CHAPTER 7

Nonlinear Behavior of Combustor Dynamics

It is linear behavior, especially linear stability, that is most easily understood and therefore has dominated discussions of combustion instabilities, particularly for solid propellant rockets. For example, the conclusion that a disturbance is unstable if the gain of energy exceeds the loss of energy in a short time interval, is founded in the first instance on linear ideas, although properly interpreted it is true generally. Because in a combustor there are many species and processes, the situation is extremely complicated. Moreover, unlike the case for linear motions, there are almost no generalizations available for nonlinear behavior to serve as the basis for classifying the results of either experiments or of theory.

The situation is simplified considerably if we restrict our attention to gas dynamics. Nonlinear behavior of disturbances in a compressible medium has long been the subject of research, steady shock waves being the most familiar phenomenon. Although there are many examples of shock waves generated in severe combustion instabilities, usually the motions do not contain shocks, or if they do, the amplitudes are small. In this chapter we examine various consequences of nonlinear gasdynamics within the framework developed in Chapters 3 and 4. Moreover, almost all of our discussion will be limited to second order nonlinear behavior, that is, to analysis in which only terms containing squares of the gasdynamic variables are considered. It appears that this approximation in fact accommodates a surprisingly large part of observed behavior, although not enough has been accomplished to assess the results in a definitive fashion.

While there is a broad spectrum of nonlinear problems that arise in combustion systems, two kinds of behavior have most recently received much of the attention: unsteady flows in solid propellant rockets; and the motions in gas turbine combustors. The first form the main subject of this chapter while the second are particularly common in systems intended for power generation. In the period stretching roughly from the early 1960s into the 1980s, for reasons earlier related, nonlinear behavior in liquid rockets attracted much interest, both in the U.S. (e.g., Sirignano 1964, Crocco 1965, Zinn 1966, Mitchell 1967) and in Russia (Natanzon 1999, where earlier work in Russia is cited and discussed at length). Nonlinear processes act to limit unsteady motions in augmentors. However, despite the work devoted to instabilities in augmentors for gas turbines over many years, relatively little seems to have been established concering the fundamental character of the instabilities and for the reasons that their amplitudes may—or may not—be limited.

Although we will not discuss nonlinear control of combustion instabilities in this book, the subject is probably more important than the lack of general interest suggests. In fact, little attention has been paid to understanding nonlinear behavior in works on control of combustion instabilities. One justification for that deficiency has been the view that if control of the oscillations works properly, it should stop the growth of the motion before its amplitude reaches a large value. There are several reasons why that reasoning is flawed:

(i) if the growth rates are unusually large, the control system may not have a sufficiently large bandwidth to be effective;
(ii) because combustion systems are intrinsically nonlinear, design of a control system based only on linear behavior may produce a control system far from optimal;

(iii) linear control demands actuation at the frequency of the oscillation to be controlled, while nonlinear control of particular types may be effective at frequencies lower than that of the oscillation being controlled;
(iv) observed nonlinear behavior contains much information about properties of the system in question and in the interests of understanding should not be ignored.

Limitations of an interpretation based entirely on linear behavior may therefore become especially evident in attempts to control an unstable motion. Existing examples of controlling combustion instabilities have almost totally ignored issues of nonlinear behavior, although such behavior is evident in all experimental work. In no demonstration, either laboratory or full-scale, have the amplitudes of the oscillations been predicted or interpreted either before or after control has been exercised. Hence nothing has been learned about why the initially unstable motions reach the amplitudes they did, or why the control system affected them in the observed way. In fact, few attempts exist to determine quantitatively the stability of motions. Consequently the subject of controlling the dynamics of combustion systems has largely been a matter at best of exercising the principles of control with little attention paid to the characteristics of the systems ('plants') being controlled. It seems that following this strategy is likely not the most fruitful way of achieving meaningful progress. Especially, this is not a sound approach to developing the basis for designing control systems. The current practice in this field is often that feedback control is designed and applied in *ad hoc* fashion for systems already built and exhibiting instabilities.[1]

A central concern of a control system designer is construction of a 'reduced order' model of the system. What that really means in the present context is the need to convert the partial differential equations of conservation developed in Chapter 3, to a finite—and probably small—system of ordinary differential equations. The analysis developed in Chapters 3 and 4 accomplishes exactly that purpose. It is not the only approach possible—e.g., although proper orthogonal decomposition has been examined briefly, in the author's experience no useful results have yet been found—but the method of modal expansion and spatial averaging has many favorable properties and has been proven to work well.

Nonlinear behavior is always present and is essential if disturbances are to have finite size in a self-excited unstable system. Thus, any considerations of limiting amplitudes—a practical matter in the treatment of instabilities in actual systems—must account for nonlinear processes. At the present time the subject is in a relatively weak state. The presence of nonlinear behavior is often remarked upon in discussions of observations. But it seems that little of practical value has been accomplished theoretically, and experimental results supporting conclusions reached in theory are almost non-existent. It does seem, however, that potentially useful theoretical results are available and some interesting opportunities exist which have not yet been explored.

The main purposes of this chapter are to examine a few results displaying some aspects of the nonlinear behavior arising from gasdynamics; and to illustrate some consequences of truncating the modal expansion, that is, what might be the consequences of reducing the order of the model. Another important issue we will examine briefly is the application of time-averaging. As the calculations in Chapter 4 showed, the great advantage of time-averaging is that it replaces N second order oscillator equation by $2N$ first order equations. That transformation enormously reduces the cost of obtaining solutions, aids theoretical work, and provides a simplified representation for application of feedback control. But as for truncation, the question arises: How accurate are the results and what are the limits of the validity of time-averaging?

It happens that both important matters of truncation and time-averaging can be investigated by applying a continuation method outlined in Section 7.7. The method has not yet been widely used but offers an efficient means for investigating solutions over wide ranges of parameters. It is a grand recipe for discovering how solutions behave as some defining quantities (such as the number of dependent variables and hence

[1] There are some recent exceptions, for example the experiments reported by Liewen *et al.* (2004).

the number of equations) is changed. Moreover, the method has been used to determine the existence of sub-critical bifurcations. It is therefore a promising approach to the practical problem of pulsed instabilities, examined in Section 7.11.

Mainly the nonlinearities due to gasdynamics are treated in this chapter. The results must be viewed with that caveat, particularly because the forms of the nonlinearities are very special, if only because the dominant coupling acts to cause energy to flow from low to high frequency waves, the tendency which produces the familiar steepening of compressive disturbances into shock waves. The results can be applied to other nonlinearities only with care because, in particular, the coupling between modes will differ from the special form provided by gasdynamics.

7.1. Early Works on Nonlinear Combustion Instabilities

It is a classical result established by Riemann (1858) and Rankine (1870) that a planar compressive wave tends to steepen, forming, in the absence of adequate dissipative processes, a shock wave as suggested by the sketch in Figure 7.1. The interpretation of this fundamental behavior rests on the fact that the propagation speed of a disturbance depends on amplitude because it depends on the temperature.[2] Thus it is mainly the change in the local speed of sound that is the cause of the steepening.

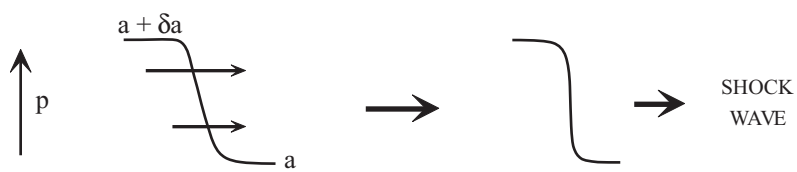

FIGURE 7.1. Steepening of a planar compressive wave into a shock wave.

The process sketched in Figure 7.1 is always active in combustion instabilities. Thus the real question in respect to observed behavior concerns the importance of wave steepening, i.e., is it a dominant process? It is never the only process at work, for in addition to those responsible for an instability (the mechanism) there are necessarily dissipative processes acting. The competition between the steepening and those processes tending to cause decay of a wave, or to modify the steepening process, is the substance of one way to view a combustion stability. This is the simplest and most fundamental basis for interpreting results found with the expansion in normal modes and spatial averaging discussed in Chapters 3 and 4.

Motivated by many observations of transverse waves in liquid and solid rockets, Maslen and Moore (1956) investigated the nonlinear problem in a circular cylinder, without combustion and flow. They were particularly concerned with steepening of transverse waves, and the accompanying change of frequency. At that time (1955) the nonlinear behavior of plane waves was quite well understood, but transverse waves had not been studied. The main difference from longitudinal waves is evident if one considers travelling waves. A wave that travels circumferentially suffers continuous reflections from the boundary. That process may be regarded as a kind of scattering which of course is absent from the case of plane wave propagation and reflection. The tendency for a wave to steepen is evidently softened in the case of transverse waves. This

[2]The ideal propagation speed of a weak isentropic disturbance is $\sqrt{\gamma RT}$ in an ideal gas, where T stands for the temperature of the medium. However, the local temperature change in an isentropic wave having local pressure δp different from the ambient value is $\delta T = \frac{\gamma-1}{\gamma} T(\delta p/p)$ while $\delta T = 0$ for an isothermal wave. For combustion instabilities, speeds of propagation are more closely given by the values for isentropic processes.

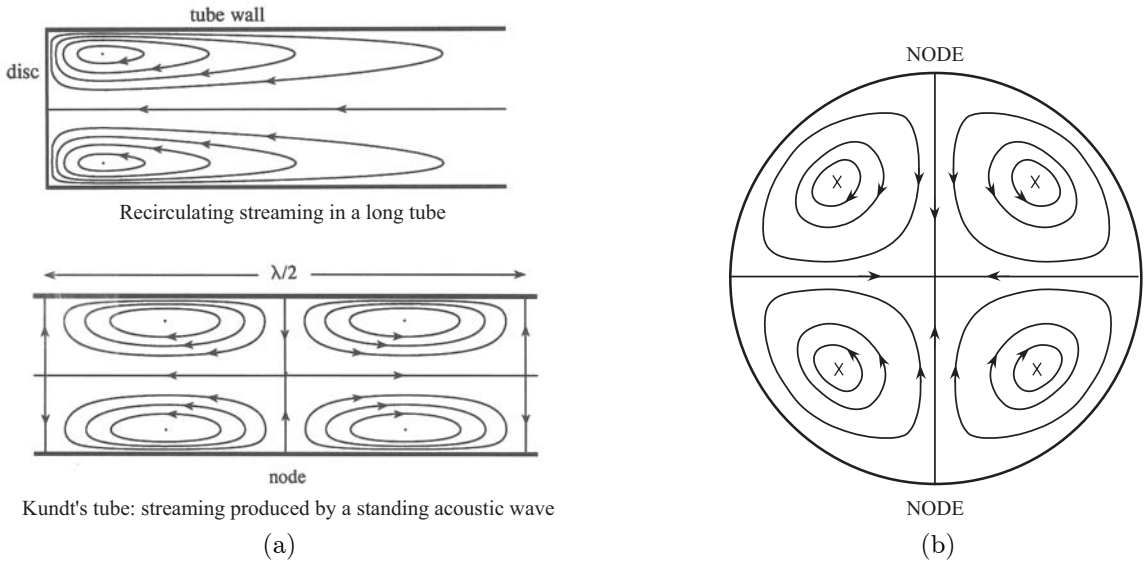

(a) (b)

FIGURE 7.2. Acoustic streaming, a consequence of small viscous effects and nonlinear acoustics (a) plane waves (Figures 5.6.6 and 5.6.7 of Howe 1998); (b) transverse standing waves in a cylinder (Maslen and Moore 1956).

result suggests what was shown to be the case by Maslen and Moore, that transverse waves will grow to higher amplitudes without the formation of shocks than will longitudinal waves.[3]

One consequence of this behavior is a quite natural development of the low order nonlinear phenomenon known as "acoustic streaming," also shown by Maslen and Moore for transverse waves. For plane wave motion parallel to a wall, a pattern of cellular motions is formed, as sketched in Figure 7.2(a). The confinement provided by the boundary causes the cells to fill the cylinder defining a transverse wave, producing a streaming motion of the form shown in Maslen and Moore's Figure 6 reproduced as Figure 7.2(b).

Much later, Flandro (1964, 1967) analyzed the problem of unwanted roll torques in solid propellant rocket motors building on the ideas of Maslen and Moore, using the formulation described here in Chapters 3 and 4; recall the remarks in Section 6.12. It's an interesting and useful analysis illustrating the procedure applied to a serious practical problem arising with a special case of combustion instability. As an example, suppose that transverse travelling waves develop in all cavities in a motor having five slots, as suggested in Figure 7.3. There is therefore an imbalance of rotating motions (an odd number of slots is required) and when the flow exhausts, a roll torque is created. The sign of the roll torque and how it is actually exerted on the motor requires careful attention to the angular momentum involved, as Flandro (1967) has shown.

Before high-speed computers became generally available, the method of characteristics was commonly used as the basis for analysis of several classes of problems involving large amplitude waves. Theoretical work in this vein seems to have originated with the analysis by Betchov (1958) who had no interest in combustion instabilities. He was concerned with oscillations in a closed tube of gas driven by an oscillating piston at one end. When viscous effects are ignored, the small amplitude motion has the familiar linear form, with the velocity given by

$$u = u_p \frac{\sin kx}{\sin kL} \cos \omega t \tag{7.1}$$

[3]Zinn (private communication) has found errors of details in the work, but Maslen and Moore's conclusions are broadly unaffected.

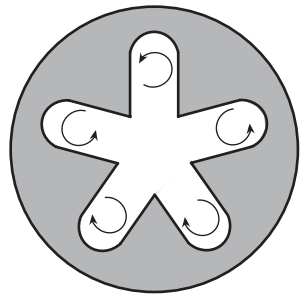

FIGURE 7.3. Finite streaming motions in a motor having five slots, giving net counterclockwise circulation (adapted from Flandro 1964).

where $\omega = kc$ and L is the length of the tube. Evidently the velocity becomes indefinitely large when $kL = \pi$. The effects of viscous friction can be computed within the linear approximation to show that they limit the amplitude. However, if the radius of the pipe is imagined to increase, frictional effects are less important, the amplitude becomes indefinitely large and nonlinear effects become more significant than viscous effects. Thus, especially so when the frequency is near resonance, nonlinear effects are increasingly significant as the amplitude increases. Not surprisingly, this problem, relatively simple and easily formulated, has attracted much attention.

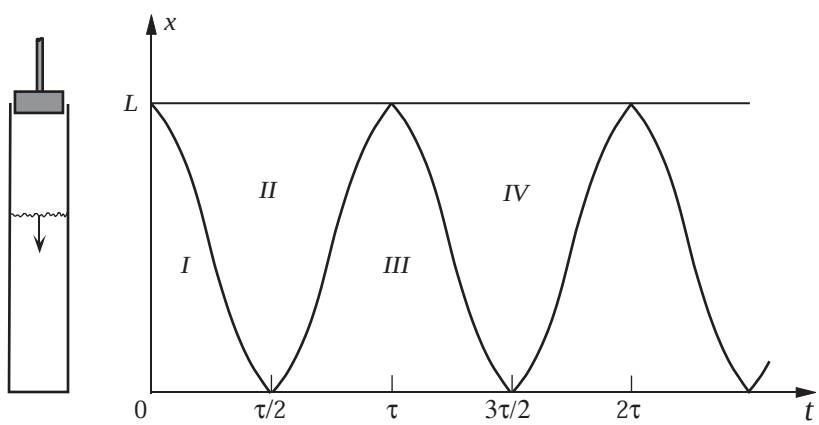

FIGURE 7.4. An oscillating shock wave in a closed tube (Betchov 1958).

On physical grounds, one may anticipate that if the amplitude and frequency of the piston's oscillatory motion are fixed, the motions of the gas will eventually settle down to a periodic form. Moreover, to emphasize the nonlinear effects, one may suppose that the periodic motion consists of a shock travelling back-and-forth in the tube with period τ. Figure 7.4, adapted from Betchov's paper, is an approximation to the flow showing only the shock wave. Betchov analyzed this problem using the method of characteristics as explained by Courant and Friedrichs (1948) and by Shapiro (1953). His discussion of the analysis includes useful comments interpreting the formalism in physical terms.

Chu (1963) and Chu and Ying (1963) analyzed a similar problem which is much more difficult to solve, although it remains quite simple compared to actual problems. A source of waves is contained in the tube, Figure 7.5, but to simplify the analysis, the source has no extent in space and is placed at the midpoint of

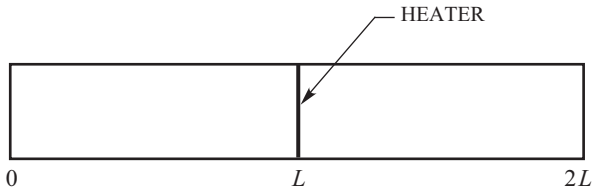

FIGURE 7.5. Closed tube containing heater at its midpoint.

the tube.[4] There is no flow in the tube but the source emits heat at a rate proportional to the local pressure fluctuation (Chu) or in addition the rate is modulated sinusoidally (Chu and Ying):

$$\text{heat release rate} \sim \begin{cases} \delta p & \text{(Chu)} \\ \delta p \sin \Omega(t + t^0) & \text{(Chu and Ying)} \end{cases} \tag{7.2}$$

Chu solved the problems of the initial growth of a disturbance, and self-sustained periodic oscillations. In both cases the fluid motion is essentially that associated with a single shock wave propagating in the tube and reflecting from the end closures. The calculations were done using a perturbation form of the method of characteristics due to Lin (1954), which in turn was suggested by the method introduced by Lighthill (1949).

The analysis by Chu and Ying was motivated mainly by the motions observed in a Rijke tube (Section 2.7) but also by combustion instabilities. Perhaps the most important aspect of this work is application of Lin's formulation of the method of characteristics to nonlinear problems involving heat addition. Two earlier reports Chu (1955, 1956), are instructive discussions of these problems, but because, as in virtually all of Chu's work, no average fluid motion is accounted for, their applications to combustion instabilities are limited.

An important qualitative change in the Princeton analyses of combustion instabilities occurred in the early 1960s when the first investigations of nonlinear behavior were carried out. Refer to Table 7.1 for a summary of the works in question. Experimental results with gas-fueled rockets had shown the presence of discrete sharp-fronted waves, suggesting a model that could be analyzed using the method of characteristics[5] as first accomplished by Sirignano (1964a,b) and Sirignano and Crocco (1964). Those papers introduced several phenomena which have since been commonly found in treatments of nonlinear instabilities. Both works are based largely on the thesis by Sirignano (1964) and treat variants of the same basic problem: the motion of a shock wave in a rocket chamber having planar combustion concentrated at the head end and terminating in a choked nozzle, Figure 7.6; or unsteady flow without a shock wave. Besides the presence or absence of a shock wave, a main difference between the two works is the model used for the response of the sheet of combustion to unsteady flow conditions. In both analyses, solutions were discussed for periodic motions, the shock wave neither growing nor decaying. The authors speculate that the driving mechanism could be related to the instability in such a way that it could be investigated by observing and interpreting the waveform. That goal has been re-stated many times since but it remains unattained.

Although he used the time lag (n, τ) model exclusively in his thesis (Sirignano 1964a), Sirignano (1968), and Sirignano and Crocco (1964) represented unsteady mass flux at the head end of the rocket by a somewhat different form not containing a time lag. With steady values denoted by subscript $(\quad)_0$, Sirignano and Crocco

[4]This problem is a simplified form of that treated in Section 2.7. It is also solved (approximately) by Culick (2002). The second work shows that if a formulation based on spatial averaging is used, it is not necessary to simplify the analysis by supposing the heater to be fixed at the midpoint of the tube.

[5]There is no obvious way to extend to nonlinear instabilities the methods used by Crocco and Cheng (1956) in their analysis of one-dimensional linear instabilities, although the authors briefly discussed some aspects of nonlinear behavior.

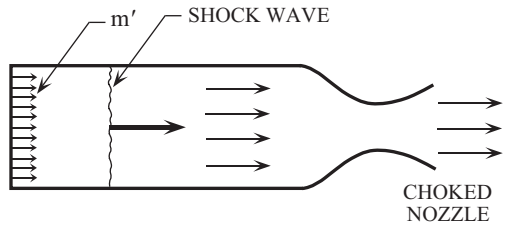

FIGURE 7.6. Model of a liquid rocket analyzed in the Princeton works. The shock wave is sometimes absent.

TABLE 7.1. Summary of Some Works from Princeton on a Theory of Combustion Instabilities.

	Combustion Model	**Wave Motion**	**Type of Mode**	**Triggering**	**Method of Analysis**
Sirignano (1964a, 1968)	$n, \tau; u'_{inj}$	Continuous Shock Waves	Axial	Inconclusive	Characteristics
Sirignano and Crocco (1964)	n, τ	Continuous Shock Waves	Axial	—	Characteristics
Zinn (1966, 1968)	n, τ	Continuous (Irrotational)	Axial	Unstable	Expansion
Mitchell (1967)	n, τ (Distributed)	Continuous Shock Waves	Axial	Inconclusive	Chester (1964)
Mitchell, Crocco and Sirignano (1969)	$n, \tau; u'_{inj}$	Continuous Shock Waves	Axial	Inconclusive	Chester (1964)
Crocco and Mitchell (1969)	n, τ (Distributed)	Continuous Shock Waves	Axial Transverse	Inconclusive	Chester (1964)

Notes:
(i) Concentrated combustion except where noted.
(ii) $u'_{inj} \neq 0$ implies $\tau = 0$.
(iii) Triggering to stable motions may have been found to exist in some cases but the references are unclear on this point.

wrote the velocity deviation from the mean value,

$$\frac{u - u_0}{u_0} = \omega \left(\frac{a - a_0}{a_0} \right) + \delta \left(\frac{a - a_0}{a_0} \right)^2 + O\left(\frac{a - a_0}{a_0} \right) \tag{7.3}$$

and carried their analysis to second order in changes of the speed of sound. They compared their results with some observations reported by Schob, Glassman and Webb (1963) made on a gas-fired rocket. Figure 7.7 shows an example of the waveform for an instability having amplitude $\Delta p/\overline{p} = 0.115$. Note that the secondary peaks in the waveform suggest that the motion could be accurately represented by a superposition of five normal modes. Thus the observations lend support of the general model used in this book. A clear case for comparison is the example cited in Section 6.11, especially Figure 6.22.

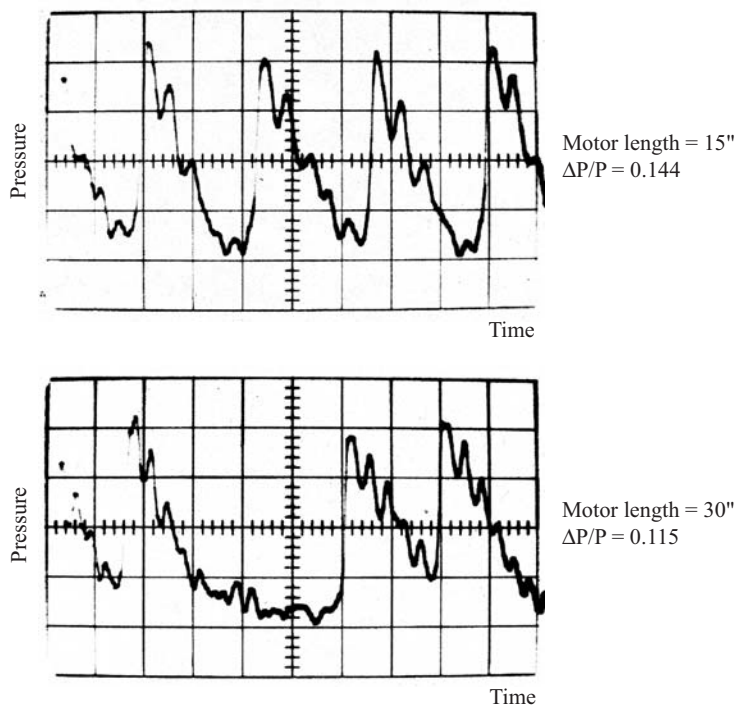

FIGURE 7.7. Waveforms observed in a gas rocket (Schob, Glassman and Webb 1963).

Sirignano (1968) analyzed the same problem using essentially the same computational methods. The main difference between that work and the calculations he did with Crocco, just mentioned, was the expression of the boundary condition at the head end,

$$\frac{\partial}{\partial t}\frac{T'}{\overline{T}} = A\frac{T'}{\overline{T}} + B\frac{p'}{\overline{p}} \tag{7.4}$$

The relation $\partial/\partial t(T'/\overline{T}) \sim A(T'/\overline{T})$ inserts a time lag in the response at the head end, distinguishing this analysis in an important qualitative way.[6] Numerical values of A and B were set according to the model for a flame response worked out by Krier *et al.* (1968). Then the results represent an approximation to the periodic motion of a shock wave in an end-burning solid propellant rocket. The behavior found is, not surprisingly, similar to that reported by Sirignano and Crocco. The idea that "information about the combustion process can be determined by experimental observation of the nonlinear waveforms" while appealingly suggested by the calculations, seems never to have been realized in practice, for any system. Mitchell, Crocco and Sirignano (1969) also examined essentially the same problem, but used a method similar to that worked out by Chester (1964).

Zinn (1966, 1968) seems to have been first in the U.S. to treat nonlinear motions not entirely in the axial direction.[7] While still analyzing the same problem shown in Figure 7.6—but, importantly, without a shock wave—he calculated results for a class of three-dimensional unsteady motions. The flow was taken to be irrotational, a restriction which can be serious under certain conditions as noted elsewhere in this book (see Chapters 3 and 4). As for most of the Princeton analyses of combustion instabilities, the $n - \tau$ model was assumed for the unsteady combustion response. Zinn obtained some results which were interpreted to

[6]In his thesis, Sirignano (1964a) had already accounted for a time lag, following earlier work on the linear problem by Crocco in several papers, and by Crocco and Cheng (1956).

[7]See also Zinn and Crocco (1967, 1968) for further details.

represent triggering but their meaning and value are doubtful because the motions were apparently found to be unstable.

First in his thesis and subsequently in collaboration with Crocco and Sirignano, Mitchell (1967) was the last of the Princeton students to analyze the problem sketched in Figure 7.6. He based his analysis on the recent work of Chester (1964) which gives results more simply than a method using characteristics, but cannot be used to study three-dimensional motions. A second advantage of the method, compared with the previous Princeton works, is the possibility of treating continuously distributed combustion. As Table 7.1 shows, Mitchell was able to treat a wider span of nonlinear problems than his predecessors at Princeton. However, his work still suffered from several serious deficiencies, notably the restriction to the $n-\tau$ model of combustion. It is not apparent from the analyses that the combustion model can easily be changed without embarking on a totally fresh analysis.

Mitchell also attempted to obtain results for triggering. However, it appears that his results share some of the same difficulties with the other Princeton works of this period. The most serious problem is that the process called 'triggering' does not produce a final state having a finite amplitude. That is, when pulsed, the system initially in a state of steady oscillation makes a transition to a condition in which the amplitude of oscillation grows without limit. Whether this sort of behavior should usefully be called 'triggering' is arguable. The definition followed in the present work is the conventional choice that triggering involves a subcritical bifurcation for which the final state is one of steady oscillation.

The theoretical ideas and approach to analyzing combustion instabilities originated by Crocco in the early 1950s dominated the field for many years in the U.S. More than three decades later the time lag was still used by some as the basis for understanding and for developing new liquid rocket engines, as discussion in Section 2.3 has shown. It is probably not an unfair characterization to note that the ideas were applied beyond their level of usefulness; progress in the design of certain aspects of liquid rockets was likely hindered. Alternative approaches were of course proposed (see Harrje and Reardon 1972) but for various reasons they were not developed extensively.

It seems that greater emphasis in the Soviet Union and Russia was placed on fundamental work directed to understanding details of the causes of instabilities. Theoretical, and some experimental, work is described in the book by Natanzon (1999). Much of the Russian experience with testing as part of liquid rocket development has been summarized by Dranovsky (2006). A discussion of those works is outside the intent of this book, but they are primary references and cannot be ignored.

Closer to the topic of the present chapter is the recent paper by French (2004). That report is a summary of progress for a program devoted to software development for predicting nonlinear combustion instabilities in solid propellant rockets. Much of the program is based on methods described in this book. The main purpose of the work is to produce a computer program capable of providing quantitative results for solid propellant rockets having quite general configurations. An example showing the growth of a finite, smooth disturbance into a steep-fronted wave is shown in Figure 7.8. That result shows clearly that the method developed here in Chapters 3–5 applies quite well to waves characterized by large gradients as well as to less abrupt disturbances.

Many computer programs have been written to compute various aspects of combustion instabilities in propulsion systems. In the past ten–fifteen years there has been increasing use of large eddy simulations (LES) to investigate flows in combustion chambers. Especially, applications to unsteady problems in gas turbines have been reported, with increasingly successful simulations of actual results found experimentally. Our purpose here is to examine some results found with the method developed in this book. The approach, based on expansion in modes and spatial averaging, seems to lend itself more effectively to understanding the physical behavior than to accurate simulation of the flows.

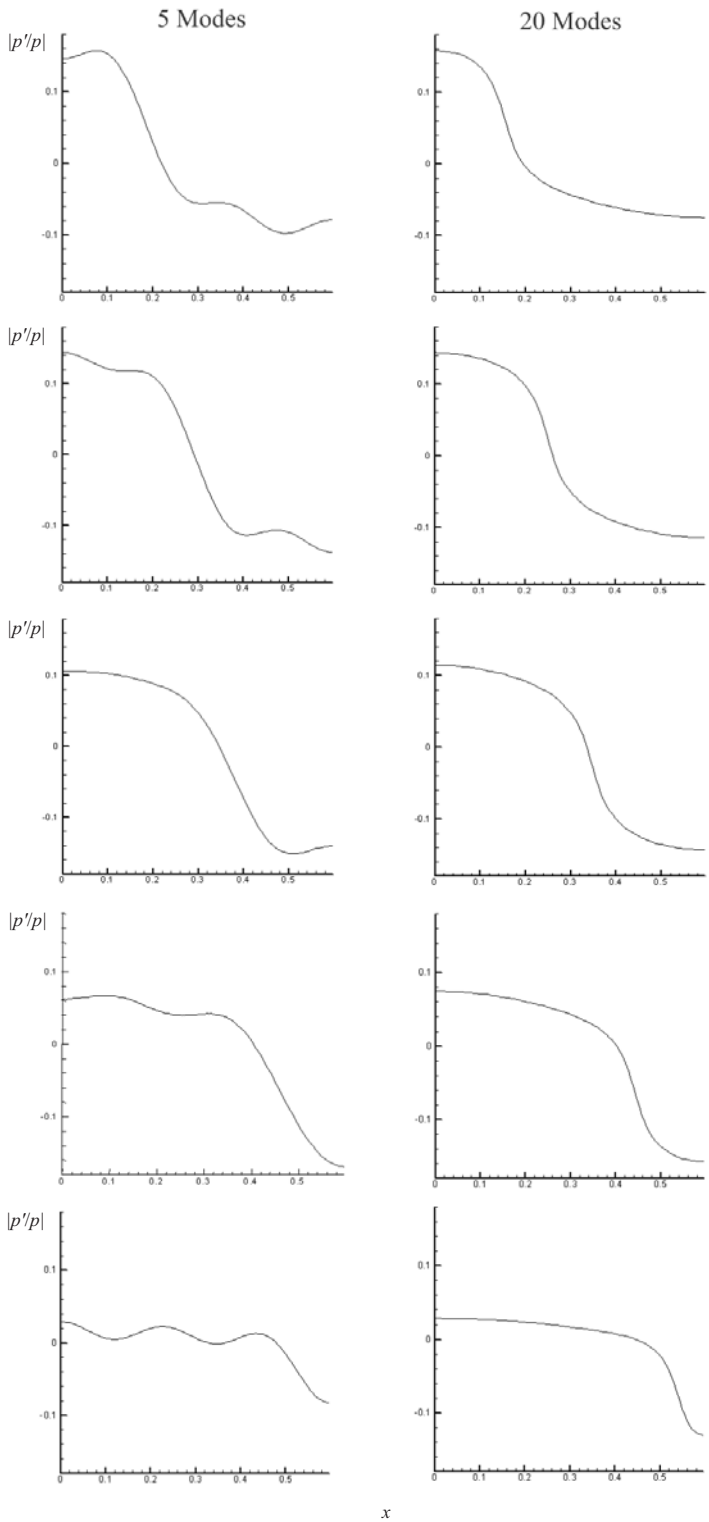

FIGURE 7.8. Steepening of a longitudinal wave travelling in a cylindrical chamber; $|p'/p|$ vs. x (French 2004).

7.2. A Single Nonlinear Mode

Interpretation of nonlinear behavior with a single mode is a sensible first step. For some purposes such a simple representation may be adequate, but experience has demonstrated that description of actual behavior must be based on more general models. The first attempt to treat a combustion instability as a single mode with the point of view taken here was Culick's (1971), an extension of earlier work on linear problems (see Sections 4.1–4.3).

Many observations suggested that point of view, but one of the clearest and most persuasive has been reproduced as Figure 1.36, taken from an oscillograph record (Perry 1970). Figure 7.9 is a drawing of the amplitude measured on Figure 1.36.

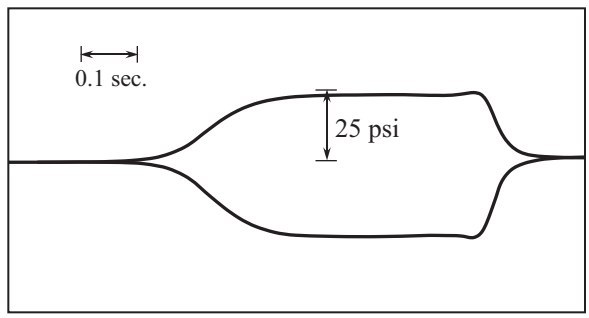

FIGURE 7.9. The envelope of oscillations for the T-burner firing shown in Figure 1.36 (Culick 1971).

The amplitude of the unstable pressure oscillation in a T-burner initially grows exponentially; levels off due to some nonlinear process; executes a limit cycle having approximately constant amplitude; and finally decays exponentially after the driving ceases, due mainly to combustion processes. The idea for a simple model of this motion was that the pressure in the burner always had the spatial distribution of the fundamental mode, $\psi(\mathbf{r})$, but with time-dependent amplitude $\eta(t)$. Thus the basic assumption was made that the pressure could be written in separable form,

$$p(\mathbf{r}, t) = \eta(t)\psi(\mathbf{r}) \tag{7.5}$$

At the time the analysis was done, the full theoretical apparatus developed here in Chapters 3 and 4 was not available. A procedure of spatial averaging was applied, similar to the method discussed in Chapter 4 but in a much simplified form. The most important difference is that nonlinear gasdynamics was not treated. Only the damping processes were ultimately taken to be nonlinear and the wave equation for the amplitude $\eta(t)$ took the form

$$\frac{d^2\eta}{dt^2} + \dot{\eta} f(\eta, \dot{\eta}) + \omega^2 \eta = 0 \tag{7.6}$$

It seemed reasonable on physical grounds to assume that $f(\eta, \dot{\eta})$ had a simple form representing possible elementary physical processes,

$$f(\eta, \dot{\eta}) = -2\alpha + \beta_1|\eta| + \beta_2\eta^2 + \gamma_1|\dot{\eta}| + \gamma_2\dot{\eta}^2 \tag{7.7}$$

Moreover, again based on experimental results, the amplitude was approximated by a sinusoid having fixed frequency ω but time-dependent amplitude $A(t)$ and phase $\varphi(t)$ to be determined,

$$\eta(t) = A(t)\sin(\omega t + \varphi(t)) \tag{7.8}$$

Familiar procedures worked out by Krylov and Bogoliubov (1947) and covered here in Section 4.5, then led to first order equations for $A(t)$ and $\varphi(t)$. For $f(\eta, \dot{\eta})$ given by (7.7), those results are

$$-\frac{1}{A}\frac{dA}{dt} = -\alpha + c_1 A + c_2 A^2 \tag{7.9}$$

$$\frac{d\varphi}{dt} = \frac{\gamma_1}{4\pi} A \tag{7.10}$$

where

$$\begin{aligned} c_1 &= \frac{2}{3\pi}(\beta_1 + 2\gamma_1\omega) \\ c_2 &= \frac{1}{8}\left(\beta_2 + \frac{3\gamma_2}{4}\omega^2\right) \end{aligned} \tag{7.11)a,b}$$

Equation (7.9) can be integrated by first factoring the right-hand side to give

$$\frac{dA}{dt} = -c_2(A - A_1)(A - A_2)A$$

of which the integral is

$$\frac{A}{A_0}\left(\frac{A_0 - A_1}{A - A_1}\right)^{a_1}\left(\frac{A_0 - A_2}{A - A_2}\right)^{a_2} = e^{\alpha t} \tag{7.12}$$

with

$$\begin{aligned} a_1 &= \frac{2\kappa}{(1+4\kappa) - \sqrt{(1+4\kappa)}} \\ a_2 &= \frac{2\kappa}{(1+4\kappa) + \sqrt{(1+4\kappa)}} \end{aligned} \tag{7.13)a,b}$$

and $\kappa = \alpha c_2/c_1^2$. The amplitude at $t = 0$ is A_0.

Very good and promising results were obtained by Culick (1971) with a linear correction to the attenuation coefficient, $\beta_2 = \gamma_2 = c_2 = 0$ so the right-hand side of (7.9) is $-\alpha + c_1 A_1$. Then one finds the simple results

$$\text{growth} \quad (\alpha > 0) \qquad \frac{A}{A_m} = \frac{\zeta e^{\frac{|\alpha|}{t}}}{1 + \zeta e^{|\alpha| t}} \tag{7.14}$$

$$\text{decay} \quad (\alpha < 0) \qquad \frac{A}{A_m} = \frac{\zeta e^{-\frac{|\alpha|}{t}}}{1 - \zeta e^{-|\alpha| t}} \tag{7.15}$$

with

$$\text{growth} \qquad \zeta = \frac{A_0/A_m}{1 - A_0/A_m} \tag{7.16}$$

$$\text{decay} \qquad \zeta = \frac{A_0/A_m}{1 + A_0/A_m} \tag{7.17}$$

For the growth of waves, after a long time ($t \to \infty$), the limiting amplitude is

$$A(t \to \infty) = \frac{\alpha}{c_1} = \frac{3\pi\alpha}{2|\beta_1 + 2\gamma_1\omega|} = A_m \tag{7.18}$$

Thus the limiting amplitude is independent of the initial amplitude A_0 as it should be if the limit cycle is unique.

The growth or decay rates for the case $\beta_2 = \gamma_2 = 0$, expressed as logarithmic slopes, are

$$\frac{1}{A}\frac{dA}{dt} = \begin{cases} \frac{|\alpha|}{1+\zeta e^{|\alpha|t}} & (\text{growth}) \\ \frac{-|\alpha|}{1-\zeta e^{-|\alpha|t}} & (\text{decay}) \end{cases} \tag{7.19)a,b}$$

which for short and long times become

$$t \to 0: \qquad \frac{1}{A}\frac{dA}{dt} \to \begin{cases} \frac{|\alpha|}{1+\zeta} & (\text{growth}) \\ \frac{-|\alpha|}{1-\zeta} & (\text{decay}) \end{cases} \tag{7.20}$$

$$t \to \infty: \qquad \frac{1}{A}\frac{dA}{dt} \to \begin{cases} 0 & (\text{growth}) \\ -|\alpha| & (\text{decay}) \end{cases} \tag{7.21}$$

Three interesting conclusions follow from (7.18) and (7.19)a,b:

(i) Both $|A_m|$ and $(d \ln A/dt)_{t\to 0}$ are proportional to $|\alpha|$; hence the initial growth rate and final amplitude increase together with $|\alpha|$. Because α represents the difference between linear driving and attenuation, increased driving produces both a larger initial growth rate and a larger final amplitude.

(ii) If the nonlinear damping is increased, the final amplitude is reduced. The initial growth rate is unaffected.

(iii) For a given $|\alpha|$ (i.e., linear contributions) and amplitude prior to decay, the initial decay rate is greater if the nonlinear coefficient of attenuation (c_1) is increased.

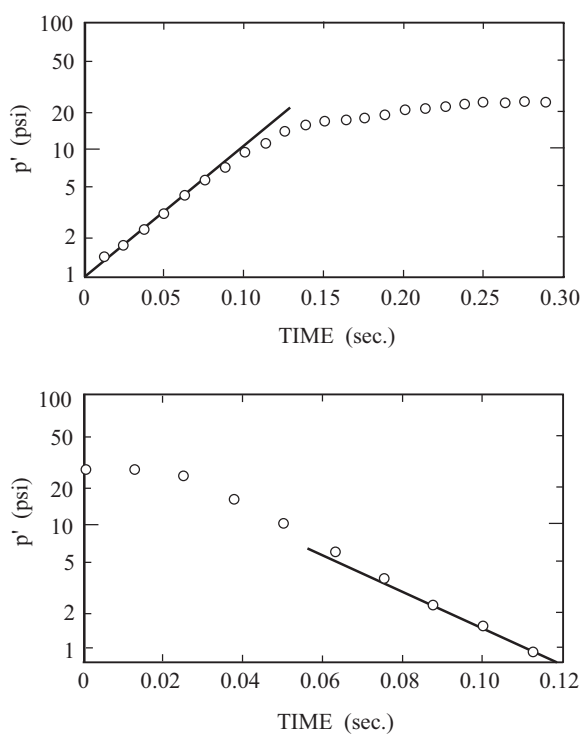

FIGURE 7.10. Data for the growth and decay periods of the firing shown in Figure 7.9.

Test data taken from the firing shown in Figure 7.9 are plotted in semi-logarithmic coordinates, Figure 7.10. The slopes of the lines shown are the values of α_g during the growth period and of α_d during decay. Figures 7.11 and 7.12 are plots of the data taken during the growth and decay periods, in coordinates giving a direct comparison with the simple theory outlined above. Apparently the behavior during both periods is quite well reproduced by this simple theory.

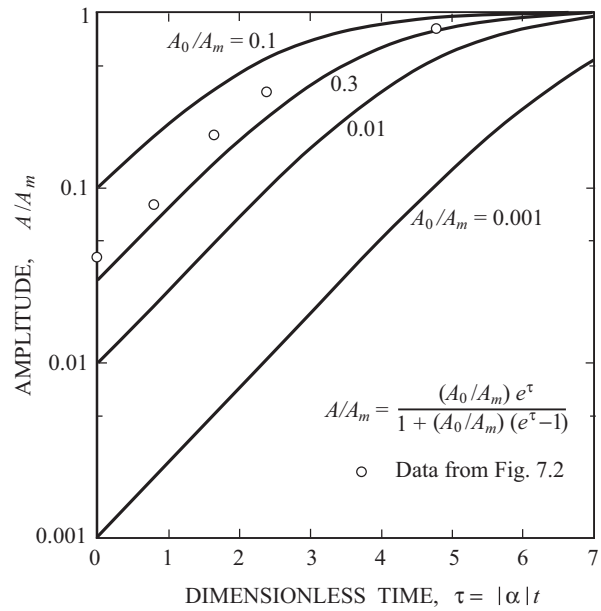

FIGURE 7.11. Nonlinear growth of oscillations for several values of the initial amplitude ratio A_0/A_m (Culick 1971).

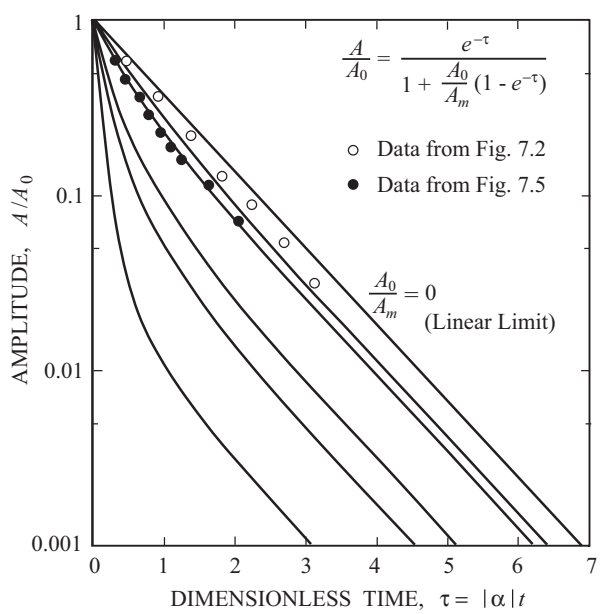

FIGURE 7.12. Nonlinear decay of oscillations for several values of the initial amplitude ratio A_0/A_m (Culick 1971).

In several respects the behavior examined in the preceding example is not a particularly difficult test of the theory worked out here. In the original work, consideration of the relatively low amplitudes present in the test discussed with Figures 7.9 to 7.12 was already recognized as a restriction. A T-burner firing at lower frequency (600 Hz, whereas the frequency of the oscillations in Figure 7.9 was 2800 Hz) exhibited more apparent nonlinear behavior, Figure 7.13. This aspect of the data was discussed in the paper, but a more important matter became clear only as the initial ideas were applied to more cases.

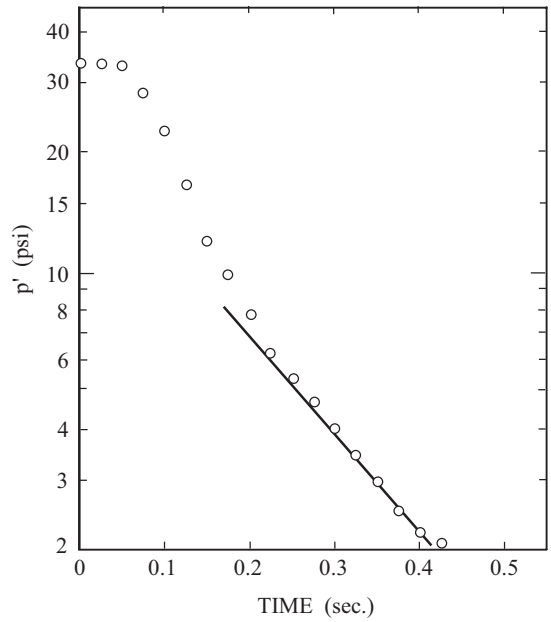

FIGURE 7.13. A T-burner firing showing stronger nonlinear behavior during the initial portion of the decay of oscillations (Culick 1971).

Immediately following the accomplishments just described, a project was begun to analyze available T-burner data to obtain values of the parameters arising with nonlinear behavior. The intent was to discover trends of the values with characteristics such as propellant composition, pressure and frequency; and eventually to attach physical meanings to the results. Considerable data was available so there was ample opportunity for enforcing consistency of the results. Although the initial results were good, a difficulty slowly became clear: A given set of data could equally well be represented by several combinations of the parameters $\beta_1, \gamma_1, \gamma_2, \ldots$. Other choices of parameters exhibited the same property. Thus it was apparently not possible to settle on unique values of empirically determined parameters. That approach to understanding nonlinear behavior failed.

As part of the effort required to carry out the failed program, it was necessary—better expressed, the opportunity was provided—to examine spectra of T-burner records. What became particularly apparent was that records which previously had been treated as 'clean', that is consisting of single frequencies, in fact often contained noticeable amounts of harmonics. That was the beginning of the author's research on systems having many degrees of freedom and concern with the importance of harmonics in combustion instabilities. The simplest case is a system having only two degrees of freedom discussed in the next section.

Representation of dynamical behavior with a single degree of freedom is enormously appealing. Not only is understanding greatly aided, but graphical representation is particularly simplified. The classic book by Minorsky (1947) contains many examples of the methods of presenting the behavior of a system. Awad (1983) and Awad and Culick (1986) used the phase plane in their discussion of nonlinear behavior. The procedure was later used by Beckstead (1987) to describe possible mechanisms. However, since the approach

is useful only for a small number of degrees of freedom, its applications are limited and, as the following remarks show, the results can be mortally misleading if the limitations are not respected.

The phase plane is usually defined with a dependent variable (displacement, say) and its rate of change (i.e., velocity) as coordinates. Thus, the equations produced by the method of averaging (Section ____) are directly applicable. As the simplest example, consider again the case treated above. The amplitude of the motion obeys (7.9) which can be written, to second order:

$$\frac{dA}{dt} = 2\alpha A + bA^2 = kA(A_1 - A) \tag{7.22}$$

If this is taken to serve as an approximation to the behavior we are concerned with here, then the second order term, bA^2, in some sense represents the effects of second order acoustics. The integral of (7.22) is

$$A = \frac{A_1}{1 + \left(\frac{A_1}{A_0} - 1\right) e^{-\alpha t}} \tag{7.23}$$

where A_0 is the initial value of A and $kA_1 = 2\alpha$. We take A to be positive, so two possibilities exist, corresponding to $kA_1 = 2\alpha$ positive or negative. Figure 7.14 shows examples for $\alpha > 0$ ('spontaneous' instability) and $\alpha < 0$ (linear stability).

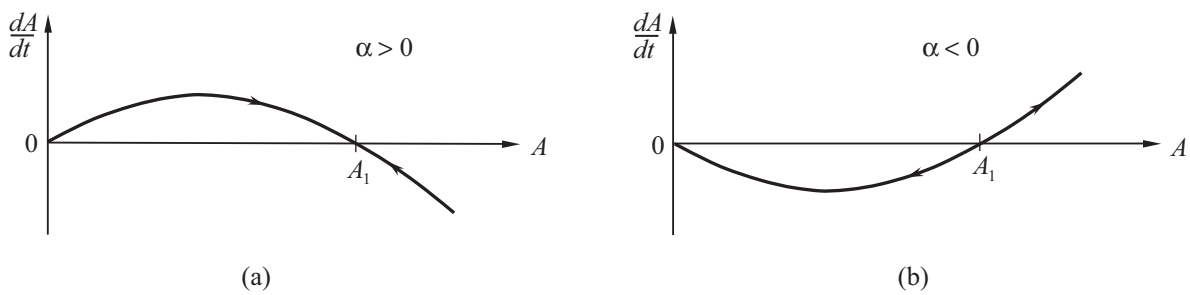

FIGURE 7.14. The two cases presented by equation (7.22).

In the case $\alpha > 0$, Figure (7.14)a, motions having any initial amplitude are unstable and eventually reach the limit amplitude A_1. This is the same behavior found with the second order acoustics equations accounting for many modes. The approximate model seems to be promising. However, the promise is tarnished for the case $\alpha < 0$, as shown in Figure (7.14)b; if the initial amplitude A is greater than A_1, the 'limit cycle' grows without limit. This behavior is not found with the complete equations (Chapter 4) for many degrees of freedom discussed in the next section.

In the late 1970s, and later, concern grew with pulsed instabilities in solid rockets. It was logical to determine first what might be predicted by the model for a single mode. The equation for a single mode, now governed by third order acoustics, is

$$\frac{dA}{dt} = kA(A_1 - A)(A_2 - A) \tag{7.24}$$

in which $kA_1 = 2\alpha$ again. A second possible form is

$$\frac{dA}{dt} = kA(A^2 - A_1^2) \tag{7.25}$$

The typical plot of (7.25) looks similar to Figure (7.14) and so is not interesting. Equation (7.24) gives the two possibilities shown in Figure 7.15. For a linearly unstable mode, $\alpha < 0$, Figure 7.15(a), the behavior is similar to that for $A < A_2$. But if the initial amplitude is larger that A_2, the motion grows without limit. This is contrary to the results of numerical calculation for cases covering many modes.

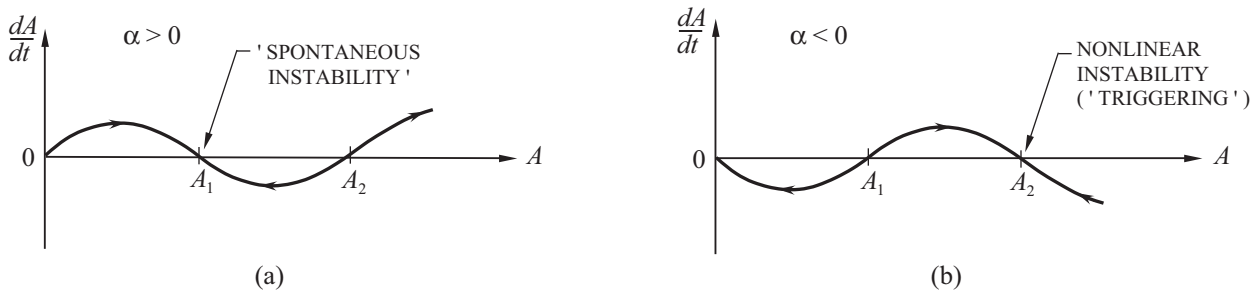

FIGURE 7.15. The two cases presented by equation (7.24). Part (b) represents a pulsed (triggered) instability.

For $\alpha < 0$, if the initial amplitude is less than A_1, the system ultimately executes a limit cycle having amplitude A_2. Thus, as shown by Figure 7.15(b), third order acoustics seem to hold the possibility of triggering.

That was an encouraging result, found at a time when interest in determining the condition for triggering, and hence learning how to avoid the phenomenon in practice, was particularly strong. Several analyses were carried out to determine how third order acoustics could be used to explain triggering (Awad 1983; Awad and Culick 1984, 1986; Yang and Culick 1986; Yang, Kim and Culick 1987, 1988, 1990). No cases of triggering were found in many examples worked out for a range of realistic conditions. It is important that those results were obtained for systems containing two or more modes.

The conclusions of several years' effort, reached not on theoretical grounds but purely by trial and error 'numerical experimenting', was that nonlinear acoustics alone did not contain the possibility of triggering to a stable limit cycle. That was an important result (albeit not strictly proved) because it implied that another nonlinear process had to be taken into account. Combustion was the obvious candidate. The matter was far from settled, however, even on practical grounds. Further exploration showed that rather special characteristics of nonlinear combustion are required. Culick, Burnley and Swenson (1995) showed that nonlinear combustion and gasdynamics together could be used to demonstrate the possibility of triggering; Burnley (1996) discussed further details in his dissertation. See also Section 7.14 here. One practical implication is that understanding pulsed instabilities requires more thorough experimental results for nonlinear characteristics—particularly of unsteady combustion—than have been obtained to date.[8]

From the practical point of view, the procedures involved here have not been developed to the level required for convenient application. And with the complications accompanying analysis accounting for two or more degrees of freedom, a simpler approach is desirable. The approximation based on a single degree of freedom is undeniably attractive. Jensen (1972), Beckstead and Jensen (1972) and Beckstead (1987) have pursued this approach, and its application to the behavior of instabilities in solid propellant rockets, further than others working in the field. They have obtained some appealing results and have emphasized several practical aspects. However, their conclusions must be viewed with caution, since they are based on a strictly flawed model having a single degree of freedom.

[8]The results cited here have apparently been obtained largely for solid propellant rockets. However, because of the generality of the procedures developed in Chapters 3 and 4, the discussion and conclusions apply equally well to any combustion system of the form treated.

7.3. The Two-Mode Approximation

This is the simplest class of problems for which nonlinear mode coupling is accommodated. Each mode is characterized by two constants: α (energy gain or loss) and θ (frequency shift). The energy gain or loss may be nonlinear—that is, α could in principle depend on amplitude—but here both α and θ are taken to be constant, characterizing entirely the linear processes. As a result of several works in the past few years, the two-mode approximation is quite well understood (Awad and Culick, 1986; Paparizos and Culick, 1989; Yang and Culick 1990; Jahnke and Culick, 1994; Culick, 1994).

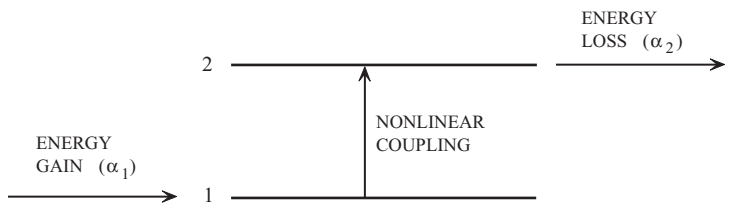

FIGURE 7.16. Energy flow in the two-mode approximation.

Only gasdynamic nonlinearities to second order are accounted for here. Their special structure allows the convenient closed form solutions to the time-averaged equations, first found by Awad (1983). The results provide much basic understanding which is applicable to more complicated nonlinear problems. For example, contrary to one's expectation based on the behavior of shock waves, nonlinear behavior in the present context need not involve large amplitudes, and the pressure oscillation may appear to be a clean sinusoid, free of significant harmonic content. The basic reason is that here the two-mode system both gains and loses energy; each interaction with the environment is necessary. Moreover, both stable and unstable limit cycles exist. In the absence of nonlinear modal coupling, or some other nonlinear process, limit cycles cannot exist.

Truncation of the modal expansion to two modes introduces errors because the flow of energy to higher modes is blocked. The amplitude of the highest mode is therefore greater than the correct value in order to provide the higher linear rate of energy loss required to sustain a limit cycle. The example in Section 6.11 showed this effect.

It's an interesting feature of the two-mode approximation that with linear gains and losses of energy, nonlinear instability (pulsing) to stable limit cycles seems not to exist. Although no rigorous proof exists, experience with many examples has shown that conclusion to be quite generally true for any number of modes if only the acoustic (gasdynamics) nonlinearities are accounted for. 'Triggering' or pulsing to stable limit cycles does occur for special forms of nonlinear energy gain from the environment (i.e., extraction from the mean flow or supply from combustion processes) as the example in Section 7.11 shows. By 'triggering' we mean here pulsing **from** a quiescent initial state or a stable limit cycle, **to** a stable limit cycle. More generally, one can imagine triggering from one stable limit cycle to another.

If we ignore linear mode coupling and account for acoustic nonlinearities to second order, the oscillator equations can be put in the form

$$\frac{d^2\eta_n}{dt^2} + \omega_n^2\eta_n = \alpha_n\dot{\eta}_n + \theta_n\eta_n - \sum_{i=1}^{\infty}\sum_{j=1}^{\infty}\left[A_{nij}\dot{\eta}_i\dot{\eta}_j + B_{nij}\eta_i\eta_j\right] + F_n^{NL} \tag{7.26}$$

where F_n^{NL} represents other nonlinear contributions. The coefficients A_{nij}, B_{nij} are defined as integrals involving the basis functions ψ_{nij}. Hence their values are fixed primarily by the geometry of the chamber in question. See Section 4.5 and Culick (1976) for additional details of the derivation of (7.26). It is a crucially important result that the nonlinear gasdynamic terms involve no cross products $\dot{\eta}_i\eta_j$ and also (not obvious

here) no 'self-coupling', terms proportional to $\dot{\eta}_n^2$ or η_n^2. Those properties seem to be the formal reasons that nonlinear (pulsed) instabilities do not exist if only these nonlinearities are included, particularly when the combustion processes are linear.

Equation (7.26) simplifies considerably for longitudinal modes. Due to orthogonality and special properties of the $\cos k_n z$, the double sum becomes a single sum and (7.26) can be put in the form (Jahnke and Culick 1994):

$$\begin{aligned}\frac{d^2\eta_n}{dt^2} + \omega_n^2\eta_n = \alpha_n\dot{\eta}_n + \theta_n\eta_n - \sum_{i=1}^{\infty}\left[C_{ni}^{(1)}\dot{\eta}_i\dot{\eta}_{n-i} + D_{ni}^{(1)}\eta_i\eta_{n-i}\right] \\ - \sum_{i=1}^{\infty}\left[C_{ni}^{(2)}\dot{\eta}_i\dot{\eta}_{n+i} + D_{ni}^{(2)}\eta_i\eta_{n+i}\right] + F_n^{NL}\end{aligned} \tag{7.27}$$

The time-averaged forms of (7.27) are

$$\begin{aligned}\frac{dA_n}{dt} &= \alpha_n A_n + \theta_n B_n + \frac{n\beta}{2}\sum^{i}\left[A_i(A_{n-i} - A_{i-n} - A_{i+n}) - B_i(B_{n-i} - B_{i-n} - B_{i+n})\right] \\ \frac{dB_n}{dt} &= -\theta_n A_n + \alpha_n B_n + \frac{n\beta}{2}\sum^{i}\left[A_i(B_{n-i} - B_{i-n} - B_{i+n}) - B_i(A_{n-i} - A_{i-n} - A_{i+n})\right]\end{aligned} \tag{7.28)a,b}$$

where, as in Chapter 3, $\eta_n = A_n\cos\omega_n t + B_n\sin\omega_n t$. For longitudinal modes, the frequencies are all integral multiples of the fundamental, a property that is crucial to the forms of (7.28)a,b. For example, for transverse modes in a cylindrical chamber, the nonlinear terms contain factors representing modulation.

For two modes, the four first order equations are

$$\begin{aligned}\frac{dA_1}{dt} &= \alpha_1 A_1 + \theta_1 B_1 - \beta(A_1A_2 - B_1B_2) \\ \frac{dB_1}{dt} &= \alpha_1 B_1 + \theta_1 A_1 + \beta(B_1A_2 - A_1B_2) \\ \frac{dA_2}{dt} &= \alpha_2 A_2 + \theta_2 B_2 + \beta(A_1^2 - B_1^2) \\ \frac{dB_2}{dt} &= \alpha_2 B_2 + \theta_2 A_2 + 2\beta B_1 A_1\end{aligned} \tag{7.29)a,b,c,d}$$

The great advantage of this system of equations is that some useful exact results can be found. One way to find them is to change independent variables to the amplitude and phases (r_n, ϕ_n) of the two modes by writing

$$\begin{aligned}\eta_1(t) &= r_1(t)\sin(\omega_1 t + \phi_1) \\ \eta_2(t) &= r_2(t)\sin(2\omega_1 t + \phi_2)\end{aligned}$$

where $r_n = \sqrt{A_n^2 + B_n^2}$. The governing equations for r_1, r_2 and the effective relative phase $\psi = 2\phi_1 - \phi_2$ are

$$\begin{aligned}\frac{dr_1}{dt} &= \alpha_1 r_1 + \beta r_1 r_2\cos\psi \\ \frac{dr_2}{dt} &= \alpha_2 r_2 + \beta r_1^2\cos\psi \\ \frac{d\psi}{dt} &= (\theta_1 - 2\theta_1) + \beta(2r_1 - \frac{r_1^2}{2}\sin\psi)\end{aligned} \tag{7.30)a,b,c}$$

where

$$\beta = \frac{\theta_2 - 2\theta_1}{2\alpha_1\alpha_2} \tag{7.31}$$

The problem of linear stability is solved directly:

$$\alpha_1, \alpha_2 < 0 \Longleftrightarrow \text{ small amplitude motions are stable} \tag{7.32}$$

7.3.1. Existence of Limit Cycles. Nonlinear behavior in general poses two basic questions:

(i) What are the conditions for existence of limit cycles?
(ii) What are the conditions that the limit cycles are stable?

Stability of a limit cycle of course is a matter entirely separate from the linear stability of small amplitude motions. We are concerned here with a system executing a steady limit cycle. If the limit cycle is stable, then if slightly disturbed, the motion will eventually return to its initial form.

In this time-averaged formulation, existence of limit cycles corresponds to existence of stationary or equilibrium points of the system (7.30)a,b,c:

$$\frac{dr_1}{dt} = \frac{dr_2}{dt} = \frac{d\psi}{dt} = 0 \Longleftrightarrow \text{ transcendental algebraic equations}$$

The solutions are

$$\begin{aligned} r_{10} &= \frac{1}{\kappa}\sqrt{-\alpha_1\alpha_2(1+\beta^2)} \\ r_{20} &= \frac{1}{\kappa}\sqrt{\alpha_1^2(1+\beta^2)} \\ \psi_o &= \tan^{-1}(-\beta) \end{aligned} \tag{7.33)a,b,c}$$

where

$$\kappa = \frac{\gamma+1}{8\gamma}\omega_1 \tag{7.34}$$

For r_{10} to be real, $-\alpha_1\alpha_2$ must be positive, implying that the constants α_1, α_2 must have opposite signs. The physical interpretation is that if the first mode is unstable, for example, $(\alpha > 0)$, then the second mode must be stable $(\alpha_2 < 0)$: the rate of energy flow into the first mode must equal the rate of loss from the second mode in order that the amplitudes be constant in time. The transfer rate upwards due to coupling must have the same value. Similar reasoning explains the case when the second mode is unstable, requiring that the first mode to be stable.

7.3.2. Stability of Limit Cycles. To determine the stability of limit cycles, the variables are written as $r_i = r_{i0} + r_i', \quad \psi = \psi_o + \psi'$ and substituted in the governing equations (7.29)a,b,c,d. The linearized equations for the disturbances are then solved for the characteristic value λ in the assumed forms $r_i' = r_{i0}' e^{\lambda t}, \cdots$. For stability, an initial disturbance must decay. Applying that requirement produces regions of stability in the plane of the parameters $\beta_o = (\theta_2 - 2\theta_1)^2/(\alpha_2 + 2\alpha_1)^2$ and α_2/α_1, shown in Figure 7.17.

There is presently no basis for understanding why stable limit cycles occur only for the special ranges of parameters shown in Figure 7.17. However, more elaborate analysis (Jahnke and Culick 1994) has shown that the result that the stability region has boundaries for finite values of α_2 and α_1 is a consequence of time-averaging. That conclusion shows the importance for both practical and theoretical reasons of assessing and quantifying as far as possible the consequences of time-averaging and truncation. Considerable progress has been made in that direction by using a continuation method to solve the systems of oscillator equations. Some results are discussed in Section 7.7.

Here it is useful to examine the details of several special cases. Figure 7.18 shows that if the parameters are chosen so that the operating point lies within the range for stable limit cycles and the first mode is unstable, truncation may have relatively small effects. On the other hand, if the limit cycle is unstable

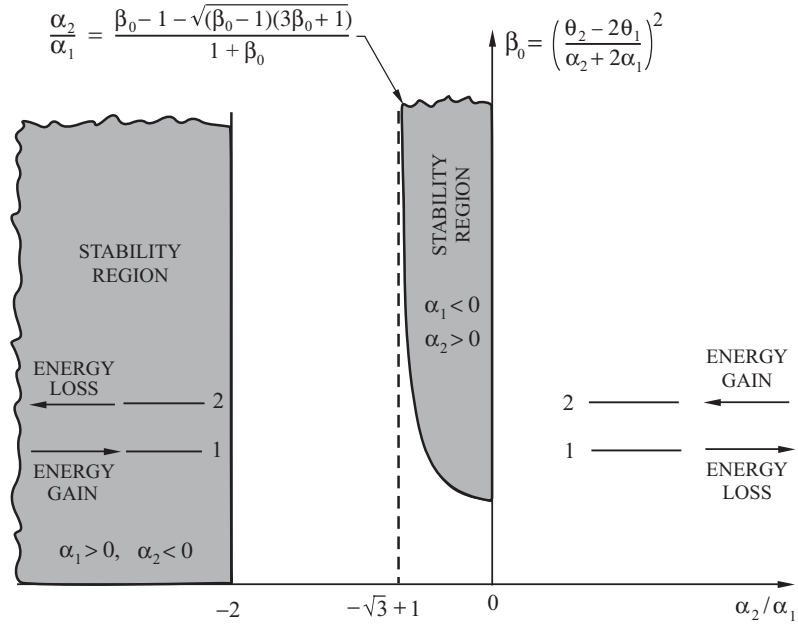

FIGURE 7.17. Regions of stability for two longitudinal modes, time-averaged equations (Awad and Culick 1986).

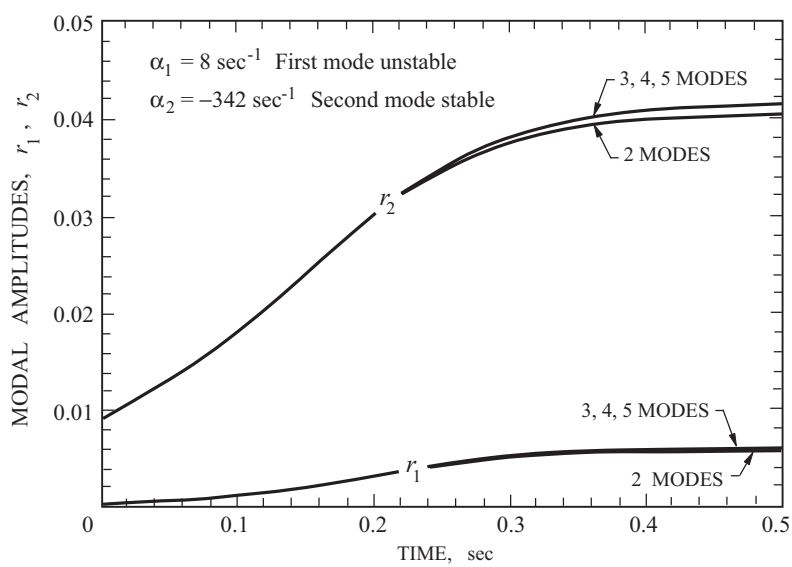

FIGURE 7.18. Effects of truncation for a stable limit cycle: first mode unstable, second mode stable (Paparizos and Culick 1989).

according to the two-mode approximation with an unstable first mode, it may become stable (with the same values of $\alpha_1, \alpha_2, \theta_1, \theta_2$) if higher stable modes are accounted for. That behavior is shown in Figure 7.19

Figure 7.20 is interesting for a quite different reason. In this case the second mode is unstable, and the motion evolves to a stable limit cycle. However, unlike the example in Figure 7.18, the amplitudes do not grow smoothly and monotonically to their values in the limit cycle. Their erratic behavior is due to the

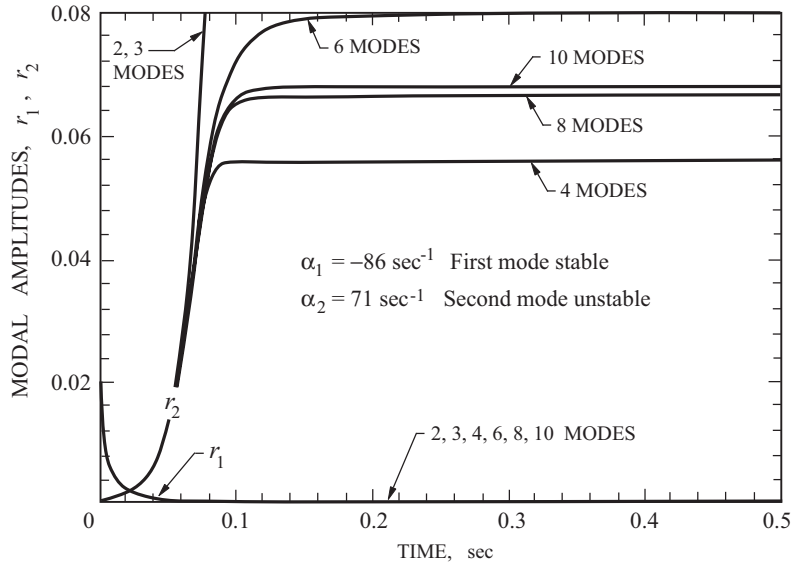

FIGURE 7.19. Effects of truncation for an unstable limit cycle: first mode unstable, second mode stable (Paparizos and Culick 1989).

fact that with the second mode unstable, energy must flow from high frequency to low frequency. That is contrary to the direction of flow imposed naturally by the fluid mechanics (of the steepening of a compressive disturbance into a shock wave). The conflict between the natural action of the nonlinear coupling on the one hand and the flow of energy imposed by energy exchange with the environment causes the amplitudes of the two modes to wander during the transient phase before finally reaching their ultimate values. More special cases are treated in the references. It is an important conclusion that truncation of the time-averaged equations for two modes will give misleading or incorrect results unless the initial state is close to the stability boundary.

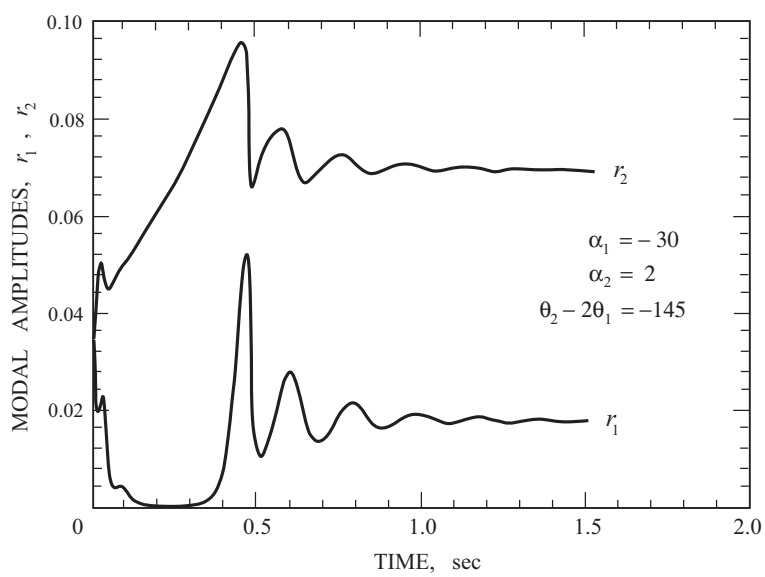

FIGURE 7.20. Development of a stable limit cycle when the first mode is stable but the second mode is unstable (Paparizos and Culick 1989).

7.4. Transverse Modes and the Method of Averaging

The term "transverse modes" refers to motions which are the simplest involving time-dependent velocity not aligned with the center-line of a straight chamber. Apart from a rectangular cross section, which is generally not a practical form for a combustion chamber, the most common geometry is a circular cylinder. Thus the classical unperturbed linear acoustic modes have the familiar separable form (Section 5.8.2), a product of a Bessel function of the radius, a trigonometric function of azimuthal angle, and a trigonometric or hyperbolic function of position along the axis. It has become customary in the field of combustion instabilities to call transverse modes any motion which has the same time variation for all degrees of freedom and the same spatial dependence in planes perpendicular to the axis of the chamber as for classical acoustic modes. We are concerned in this section with the time dependence of such motions. Their spatial forms define normal modes but the time-dependence is not simply trigonometric.

It seems a somewhat remarkable result that relatively simple conditions for existence and stability of transverse modes, in a circular cylinder, can be obtained by following the same approach used to treat purely longitudinal modes. The reason is that the time-averaged equations again have a special structure allowing construction of exact solutions for two modes. Furthermore, some results can be obtained for a special case of three modes as well. What makes these results surprising in a practical sense is that now the natural frequencies do not satisfy the conditions $\omega_n = n\omega$, and the time-averaged equations contain factors representing modulation on the right-hand side.

The set of equations valid for second order acoustics in a circular cylindrical chamber have been given by Yang and Culick (1990),

$$\begin{aligned}
\dot{A}_n = &-\frac{1}{2\omega_n}\sum_{i=1}^{\infty}\{c_{ni}[\cos(\omega_n+\omega_i)t+\cos(\omega_n-\omega_i)t] \\
&+s_{ni}[\sin(\omega_n+\omega_i)t-\sin(\omega_n-\omega_i)t]\} \\
&-\frac{1}{2\omega_n}\sum_{i=1}^{\infty}\sum_{j=1}^{\infty}\{F_{nij}a_{ij}[\cos(\omega_n+\omega_{ij^+})t+\cos(\omega_n-\omega_{ij^+})t] \\
&+G_{nij}b_{ij}[\cos(\omega_n+\omega_{ij^-})t+\cos(\omega_n-\omega_{ij^-})t] \\
&-F_{nij}d_{ij}[\sin(\omega_n+\omega_{ij^+})t+\sin(\omega_n-\omega_{ij^+})t] \\
&+G_{nij}e_{ij}[\sin(\omega_n+\omega_{ij^-})t+\sin(\omega_n-\omega_{ij^-})t]\}\,,
\end{aligned} \tag{7.35}$$

$$\begin{aligned}
\dot{B}_n = &-\frac{1}{2\omega_n}\sum_{i=1}^{\infty}\{C_{ni}[\sin(\omega_n+\omega_i)t+\sin(\omega_n-\omega_i)t] \\
&+S_{ni}[-\cos(\omega_n+\omega_i)t+\cos(\omega_n-\omega_i)t]\} \\
&+\frac{1}{2\omega_n}\sum_{i=1}^{\infty}\sum_{j=1}^{\infty}\{F_{nij}a_{ij}[\sin(\omega_n+\omega_{ij^+})t+\sin(\omega_n-\omega_{ij^+})t] \\
&+G_{nij}b_{ij}[\sin(\omega_n+\omega_{ij^-})t+\sin(\omega_n-\omega_{ij^-})t] \\
&-F_{nij}d_{ij}[\cos(\omega_n+\omega_{ij^+})t-\cos(\omega_n-\omega_{ij^+})t] \\
&+G_{nij}e_{ij}[\cos(\omega_n+\omega_{ij^-})t-\cos(\omega_n-\omega_{ij^-})t]\}\,,
\end{aligned} \tag{7.36}$$

where

$$\begin{aligned}
\omega_{ij^+} &= \omega_i+\omega_j; & \omega_{ij^-} &= \omega_i-\omega_j; \\
C_{ni} &= \omega_i D_{ni}A_i+E_{ni}B_i; & S_{ni} &= -\omega_i D_{ni}B_i+E_{ni}A_i; \\
F_{nij} &= \omega_i\omega_j A_{nij}-B_{nij}; & G_{nij} &= \omega_i\omega_j A_{nij}+B_{nij};
\end{aligned}$$

$$a_{ij} = \frac{1}{2}(A_iA_j - B_iB_j); \qquad b_{ij} = \frac{1}{2}(A_iA_j - B_iB_j);$$
$$d_{ij} = \frac{1}{2}(A_iB_j - A_jB_i); \qquad e_{ij} = \frac{1}{2}(A_iB_j - A_jB_i).$$

We follow the example worked out by Yang and Culick (1990) and consider three transverse modes: the first and second tangential and the first radial, having the following wave numbers and mode shapes:

First Tangential Mode (1T)

$$\kappa_1 R = 1.8412;\ \psi_1 = \cos\theta J_1(\kappa_1 r),\ \psi_4 = \sin\theta J_1(\kappa_1 r), \tag{7.37}$$

First Radial Mode (1R)

$$\kappa_2 R = 3.8317;\ \psi_2 = J_0(\kappa_2 r), \tag{7.38}$$

Second Tangential Mode (2T)

$$\kappa_3 R = 3.0542;\ \psi_3 = \cos 2\theta J_2(\kappa_3 r),\ \psi_5 = \sin 2\theta J_2(\kappa_3 r). \tag{7.39}$$

To simplify writing we have defined $\kappa_1 = \kappa_{11}$, $\kappa_2 = \kappa_{01}$, $\kappa_3 = \kappa_{21}$. The inclusion of both azimuthal eigenfunctions for tangential modes of oscillations allows the possibility of either standing or spinning waves, or a combination of both. Only standing modes will be treated here. The corresponding coefficients F_{nij} and G_{nij}, have non-zero values. Self-coupling terms therefore arise only in the equations for the radial mode, while the nonlinear behavior of the tangential modes is mainly determined by cross-coupling. However, the self-coupling terms in the equation for the radial mode drop out after time-averaging and do not affect the results obtained here.

We will treat standing transverse oscillations; only the mode functions ψ_1, ψ_2 and ψ_3 need to be retained. Moreover, with time-averaging, terms containing oscillations at frequencies greater than half the normal frequencies drop out (see Yang and Culick 1990) and the equations for A_n and B_n become

First Tangential Mode (1T)

$$\begin{aligned}\frac{dA_1}{dt} = &\ \alpha_1 A_1 + \theta_1 B_1 \\ &+ a_1(A_1A_2 + B_1B_2)\cos\Omega_1 t + a_2(A_1A_3 + B_1B_3)\cos\Omega_2 t \\ &+ a_1(A_1B_2 - A_2B_1)\sin\Omega_1 t + a_2(A_1B_3 - A_3B_1)\sin\Omega_2 t,\end{aligned} \tag{7.40}$$

$$\begin{aligned}\frac{dB_1}{dt} = &-\theta_1 A_1 + \alpha_1 B_1 \\ &- a_1(A_1A_2 + B_1B_2)\sin\Omega_1 t - a_2(A_1A_3 + B_1B_3)\sin\Omega_2 t \\ &+ a_1(A_1B_2 - A_2B_1)\cos\Omega_1 t + a_2(A_1B_3 - A_3B_1)\cos\Omega_2 t,\end{aligned} \tag{7.41}$$

First Radial Mode (1R)

$$\frac{dA_2}{dt} = \alpha_2 A_2 + \theta_2 B_2 + b_1(A_1^2 - B_1^2)\cos\Omega_1 t - b_1(2A_1B_1)\sin\Omega_1 t \tag{7.42}$$

$$\frac{dB_2}{dt} = -\theta_2 A_2 + \alpha_2 B_2 + b_1(A_1^2 - B_1^2)\sin\Omega_1 t - b_1(2A_1B_1)\cos\Omega_1 t, \tag{7.43}$$

Second Tangential Mode (2T)

$$\frac{dA_3}{dt} = \alpha_3 A_3 + \theta_3 B_3 + b_2(A_1^2 - B_1^2)\cos\Omega_2 t - b_2(2A_1B_1)\sin\Omega_2 t \tag{7.44}$$

$$\frac{dB_3}{dt} = -\theta_3 A_3 + \alpha_3 B_3 + b_2(A_1^2 - B_1^2)\sin\Omega_2 t - b_2(2A_1B_1)\cos\Omega_2 t, \tag{7.45}$$

where

$$\alpha_n = -\frac{D_{nn}}{2}; \qquad \theta_n = -\frac{E_{nn}}{2\omega_n}, \; n = 1, 2, 3;$$
$$a_1 = -\frac{1}{4\omega_1}(G_{112} + G_{121}) = 0.1570\left(\frac{\bar{a}}{R}\right);$$
$$a_2 = -\frac{1}{4\omega_1}(G_{113} + G_{131}) = -0.0521\left(\frac{\bar{a}}{R}\right);$$
$$b_1 = -\frac{1}{4\omega_2}F_{211} = -0.1054\left(\frac{\bar{a}}{R}\right);$$
$$b_2 = -\frac{1}{4\omega_3}F_{311} = 0.1873\left(\frac{\bar{a}}{R}\right);$$
$$\Omega_1 = 2\omega_1 - \omega_2 = -0.1493\left(\frac{\bar{a}}{R}\right);$$
$$\Omega_2 = 2\omega_1 - \omega_3 = 0.6282\left(\frac{\bar{a}}{R}\right)$$

7.4.1. Periodic Limit Cycles for Transverse Modes.

(a) *First Tangential and First Radial Modes.*

Write $A_n(t)$ and $B_n(t)$ in terms of amplitude and phase, which serve as radial coordinates:

$$A_n(t) = r_n(t)\cos\Phi_n(t) \qquad B_n(t) = r_n(t)\sin\Phi_n(t) \tag{7.46)a,b}$$

Now substitute (7.46)a,b in (7.40)–(7.43), neglect the second tangential mode, and rearrange the results to give

$$\frac{dr_1}{dt} = \alpha_1 r_1 + a_1 r_1 r_2 \cos(2\Phi_1 - \Phi_2 + \Omega_1 t), \tag{7.47}$$
$$\frac{dr_2}{dt} = \alpha_2 r_2 + b_1 r_1^2 \cos(2\Phi_1 - \Phi_2 + \Omega_1 t), \tag{7.48}$$
$$\frac{d\Phi_1}{dt} = -\theta_1 - a_1 r_2 \sin(2\Phi_1 - \Phi_2 + \Omega_1 t), \tag{7.49}$$
$$\frac{d\Phi_2}{dt} = -\theta_2 - b_1 \frac{r_1^2}{r_2} \sin(2\Phi_1 - \Phi_2 + \Omega_1 t). \tag{7.50}$$

All of these equations have a common time-varying term $2\Phi_1 - \Phi_2 + \Omega_1 t$ in the sinusoidal functions. For convenience, we may combine (7.49) and (7.50) to simplify the analysis. Thus (7.47)–(7.50) reduce to

$$\frac{dr_1}{dt} = \alpha_1 r_1 + a_1 r_1 r_2 \cos X, \tag{7.51}$$
$$\frac{dr_2}{dt} = \alpha_2 r_2 + b_1 r_1^2 \cos X, \tag{7.52}$$
$$\frac{dX}{dt} = -2\theta_1 + \theta_2 + \Omega_1 - \left(2a_1 r_2 + b_1 \frac{r_1^2}{r_2}\right)\sin X, \tag{7.53}$$

where

$$X(t) = 2\Phi_1 - \Phi_2 + \Omega_1 t. \tag{7.54}$$

Figure 7.21 shows two results for different initial conditions. The eventual values of the amplitude are the same in the two cases, an example of the (apparently) general result for these equations that the limit cycle (if it exists) is independent of the initial conditions. The property has not been proved; it holds at most if the

only nonlinear process is given by the fluid mechanics, but seems not to be restricted only to second-order acoustics. Yang, Kim and Culick (1990) demonstrated the same result for third-order acoustics.

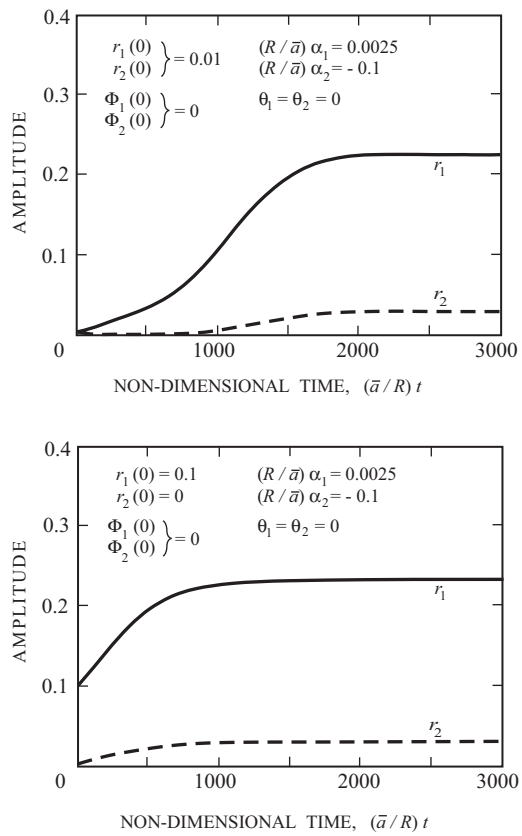

FIGURE 7.21. Amplitudes in two limit cycles involving the first tangential and first radial modes only, based on the time-averaged equations. The two cases are for different initial conditions (Yang and Culick 1990).

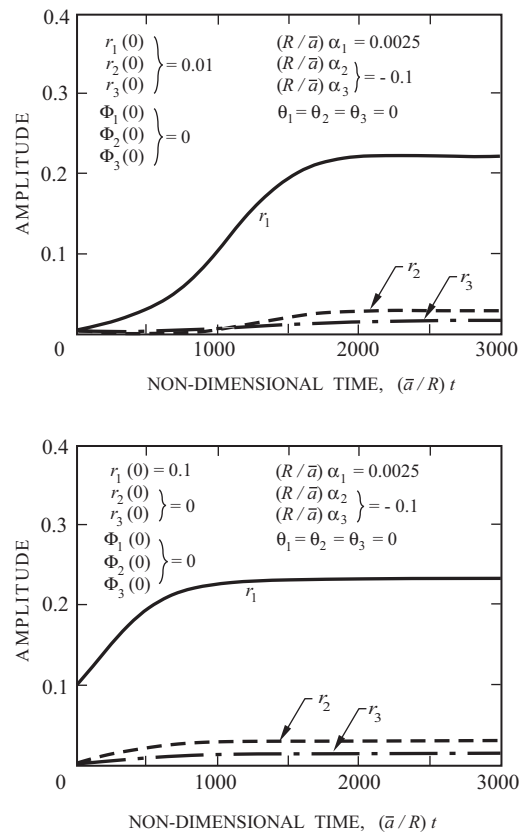

FIGURE 7.22. An example of limit cycles for three normal modes, 1T/1R/2T accounted for; two cases of initial conditions are shown (Yang and Culick 1990).

Although closed form solutions to (7.51)–(7.53) have not been found, a great deal of information can be gained by examining the conditions for periodic limit cycles. The idea is to seek solutions for r_1, r_2, X when they are independent of time, and formulate the conditions that must be satisfied for those solutions to be real. The procedure has been worked out by Yang and Culick (1990) giving $\alpha_1\alpha_2 < 0$, as shown already for two longitudinal modes; the condition must be true according to a physical argument already given. It also follows from the calculations that the amplitudes in the limit cycle are given as

$$\begin{aligned} \eta_{16} &= r_{20}\sin\left[(\omega_1+\nu_1)t+\xi_1\right] \\ \eta_{20} &= r_{20}\sin\left[2(\omega_1+\nu_1)t+\xi_2\right] \end{aligned} \qquad (7.55)\text{a,b}$$

where ν_i and ξ_i are constants. Thus, the amplitude of the second mode oscillates at twice the frequency of the first mode *in the limit cycle.* This must be true for the limit cycle to be periodic. The result was first established by Powell (1970) and reported by Zinn and Powell (1971) for transverse modes.

The conditions for stability of these limit cycles have also been given by Yang and Culick (1990),

$$\begin{aligned} \alpha_1 + \alpha_2 &< 0 \\ 2\alpha_1 + \alpha_2 &< 0 \\ \alpha_1\alpha_2 &< 0 \end{aligned} \qquad (7.56)\text{a,b}$$

These conditions and their derivation are given in the reference.

Because of the difference in frequencies of the first radial and second tangential modes, the 1T/1R and 1T/2T limit cycles have quite different characteristics (quantitatively). The matter is discussed in some detail by Yang and Culick (1990) where the relevant energy equations are also considered. The examples of the 1T/1R and 1T/2T limit cycles form a very useful comparison of limit cycles existing with only two modes.

(b) *Periodic Limit Cycles for Three Modes.*

It came originally as a pleasant surprise that a limit cycle for three modes can be analyzed with the same procedures used for two modes. Much of the detail has been given by Yang and Culick (1990) and will not be repeated here. Only the case 1T/1R/2T has been worked out; it is simply not known *a priori* how cases can be solved in this way. Figure 7.22 shows limit cycles computed for two sets of initial conditions. The amplitudes for long times are evidently independent of initial conditions. In this case the frequencies for $t \to \infty$ are $\omega_1 + \nu_1$, $2(\omega_1 + \nu_1)$, $2(\omega_1 + \nu_1)$ where ν_1 is constant.

7.5. Observations of a Spinning Transverse Mode

Many years ago there were several reports of observational results for travelling waves interpreted as 'spinning' transverse modes. Owing to limitations of the instrumentation, the results depend to some extent on the interpretational powers of the observers. For example, following the early conjecture by Smith and Springer (1953) that the instabilities they had observed appeared to be longitudinal detonation waves, that idea was extended to be the basis for interpreting waves that appeared to rotate about the axis of the chamber (Denisov *et al.* 1962, Krieg 1962, Nicholls and Cullen 1965, Oppenheim and Laderman 1965). The most complete and convincing results were reported by Clayton, Rogero and Sotter (1968) which we summarize here.[9]

Figure 7.23 is a picture of the wave, inferred by Clayton *et al.* from data obtained with pressure transducers installed on the injection face and on the chamber wall. The chamber; one unlike injector element; and the device used for pulsing are shown in Figure 7.24. Fifty-two injection elements were mounted in the injection plane at the head end of motor. The pulsing device is so positioned that it is not surprising that a spinning tangential wave was initiated by the pulsing. Both clockwise and counterclockwise rotations occurred, depending on, among other quantities, the relative circumferential positions of the pulses and the pattern of injection elements. This feature of the experimental situation was only remarked upon in the paper and was not explored further. The authors also noted that in a different but similar engine, the unstable mode appeared without pulsing. No further details were given and the problem seems not to have been treated theoretically (see Footnote 9). In particular, there are presently no results—theoretical or experimental—showing that a spinning mode of the sort reported may be a detonation wave rather than a large amplitude acoustic wave, or shock wave.

[9]Flandro (private communication) renewed the author's interest with his recent 2004 remark that he is engaged in work on this problem.

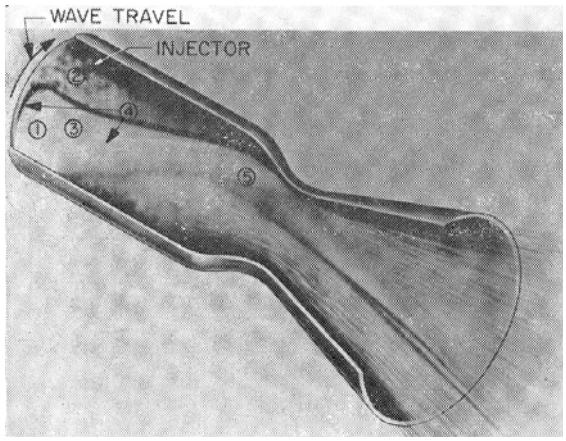

FIGURE 7.23. Sketch of the interpretation as a 'detonation' wavefront. 1 Shock wave rotating within sensitive reaction zone near injector, strong coupling between wave environment, and energy release from reactants. 2 Fresh reactants continuously replenished during wave rotation period. 3 Frontal surface inclined to chamber longitudinal axis and oriented nonradially in planes of chamber cross section. 4 Intersection of wave with chamber boundaries. 5 Possible helical path of burned gas immediately following the wave (Clayton, Rogero and Sotter 1968).

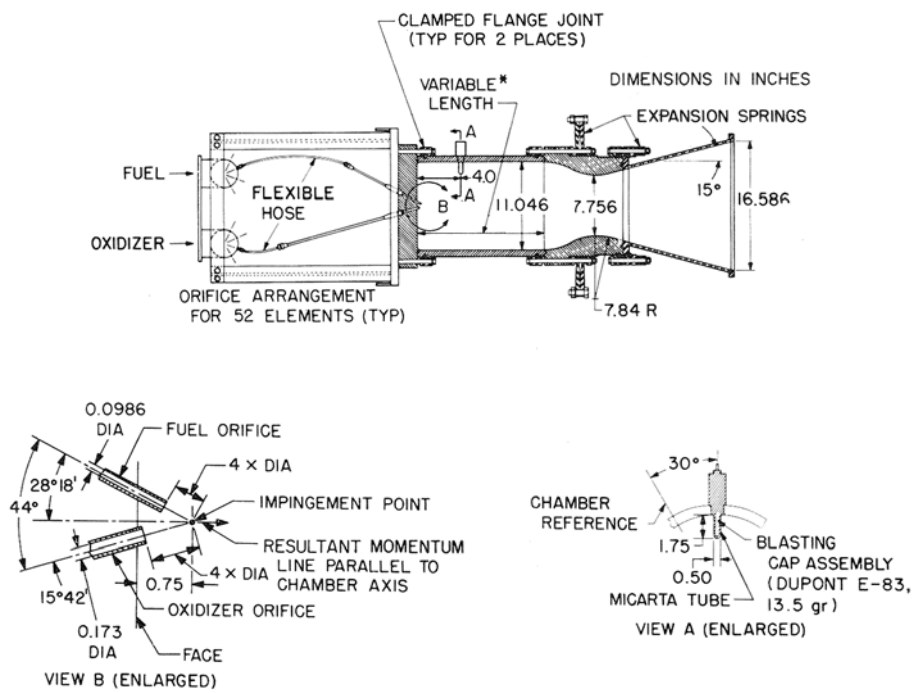

FIGURE 7.24. The test engine, 20,000 lbf-thrust engine and components (Clayton, Rogero and Sotter 1968).

7.6. Remarks on Truncation and Reduced-Order Modeling

As a practical matter, the problem of establishing a reduced-order approximation occupies an extremely important position. In general, the term 'reduced-order' has qualitative implications that the formal description of a physical system is simplified because the governing set of differential equations has a lower order. A

major problem is determining the extent to which the description of the physical system is imperfect: How good is the approximation? In the present context, an (almost) equivalent question is: How many modes must be considered in a given problem to obtain 'good' results? We have already seen simple special cases treated with the method of time-averaging; some results are given, for example, in Figures 7.18 and 7.19. Some results for more difficult problems are given in Section 7.7.

Reduced-order modeling has become an active area of concern during the past few years owing to its immediate applications in problems of active control. We will discuss the subject further in Chapter 9.

7.7. Application of a Continuation Method

Much of the work during the past decade at Caltech on chamber dynamics has been directed to understanding the extent to which nonlinear behavior can be explained on the basis of nonlinear gasdynamics. The reasoning is first that we know the model of gasdynamics—the Navier-Stokes equations for compressible flow—so we can do accurate analysis; and second, those features that cannot be explained must be due to other causes so, by elimination we have some guidelines for what we should seek in other processes. Experience has shown that 'other processes' is this context most probably means combustion.

To carry out this program with numerical simulations—after all, few exact results exist—would be a formidable task because of the number of characteristic parameters. The parameter space comprises those quantities defining the geometry of a chamber and two parameters (α_n, θ_n) characterizing linear behavior of each mode. The effect required to search the parameter space is much reduced by applying a continuation method. The procedure is an efficient systematic means of locating values of parameters for which the dynamical behavior suffers a qualitative change, i.e., bifurcation points. The simplest—almost trivial—example is the Hopf bifurcation point which arises when, for a stable system, one of the values α_n changes from a negative to a positive value; the system becomes linearly unstable and under suitable conditions the motion develops into a stable limit cycle. In fact, linear instability is not always such a simple matter. We have found cases with special sorts of nonlinear processes for which a Hopf bifurcation may occur when the critical value of α_n is non-zero.

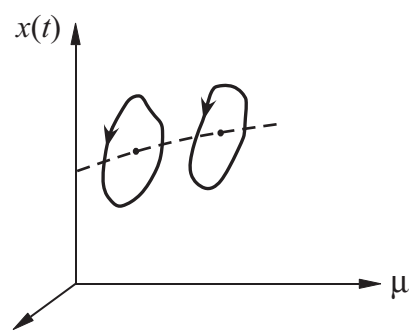

FIGURE 7.25. Schematic illustration of the continuation method applied to limit cycles.

The essential idea of applying a continuation method to limit cycles is illustrated in Figure 7.25 where the variables of the motion are $x(t)$ and μ is the parameter in question, the bifurcation parameter. A continuation method is a computational (numerical) scheme for following, in this case, the changes of a period solution—a limit cycle—as the values of one or more parameters are changed. A picture like Figure 7.25 is impossible to draw for more than three coordinates, so the conventional display of information is a bifurcation diagram in which the amplitude of one variable in the limit cycle is plotted versus the parameters varied as the continuation method is applied. Figure 7.26 shows two examples, a Hopf bifurcation, also called

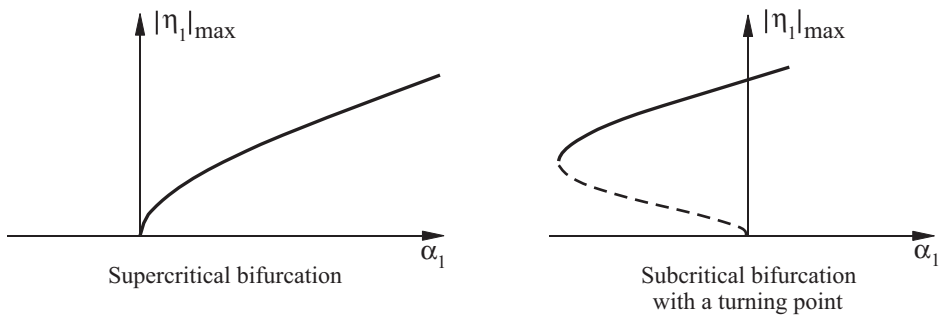

FIGURE 7.26. Two examples of bifurcation.

a *supercritical bifurcation*; and a *subcritical bifurcation* with a turning point. Those are the two types of bifurcation most common in the present context.

A bifurcation diagram is a locus of equilibrium points traced as the bifurcation parameter is changed. As a practical matter, a continuation method is more systematic and cheaper to use than numerical simulations. We have successfully used a continuation method developed by Doedel and colleagues (Doedel *et al.* 1991a,b; Doedel *et al.* 1997) to investigate four classes of problems:

(i) consequences of time-averaging
(ii) consequences of truncating the modal expansion
(iii) influences of the linear parameters (α_n, θ_n) on nonlinear behavior
(iv) pulsed instabilities (triggering): the conditions for existence of stable limit cycles in a linearly stable system.

The problems (i) and (ii) are central to the matter of constructing reduced-order models. Hence it is important to emphasize that in our view, application of the continuation method to investigate the consequences of time-averaging and truncation is part of the procedure for establishing the validity of reduced order models within the framework of analysis based on modal expansion and spatial averaging.

The continuation method is a powerful means for investigating many nonlinear problems in the classes listed above. Commercial software is available for this purpose. For more extensive discussions see Jahnke and Culick (1994); Burnley (1996); Burnley and Culick (1996); and Ananthkrishnan, Deo and Culick (2002). As an illustration we quote here some results for limit cycles in systems of longitudinal modes when only the gasdynamical nonlinearities are accounted for. We are interested in the consequences of truncation with time-averaging.

In Section 7.3 we cited a few results for the limiting case of two modes described by the four equations found with time-averaging. Figure 7.27 shows the special example of the effect of truncating the series expansion for the time-averaged system: Increasing the number of modes apparently widens the region of stability. In fact, use of the continuation method has established the result that the existence of a region of stability for limit cycles with two modes is due to truncation. When the first mode is unstable, stable limit cycles exist for all values of α_1, if more than two modes are taken into account. That is true even if the original oscillator equations are used.

Figure 7.28 shows that if time-averaging is not used, there is a turning point in the bifurcation diagram. Moreover, the boundary of stability persists for the time-averaged equations but moves to larger values of α, as the number of modes is increased. Figure 7.29 is the result for the time-averaged equations and Figure 7.30 shows the case of 4 modes computed for the full oscillator equations.

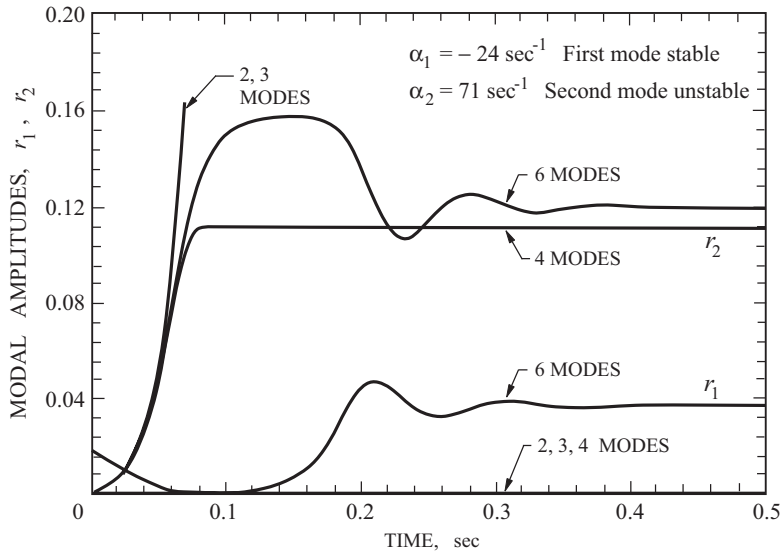

FIGURE 7.27. The effects of truncation for a two-mode system: second mode unstable, all other modes stable (Paparizos and Culick 1989).

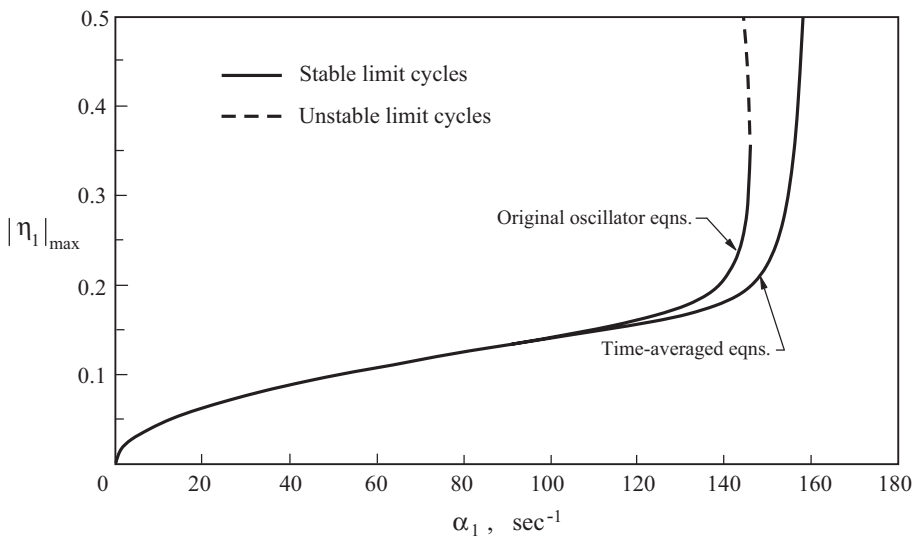

FIGURE 7.28. Effect of time-averaging for two modes (Jahnke and Culick 1994).

It seems true that if the system is only slightly unstable, then the system of time-averaged equations for two-longitudinal modes is a good approximate model for investigating nonlinear behavior. However, if one is generally interested in producing reduced order models, the effects of truncation and time-averaging should be investigated. Applying a continuation method seems to be the best approach for doing so. It is a quick and inexpensive way to learn a great deal about a system.

Ananthkrishnan *et al.* (2005) have given the first analysis addressing the practical question of how many—or perhaps more accurately, how few—modes are required to obtain faithful results. The reasoning is based on properties of the energy transfer between modes, with the full second-order equations used for the formal description of longitudinal modes. Thus, errors accompanying application of time-averaging are absent. The

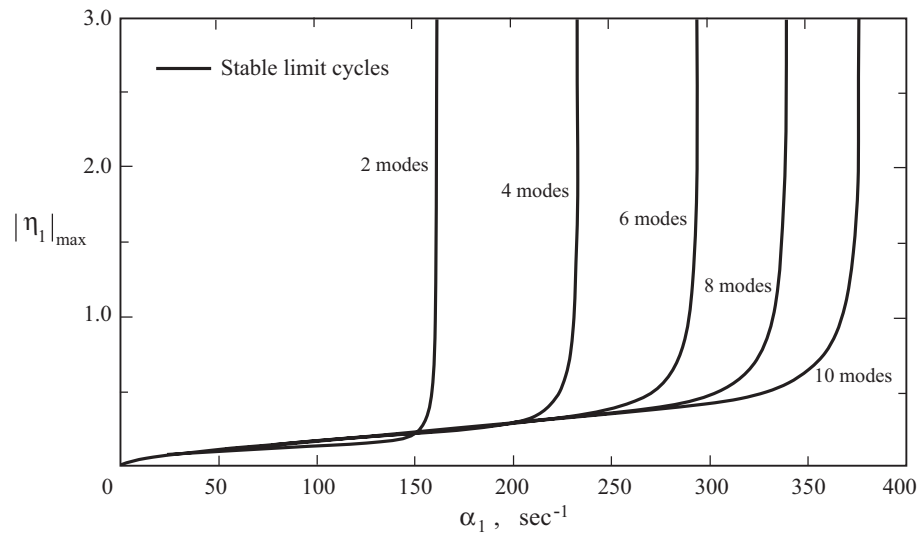

FIGURE 7.29. Solutions with truncation of the time-averaged equations (Jahnke and Culick 1994).

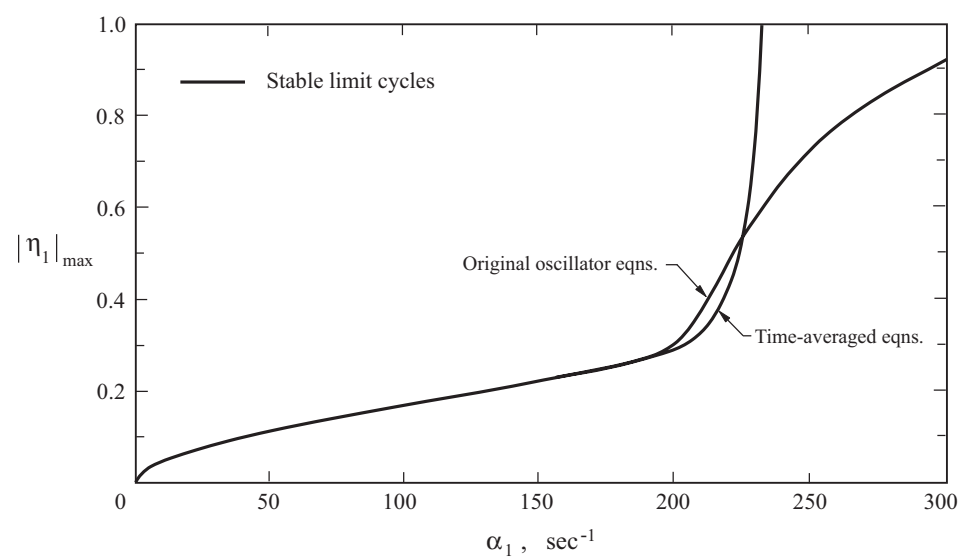

FIGURE 7.30. Maximum amplitude of η_1 in the limit cycle: four modes, comparison of results for the full oscillator and the time-averaged equations (Jahnke and Culick 1994).

view is maintained that the global behavior is dominated by the fluid mechanics represented by the second-order terms in equation (7.27). We emphasize again that the results will be special because the nonlinear terms involve only squares ($\eta_r \eta_s$ and $\dot{\eta}_r \dot{\eta}_s$) and no quadratic terms such as $\eta_r \dot{\eta}_s$. That property alone has much to do with the conclusions reached.

The reasoning is covered thoroughly in the reference and will not be reproduced here. An important conclusion is that for correct qualitative analysis of the motion when the first mode is unstable requires four modes: the unstable mode (mode 1); the coupled mode (mode 2) and energy sinks (modes 3 and 4). If the second mode is linearly unstable, at least the first eight modes must be retained. Reported results by Janke

and Culick (1994), Burnley (1996), and Culick, Burnley and Swenson (1995) support the point. See also the more carefully argued conclusions reached by Ananthkrishnan *et al.* (2005).

A second conclusion of the last work is that theoretical justification can be given to the idea that the second-order gasdynamic nonlinearities alone will not produce subcritical bifurcations, i.e., 'triggered' limit cycles. As we have discussed, various works carried out over roughly two decades suggested this result but no substantial proof had been previously found. The paper also contains further investigation of triggering with second-order gasdynamics and nonlinear velocity coupling.

In a general respect, the work reported by Ananthkrishnan *et al.* shows most clearly the usefulness of a continuation method as a tool for investigating and understanding nonlinear behavior.

7.8. Recirculation Zones, Hysteresis and Control of Combustion Instabilities

The existence of hysteresis in the dynamical behavior of combustions is both an interesting phenomenon to investigation and a characteristic that has potentially important practical consequences. It seems that the first evidence for hysteresis in combustors was found by Russian researchers concerned with instabilities in liquid rockets (Natanzon *et al.* 1978, 1992; Natanzon 1999). In that case, Natanzon and his co-workers proposed bifurcation of *steady states* of combustion, and the associated hysteresis, as a possible explanation for the random occurrences of combustion instabilities. The Russian workers were in a special situation affording them the opportunity to make such observations. The large Russian boosters were designed to use many (as many as thirty-three) liquid rocket engines in a single stage. Hence large numbers of nominally identical engines were manufactured and tested for operational use. Sufficient data were obtained that statistical analysis of the behavior could be carried out. A basis therefore existed for identifying random behavior. More information is available in Natanzon's monograph, including interesting discussions of experimental work. The results are convincing arguments for the basic importance of hysteresis, which may have widespread implications. The idea is the following.

In a liquid rocket many zones of recirculation are created at the injector where jets of liquid fuel and/or oxidizer enter the chamber. As an approximation, one may regard a recirculation zone as a chemical reactor whose behavior is known to be well-characterized by the temperature of the incoming gases entrained from the environment, and the average temperature within the zone. A fairly simple calculation based on consideration of energy and mass flows leads to the results sketched in Figure 7.31. The upper and lower branches of the hysteresis loop represent different branches of stable combustion. Those states have different influences on the state of combustion in the chamber. It was Natanzon's assertion that the state associated with the lower branch in Figure 7.31 (the cold recirculation zone) is more unstable and prone to lead to combustion instabilities. Which branch is reached depends on the history of the engine, starting from ignition or some other sort of abrupt transient. The final state of a recirculation zone depends on random 'accidents' of history. Therefore, random occurrences of combustion instabilities may be observed. Figure 7.32 is a sketch of a possible recirculation zone and adjacent flow of a fuel or oxidizer jet. This model has been used as the basis for numerical calculations supporting Natanzon's proposal (Natanzon 1999).

In the mid-1980s, research with a dump combustor at Caltech revealed the presence of a different kind of hysteresis of dynamical states of combustion (Smith, 1985; Sterling, 1987). The combustor has been described in Chapter 1, Figure 1.17; Figure 7.32 shows the inlet region and the recirculation zone at a dump plane during steady combustion. The combustor showed combustion instabilities in the neighborhood of the stability boundary defined in the plane of flow rate and equivalence ratio, Figure 7.33(a). Figure 7.33(b) shows an idealized hysteresis loop, observed as dependence of the level of pressure oscillation on equivalent ratio with the total flow rate held constant. This sort of behavior has been observed also in other dump

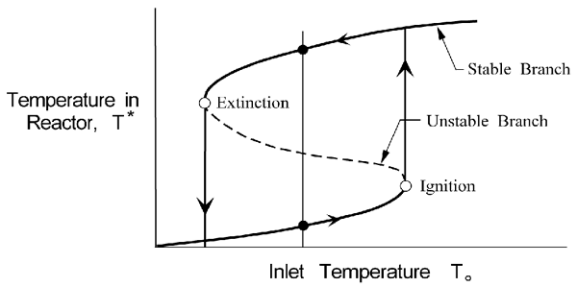

FIGURE 7.31. Hysteresis loop for a recirculated zone idealized as a simple chemical reactor.

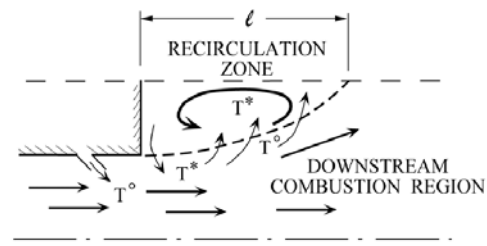

FIGURE 7.32. Sketch of a recirculation zone formed by a jet of fuel or oxidizer (adapted from Natanzon 1999).

combustors as well as in a flame-driven Rijke tube (Seywert, 2001) and in an electrically driven Rijke tube (Matveev, 2002; Matveev and Culick, 2002a,c); see Section 2.7.

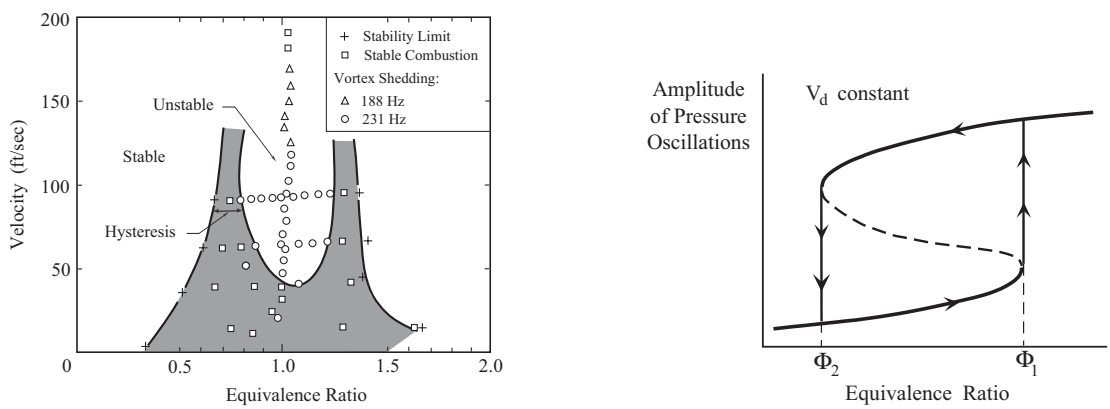

(a) (b)

FIGURE 7.33. (a) Stability boundary (Sterling 1987) and (b) an idealized hysteresis loop suggested by the data shown in (a) for the Caltech dump combustor.

Recent experimental works (Knoop *et al.* 1996; Isella *et al.* 1996) have established the physical nature of the hysteresis in this case and have shown how active control can be used to extend the range of steady operation into the hysteretic region. High speed films have confirmed that the upper branch of the loop is associated with shedding of large vortices which, causing periodic combustion of entrained reactants sustain high amplitude pressure oscillations. The lower branch is associated with relatively quiet combustion in a shear layer shed from the lip at the inlet.

Familiar considerations of dynamical behavior suggest that it should be possible to achieve pulsed transitions between the two branches of stable dynamical states. Those processes were demonstrated by Knoop *et al.* and Isella *et al.* by injecting pulses of fuel at the inlet plane. Single pulses of fuel cause transition from the upper to the lower branch. Thus with suitable sensing and actuation it is possible always to maintain the low level of oscillations (effectively 'noise') within the zone where hysteresis exists.

Figure 7.34(a) shows the modified step allowing injection of pulses; Figure 7.34(b) shows an example of the hysteresis observed. Examples of the unsteady pressure found during stable burning and unstable burning, on the lower and upper branches respectively, of the hysteresis loop are reproduced in Figure 7.34(b).

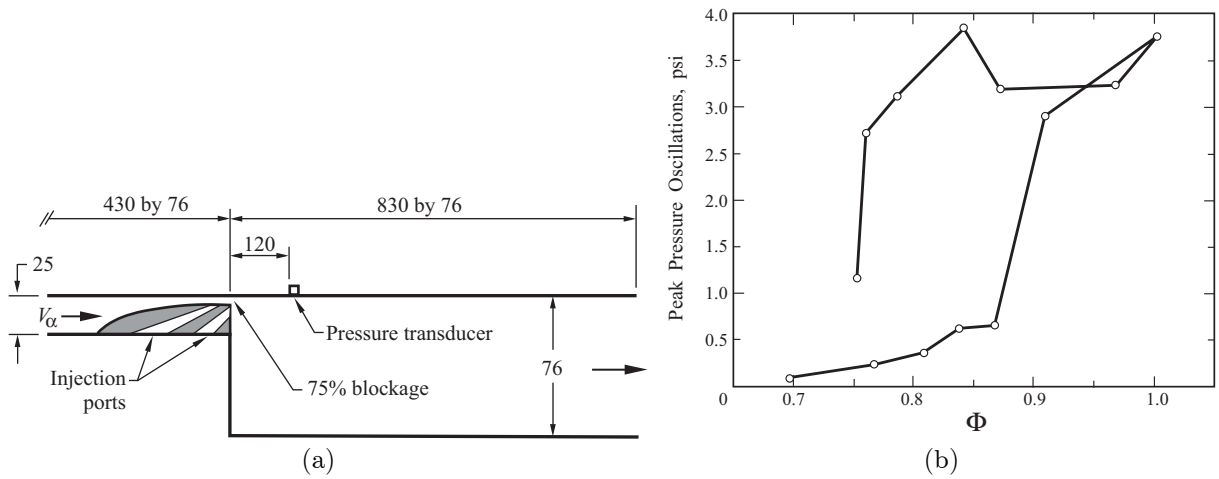

FIGURE 7.34. (a) Sketch of the dump combustor modified to allow injection of pulses; (b) hysteresis observed in the apparatus shown in (a) (Isella, Seywert, Culick and Zukoski 1997).

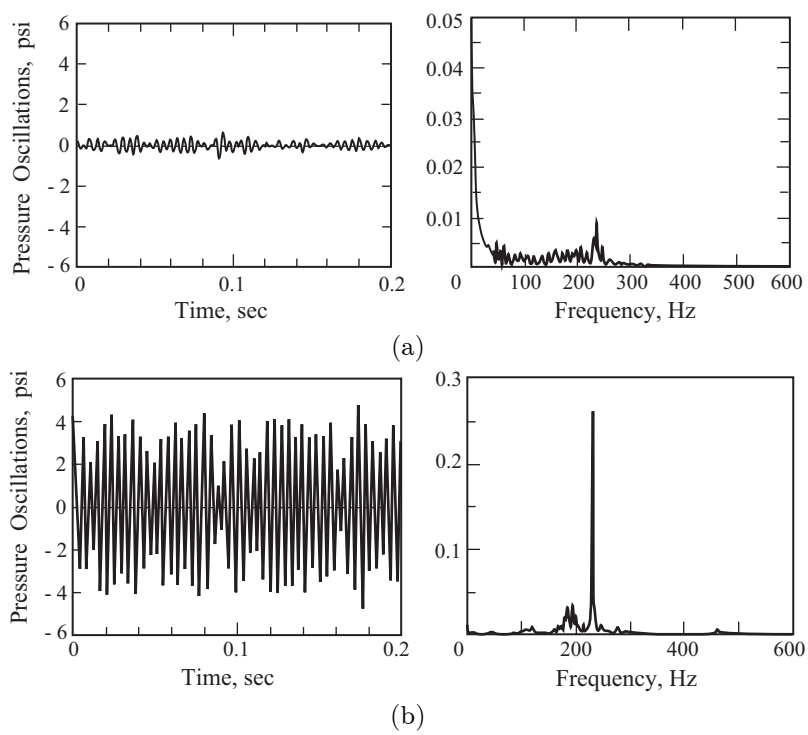

FIGURE 7.35. Pressure traces and spectra for the two branches of the hysteresis loop. (a) stable burning on the lower branch; (b) unstable burning on the upper branch. (Isella, Seywert, Culick, and Zukoski 1999).

The idea motivating the series of tests (carried out as a project in a student laboratory course) was the following theoretical notion. If the combustor were operating in an unsteady state on the upper branch of the hysteresis loop, Figure 7.34(b), then it should be possible, by pulsing, to cause the system to undergo

a transition to the lower branch, hence reducing the amplitude of the oscillations. Originally it seemed necessary that fuel be used, because combustion was assumed to be the origin of the behavior. In the event, it happened that a pulse of nitrogen would also cause a transition, but not always. Thus the behavior, not surprisingly, involves a combination of combustion processes and the fluid mechanics of the separation zone.

Figure 7.36 shows the time history of oscillations in an interval including the introduction of a pulse. The series of circled numbers in part (b) identify times when high speed shadowgraphs were taken of flow immediately downstream of the step. An example of the results is shown in Figure 7.37. The solid lines approximately indicate instantaneous lines of flow. The test results confirmed the authors' guess *a priori* that the origin of the strong oscillations was associated with combustion in a separated region of recirculation at the step. Relatively quiet behavior accompanies combustion in turbulent shear layer.

Further discussion of the effects of pulsing is given in the references, but many details remain unexplained in terms of fundamental causes. For example, the consequences of using a noncombustible injected gas, mentioned above, are similar but not as inevitable as those just described. Interactions of strong acoustic waves, secondary (including pulsed) flows and recirculation zones are likely to be more important to the unsteady behavior of combustors than the present level of understanding may suggest.

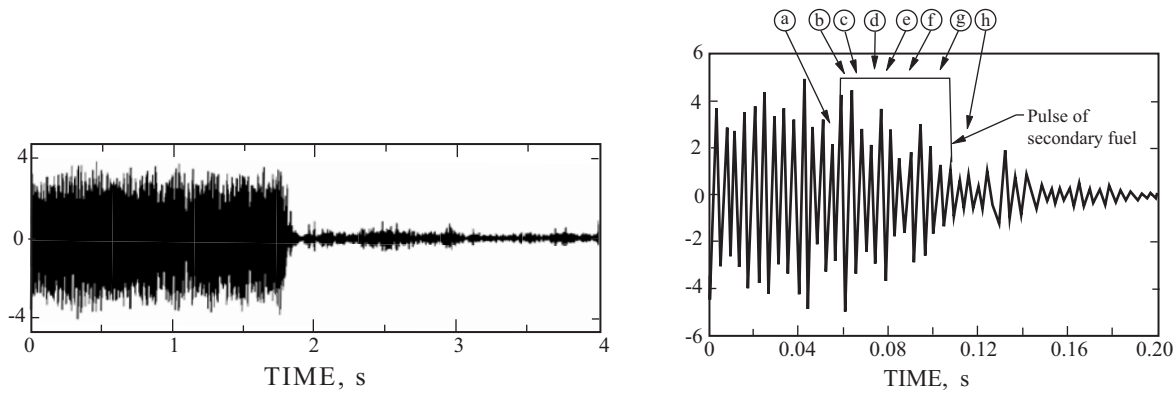

FIGURE 7.36. Time history of a portion of trace. (a) low resolution showing quenching pressure oscillations by a pulse; (b) high resolution showing times of the photographs in Figure 7.37 (Isella, Seywert, Culick and Zukoski 1997).

The behavior shown with a pulsed recirculation zone is a form of nonlinear control. Although it has been demonstrated only for the range of equivalence ratio covering the zone of hysteresis, it is an important demonstration of active control at a frequency far less than the frequency of the oscillations. That is a significant characteristic because if the reduced bandwidth required of the control system, particularly the actuation, is smaller, the demands placed on the equipment are reduced. See Chapter 9 for further comments.

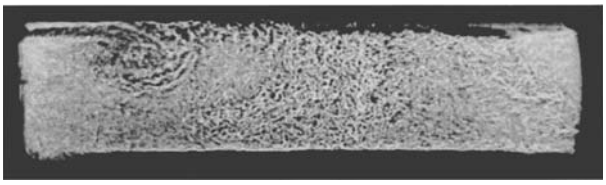

$t = -3$ ms
Large vortex shedding during unstable combustion.
(a)

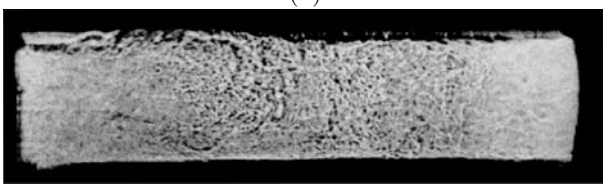

$t = 1.4$ ms
Pulse of secondary fuel inhibits formation of next vortex.
(b)

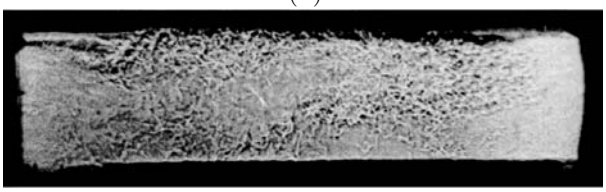

$t = 8$ ms
Recirculation zone forms at dump plane.
(c)

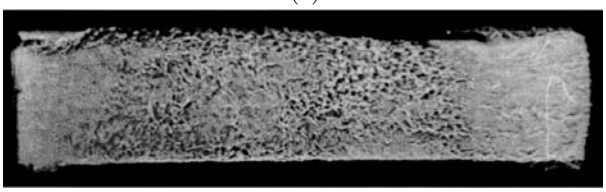

$t = 14$ ms
Recirculation zone spreads downstream.
(d)

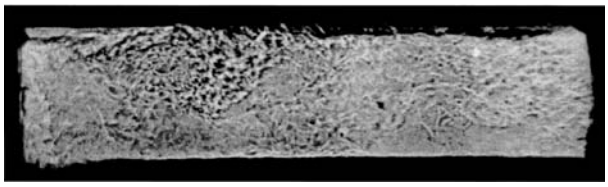

$t = 18$ ms
Recirculation zone shrinks.
(e)

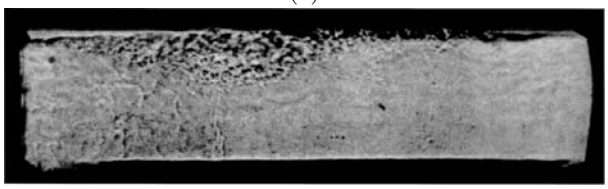

$t = 30$ ms
Stable combustion state beginning to form.
(f)

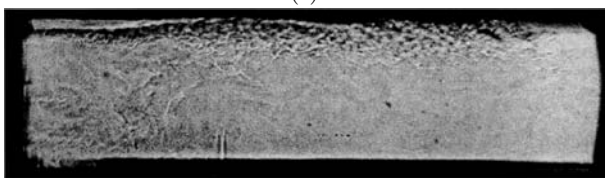

$t = 41$ ms
Disturbances have completely disappeared.
(g)

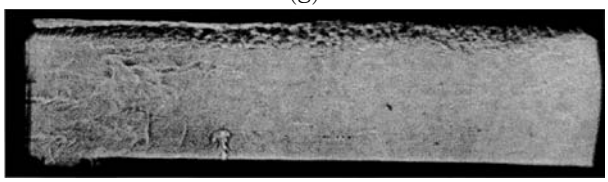

$t = 56$ ms
Turbulent shear layer burning (stable combustion).
(h)

FIGURE 7.37. Shadowgraphs of the transition induced by a single pulse initiated at $t = 0$ (Isella, Seywert, Culick and Zukoski 1997).

7.9. Representing Noise in Analysis of Combustor Dynamics

Generation and emission of noise is a characteristic feature of all combustors. The difference in sound level produced by a burning jet contrasted with an unburning jet, for example, is obvious and convincing evidence of the phenomenon. Combustion noise has long been studied—see, for example, early interest by Lord Rayleigh (1945)—and in the past fifty years, has been through several periods of increased emphasis, followed inevitably by general papers such as those by Strahle (1971, 1978, 1985) convey the vicissitudes of the field. Currently the developments of large numerical simulations (e.g. LES) hold promise for increased understanding. It appears that good experimental results may be more difficult to acquire.

Considerable experience during the past five decades has established the result that combustion noise is a minor part of the noise produced by a gas turbine; see, for example, Cumpsty (1979) and Cumpsty and Marble (1977). Hence, interest in the subject has not been motivated and sustained by practical considerations of noise pollution of the environment. The energy contained in the noise field of a combustor, and the power radiated, do not have serious environmental consequences in the same sense as, for example, jet noise does. Our concern here is relatively narrow, related to possible causes or effects of combustion instabilities, and especially how noise may be included in the framework we have been discussing.

Even a small laboratory combustor radiates considerable noise, generated by turbulent motions (often called 'combustion noise') within the chamber. See, for example, the spectrum reproduced earlier as Figure 1.18. The scaling laws are not known, but it is obvious to any bystander that a full-scale combustor of any sort is noisy indeed. Presently it is not well understood how important noise is to the behavior of combustion instabilities or to the application of feedback control. The purpose of this section is to introduce a means for investigating those matters within the framework developed in Chapters 3 and 4.

There are three sorts of problems that will arise:

(i) formal incorporation of noise (stochastic) sources in the framework of spatially averaged equations for unsteady motions in a combustor;
(ii) modeling the noise sources;
(iii) solving the stochastic differential equations.

The first step, as explained in Section 3.1, is to apply the principle of splitting small disturbances into the three basic modes of propagation: acoustic waves, vorticity waves, and entropy waves. All of the discussion so far in this book has been devoted to the acoustic field. Noise is associated with the random motions comprising mainly vorticity but also entropy (or temperature) waves in a combustion chamber. Our concern in the present context is directed chiefly to interactions of those motions with the acoustic field. The formal representation will be relatively simple and intuitively persuasive, but modeling the details remains to be accomplished. Numerical results require assumptions that cannot be justified *a priori.*

Following the principle of splitting, we write the flow variables as sums of the three contributions, one each corresponding to the three modes of motion:

$$\begin{aligned} p' &= p'_a + p'_\Omega + p'_s \\ \mathbf{\Omega}' &= \mathbf{\Omega}'_a + \mathbf{\Omega}'_\Omega + \mathbf{\Omega}'_s \\ s' &= s'_a + s'_\Omega + s'_s \\ \mathbf{u}' &= \mathbf{u}'_a + \mathbf{u}'_\Omega + \mathbf{u}'_s \end{aligned} \qquad (7.57)\text{a,b,c,d}$$

Subscripts $(\quad)_a$, $(\quad)_\Omega$, $(\quad)_s$ denote acoustic, vortical and entropic contributions. Once again, the ordering procedure explained in Chapters 3 and 4 allows us to derive meaningful results by considering only the first order components. Hence we assume that only the acoustic waves contain pressure fluctuation; in this linear limit, only the waves of vorticity contain vorticity fluctuations; and only the entropy waves have fluctuations of entropy. The velocity field possesses contributions from all three modes.

The idea then is to substitute the assumed general forms of the variables in the primitive equations of motion expanded to third order in the fluctuations. Then form the nonlinear equation for the pressure and apply spatial averaging. This procedure was first reported by Culick *et al.* (1992) but in revised and corrected form by Burnley (1996) and Burnley and Culick (1999). Eventually one finds the oscillator equations,

$$\ddot{\eta}_n + \omega_n^2 \eta_n = F_n$$

but now F_n contains stochastic sources. The 'general' form of F_n is

$$-\frac{\bar{p}E_n^2}{\bar{a}^2}F_n = \bar{\rho}I_1 + \frac{1}{\bar{a}^2}I_2 + \bar{\rho}I_3 + \frac{1}{\bar{a}^2}I_4 + \bar{\rho}I_5 + \oint\!\!\oint \left[\rho\frac{\partial \mathbf{u}'}{\partial t}\cdot\hat{u} + \bar{\rho}\frac{\partial \mathbf{u}'}{\partial t}\right]\cdot\hat{\mathbf{n}}\psi_n dS - \int \boldsymbol{\mathfrak{F}}'\cdot\nabla\psi_n dV + \frac{1}{\bar{a}^2}\int\frac{\partial \mathcal{P}'}{\partial t}\psi_n dV$$

where

$$I_1 = \int [\bar{\mathbf{u}}\cdot\nabla\mathbf{u}' + \mathbf{u}'\cdot\nabla\bar{\mathbf{u}}]\cdot\nabla\psi_n dV$$

and similar definitions for the remaining integrals I_1. See Annex D and the references for details.

Then the unsteady velocity field is split according to (7.57)a,b,c,d. Eventually, re-arrangement and application of the assumptions discussed above leads to the result

$$\begin{aligned}\ddot{\eta}_n + \omega_n^2\eta_n = 2\alpha_n\dot{\eta}_n + 2\omega_n\theta_n\eta_n - \sum_{i=1}^{\infty}\sum_{i=1}^{\infty}[A_{nij}\dot{\eta}_i\dot{\eta}_j + B_{nij}\eta_i\eta_j] \\ + \sum[\xi_{ni}^v\dot{\eta}_i + \xi_{ni}\eta_i] + \Xi_n + \left(F_n^{NL}\right)_{other}\end{aligned} \tag{7.58}$$

where the ξ_{ni}^v, ξ_{ni} and Ξ_n are stochastic sources defined as integrals over the vortical and entropic fluctuations of the velocity. See the references cited above for details.

No intensive modeling based on experimental, theoretical or phenomenological grounds has been accomplished. Explicit results have been obtained by approximating the stochastic sources as white noise processes having properties chosen to be realistic, i.e., the results seem to be reasonably consistent with available measurements of actual behavior.

Two types of stochastic influences arise in (7.58):

(i) ξ_{ni}, ξ_{ni}^v represent stochastic influences on the 'spring' or natural frequency of the nth mode and on the damping or growth rate. These are formally referred to as 'multiplicative noise sources' because they appear as factors multiplying the dependent variables, the displacement and velocity of the nth oscillator. (Stratonovich 1963)

(ii) ξ_n represents a stochastic driving source causing excitation of the nth oscillator even in the absence of driving by combustion processes; the Ξ_n are formally called 'additive noise sources'.

It is evident from the form of (7.58) that the random character of the stochastic sources will appear as random fluctuations imposed on the amplitudes $\eta_n(t)$ of the acoustic modes, exactly the sort of behavior found experimentally. Thus, Fourier synthesis of the pressure field, the modal expansion, continues to serve as a good approximate representation of the deterministic results can be obtained by retaining only a small number of terms.

Results were obtained first for the simplest case of two modes, with noise sources only in the fundamental mode. Nonlinear gasdynamic coupling transfer stochastic behavior to the second mode. Computations have been carried out using a Monte-Carlo method to give probability density functions, with the equations written in the Stratonovich form of stochastic differential equations (Burnley, 1996). Figure 7.38 shows the pressure trace and spectrum for a simulation in which the first mode is unstable.

This method of accounting for noise in a combustor seems to be very promising. However, modeling the noise sources is in a primitive state, and comparisons of results with experimental observations can only be done qualitatively.

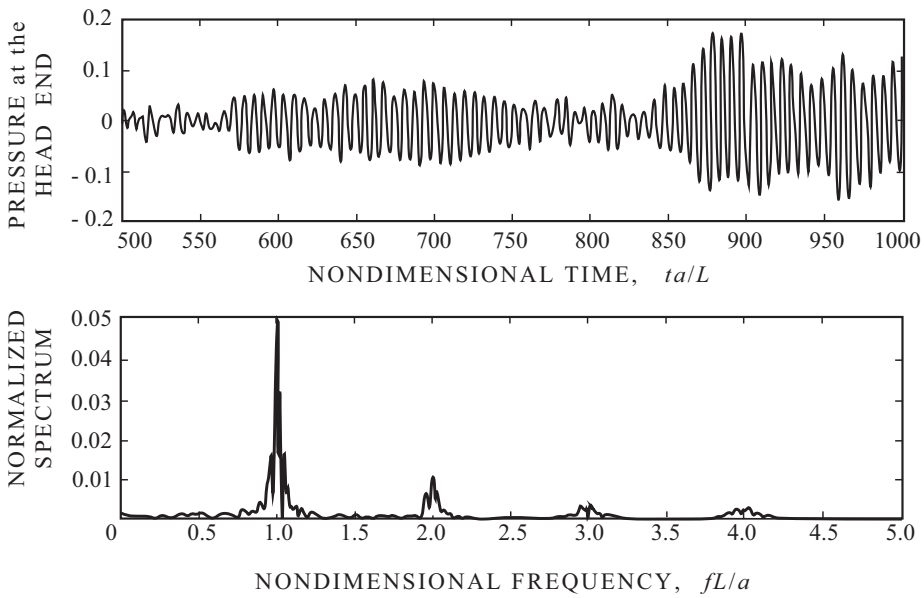

FIGURE 7.38. Pressure trace and spectrum for a simulation with noise; four modes included, first mode unstable (Burnley and Culick 1996).

7.10. System Identification for Combustor Dynamics with Noise

Use of system identification in the field of combustor dynamics seems to have been developed first by Russian groups as part of their development of liquid rocket engines, beginning perhaps as early as the 1950s but certainly in the 1960s (Agarkov *et al.* 1993).

In several papers during the 1980s, Hessler (1979, 1980, 1982); and Duer and Hessler (1984); and more recently Hessler and Glick (1998), have asserted that the oscillations observed as combustion instabilities in solid rocket motors are *driven* rather than *self-excited.* The sources of the driving—i.e., the 'mechanisms'—are supposed to be either vortex shedding or noise. Hessler and co-workers conclude that the properties of the noise measured in a stable chamber can be used as the basis for infusing properties of the primary mechanism causing instabilities when they arise or more correctly, such data will provide quantitative information about the static stability margins—how close the dominant acoustic modes are to becoming unstable.

The basic idea is sound. When the mechanisms are interpreted as driving forces independent of the acoustic field, and they are assumed to be broad-band, then the acoustic modes are excited to amplitudes related directly to the amount of damping (α_n). Hence the idea is to process noisy records in such a fashion as to extract the values of the linear parameters (α_n, θ_n). The proposed method can be tested using the oscillator equations with some sources derived in the preceding chapter.

Seywert (2001) and Seywert and Culick (1999) have reported results of some numerical simulations carried out to check the idea just described. In particular, the main purpose was to determine the accuracy with which the experimental method would give the linear parameters. The procedure is straightforward. To be definite and to keep the computations within practical bounds, we consider a system of four modes, each containing noise sources which, as explained in Section 7.9, are assumed to be white noise. The amplitudes of the noise (rms values) are selected so that random amplitude fluctuations in the pressure spectrum have values in the ranges experimentally observed (Seywert and Culick).

Three types of problems arise, associated with the three types of noise sources: additive noise, Ξ_n; and two kinds of multiplicative noise, ξ_n^v which affects mainly the growth and decay rates, and ξ_n which causes random variations of the frequency. In all cases we are concerned here with discovering the ways in which noise affects the result of system identification. The idea is to select values of the α_n, θ_n and carry out numerical simulations. Then the data are processed to give values of the α_n, θ_n which now have mean values and some uncertainties due to the presence of the noise. The questions to be answered are: How close are the mean values to the time values used as inputs? and How large are the uncertainties? These are important practical matters. If the method is effective, then data from hot firings of full-scale combustors could be used to infer the linear parameters characterizing the dynamics represented by several modes. Those parameters identify the poles of the response function of the chamber. Hence a relatively straightforward process would give the information required to proceed with designing a linear control system.

Actually there are two ways to get the information: process pressure records naturally occurring; or process the pressure record following a pulse. The method of pulsing has long been used as means of assessing the stability margin of liquid rockets (Harrje and Reardon, 1972). Both methods have been used for a stable system of four longitudinal modes having the parameters given in Table 7.2; the fundamental frequency is 900 s^{-1}. Figure 7.39 shows a simulated pressure trace and Figure 7.40 shows its power spectrum and construction using Berg's method.[10]

TABLE 7.2. Values of the Linear Parameters.

mode	1	2	3	4
$\alpha_n(s^{-1})$	-50	-375	-584	-889
$\theta_n(s^{-1})$	12.9	46.8	-29	-131

Without good data for the noise in an actual combustor and no model, we assume white noise sources. Their amplitudes are chosen so that the average (rms) values of the simulated pressure records are reasonable Table 7.3 shows the relation between the rms value of the system response ($p'/\bar{p}$) and the noise power of Ξ. The 'noise power' cannot be measured, being the height of the power spectral density of the noise. Figure 7.41 gives a more detailed picture, showing how the amplitudes of the spectra of the four modes increase with noise power.

TABLE 7.3. Relation Between the Noise Power of Ξ_n and the rms Value of the Simulated Pressure Fluctuation.

Noise Power of Ξ_n	rms Values of $p'/\bar{p}$
10^1	.005%
10^3	.05%
10^5	.5%

[10]Berg's method is a standard method of signal processing, widely available. We have used the software included in the Signal Processing Toolbox, an extension of MATLAB.

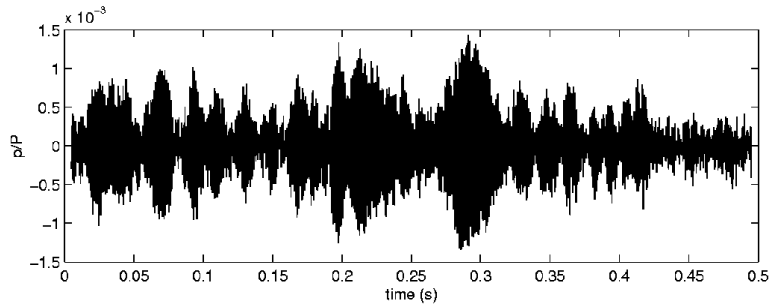

FIGURE 7.39. Simulated pressure trace with noise; all modes stable.

In Figure 7.42, a simulated response to a pulse is fitted by the superposition of four modes:

$$\frac{p'}{\bar{p}} = \sum_{i=1}^{4} A_i e^{\alpha_i t} \cos(\omega_i t + \phi_i)$$

The parameters A_i, α_i, ω_i, ϕ_i are fitted using a least squares method.

We use the noise power as a parameter. Figure 7.43 shows an example of the sort of results one finds for multiplicative noise in the modal damping ($\xi_n^v \neq 0$; $\xi_n = 0$; $\Xi_n = 0$). The corresponding results of using the pulse method are given in Figure 7.44.

We conclude from these results that substantial errors may accompany system identification in the presence of realistic (we believe) noise. How significant the errors are depends on the particular application at hand and on how small the stability margins are. For a weakly stable system, values of the margins

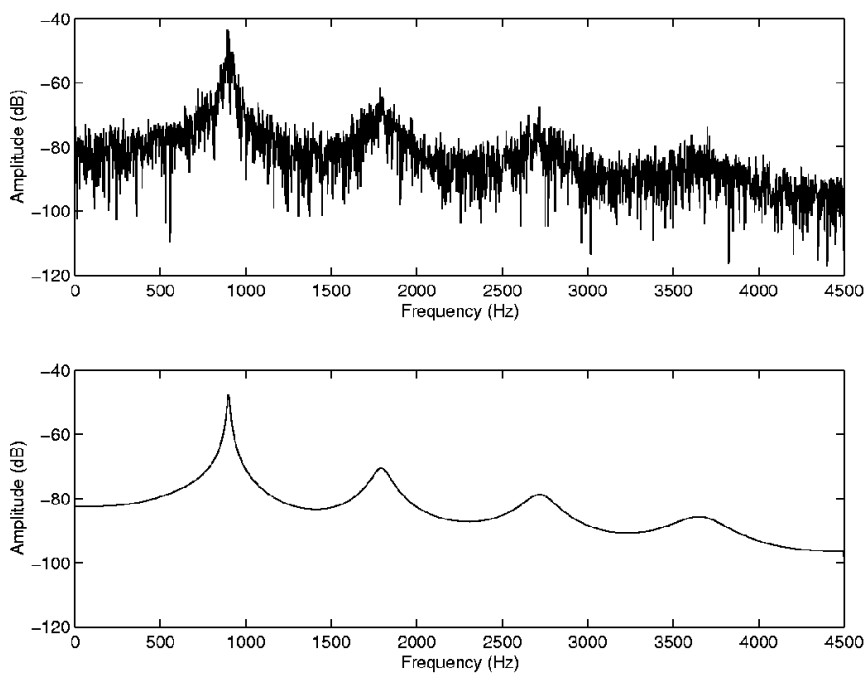

FIGURE 7.40. Application of Berg's method: power spectrum of the pressure trace in Figure 7.39 and its reconstruction.

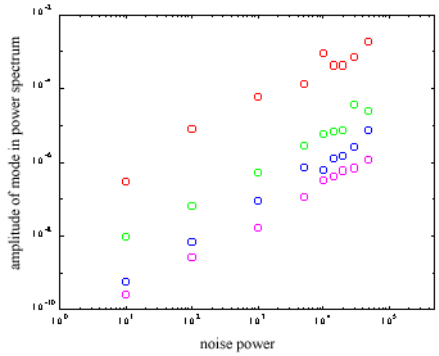

FIGURE 7.41. Dependence of the peak amplitudes of the power spectra for four modes, on noise power.

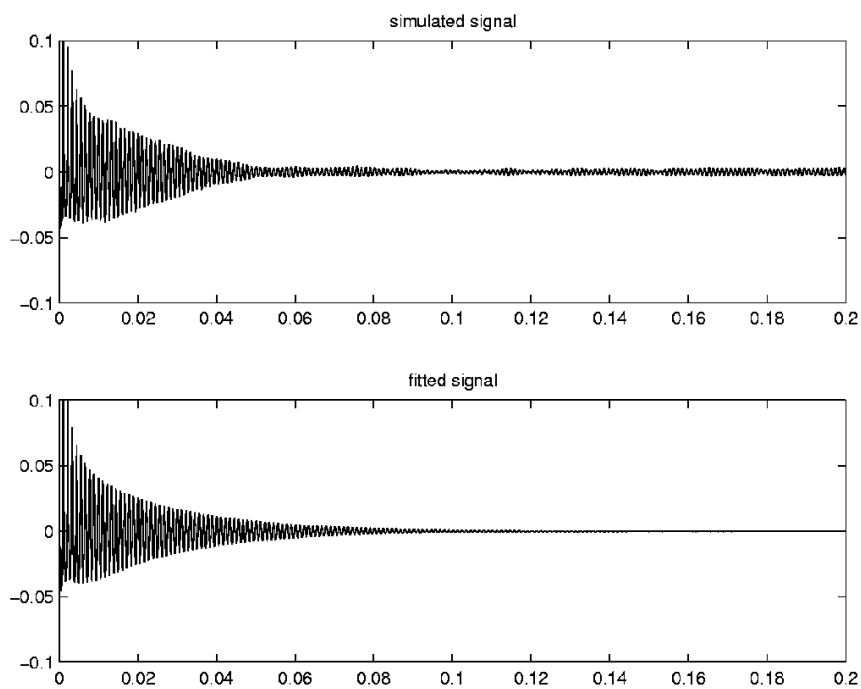

FIGURE 7.42. Reconstructed pressure trace for the transient response excited by a 10% pulse.

determined in this way are suspect because of the finite uncertainties. The results would therefore not be useful as a basis for representing the combustor's response function.

It should be clear from the nature of the methods described here that the system must be stable (i.e., all modes must be stable) for this application. For example, if data (simulated) for a limit cycle are processed in this fashion, the inferred values of α_n, θ_n have no apparent connection with the correct values.

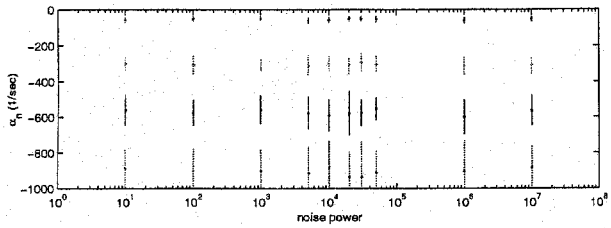

Noise	α_1	α_2	α_3	α_4
10^1	-57±14	-301±31	-560±84	-886±98
10^2	-51±13	-307±52	-576±75	-903±126
10^3	-47±11	-307±38	-558±78	-901±117
10^4	-56±16	-300±51	-591±88	-883±150
10^5	-59±18	-310±53	-598±95	-914±128
10^6	-53±15	-310±46	-564±84	-905±172
10^7	-59±19	-313±44	-591±83	-887±124
correct	-50	-325	-584	-889

FIGURE 7.43. Values of decay rates (modal attenuation) found with Berg's method with multiplicative (ξ_n) noise.

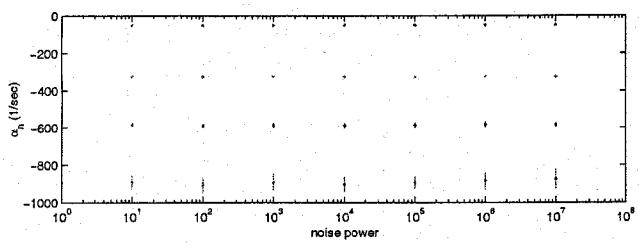

Noise	α_1	α_2	α_3	α_4
10^1	-50±2	-323±6	-584±9	-889±35
10^2	-50±2	-325±5	-589±8	-908±36
10^3	-50±2	-322±4	-587±10	-891±44
10^4	-50±3	-326±5	-589±8	-902±37
10^5	-49±3	-326±4	-586±12	-895±35
10^6	-50±2	-324±4	-582±15	-886±43
10^7	-49±3	-327±4	-583±11	-877±51
correct	-50	-325	-584	-889

FIGURE 7.44. Values of decay rates (modal attenuation) found with the method of pulsing.

7.11. Pulsed Instabilities; Subcritical Bifurcations

Pulsed instabilities are produced by a process sometimes called 'triggering.' We suppose that the dynamical system, here a combustor, is stable; that is, small disturbances decay to vanishingly small amplitude. It often happens that a real system behaves differently if it is exposed to a finite disturbance. There are three possibilities: the subsequent motion decays; the induced motion grows without limit; or the motion settles into some form having finite maximum size which, if periodic, is called a limit cycle. It is the last case that concerns us in this section. We explicitly exclude from our considerations the possibility that the system may enter an uncontrolled motion. (See Table 7.1 for contrary cases.) Whatever may be the form—i.e., the shape in time—of the initial disturbance, the overall process is generally called 'pulsing.'

Unfortunately, at the time of writing we do not have information about the history or current practice of pulsing in Russia. It has been and still is an important part of the development of Russian rockets. The subject is covered in the monograph by Dranovsky (2006), including results obtained in the early 1990s.

As we have already explained, pulsed instabilities include several practical problems involving the initiation of oscillations. It often happens that an instability is born during or soon after ignition of the device. A rocket, liquid or solid, may suffer a rapid rise of pressure followed by an overshoot of pressure. Oscillations may be a result, the Russian RD-0110 being just one example; see Chapter 1, and the remarks accompanying Figures 1.13–1.15. Sufficiently large pulses to excite instabilities may also be produced by material passing through the nozzle. For example, in large solid rockets, liquid Al_2O_3 exhausted as streamers, originating from the cavity surrounding the inlet to the nozzle, has been observed to produce small disturbances of chamber pressure, a consequence of a temporary reduction of throat area. Inadvertent and undesirable reductions of throat area are always possible. For these reasons, understanding the causes and consequences of finite pulses is an important theoretical and practical matter.

Pulsing without intent to cause instabilities has become a standard means of ranking or rating liquid rocket motors especially. The method has been used less widely for solid rockets. For both solid and liquid

rockets, repeated pulsing with different size pulses forms the basis for assessing the relative stability of a motor. For solid rockets, the time of pulsing during a firing is a second, but not necessarily secondary, variable. The procedure may also be used, for example, to assess the effect of modifications of the design on stability. Presently the status of calculating the unsteady flow is such that it is not possible to predict meaningful results.

In this section we are concerned mainly with the development of waves in a chamber following a pulse. It is not yet possible to predict completely the conditions under which an instability may develop. As an aid to interpreting the behavior, we will use results we have developed in Chapters 3 and 4. However, the available conclusions for the behavior and properties of pulses in a combustion chamber are few and quite limited; much remains to be done before the subject may be considered understood.

7.11.1. Pulsing Solid Propellant Rockets. Dickinsen (1962)[11] first reported pulsed instabilities, in a simple solid propellant rocket, a circular cylinder having diameter eight inches and initial port four inches in diameter.[12] Reports of the work in detail were given by Brownlee (1963) and Brownlee and Roberts (1963). Figure 7.45 shows a typical pressure record; see also Figure 1.42. Later, in similar tests, Brownlee and Kimball (1966) were able to use schlieren apparatus to show directly the discrete nature of the waves. An example is reproduced in Figure 7.46. The presence of the longitudinal wave train caused a continual rise of chamber pressure until a safety diaphragm failed. Note that the amplitude of the travelling waves became as large as (approximately) 30% of the mean pressure. Several characteristics distinguished this instability from previous works, such as those at NOTS, China Lake, which were concerned with spontaneous instabilities:

(i) All of the propellants tested, even with nineteen percent aluminum, would, under appropriate conditions, support pulsed instabilities;
(ii) The instabilities always involved longitudinal (axial) waves, as shown in Figure 7.47;
(iii) The instability always produced increases in the mean pressure, the average burning rate, and the thrust, compared with their values in the absence of an instability;
(iv) At sufficiently high chamber pressure, all the propellants tested would support pulsed instabilities;
(v) Propellants having higher burn rates at a given pressure could be operated at higher chamber pressures before pulsed instabilities could be produced;
(vi) Propellants more susceptible to erosive burning also exhibited more severe instabilities in the axial mode.

In a paper covering solid rockets more broadly, Dickinson and Jackson (1963) included Figure 7.47(a), a useful presentation of the stability boundaries for three propellants whose properties were not disclosed. Examples of the sort of data obtained in those tests are reproduced in Figure 7.47(b) showing the shift of the stability boundary with chamber pressure (throat diameter). Like many details of stability behavior, the result shown is likely to be in fact dependent on the propellant used. Thus, generalizing on the basis of results for one propellant should not be done. In a subsequent paper, Roberts and Brownlee (1971) clearly made the point by testing 54 propellants (polybutadiene and polyurethane binders) to show that a stability criterion proposed by Capener, Dickinson and Kier (1967) did not hold generally.

The tests analyzed by Brownlee *et al.* served to clarify one type of instability and established stability boundaries for the propellants tested. Unfortunately, the results contain almost no information in respect to the influence of particular propellant properties. It was also not an intent of the work to investigate the properties of the wave motions or the dependence of the instabilities on the geometry of the combustor.

[11] The method of pulsing had apparently been in use for two years or so before this first report was made.

[12] The Canadian work described in this section was carried out to support development of the Black Brant sounding rocket. Hence the test conditions don't span the ranges one might prefer, to define the problem completely.

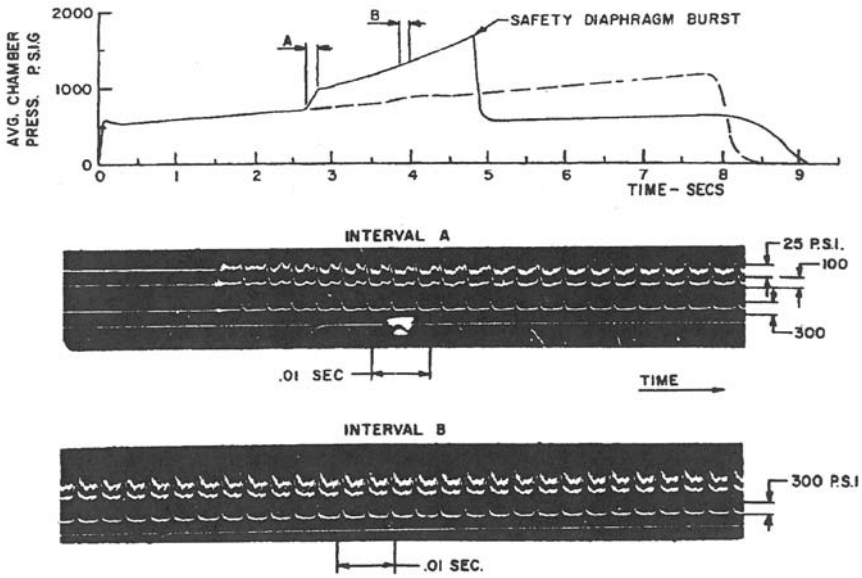

FIGURE 7.45. A pulsed instability initiated in an 80 inch long motor by a small explosive charge (Dickinson 1963; Brownlee and Roberts 1963).

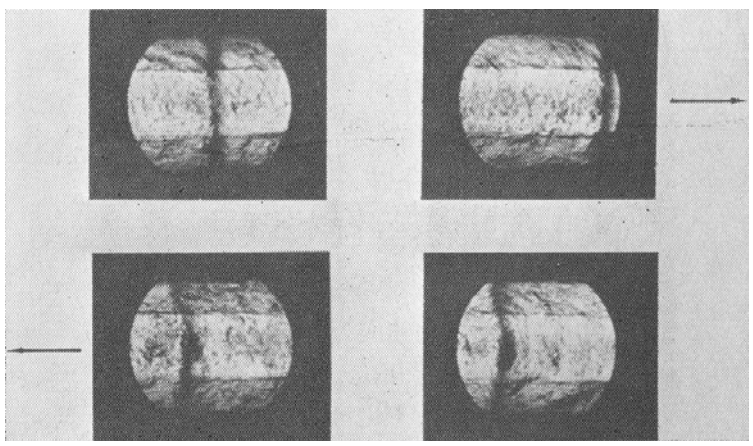

FIGURE 7.46. Picture taken with schlieren apparatus midway between the head-end and the nozzle (Brownlee and Kimbell 1966).

A program carried out at the Stanford Research Institute in the mid and late 1960s was not connected to a development effort and was therefore free to explore more basic questions. The main accomplishments were reported by Capener, Dickinson and Kier (1967); and Marxman and Wooldridge (1968, 1969). Unlike the works described above, these investigations placed considerable emphasis on the influence of propellant composition on the combustion instability leading to large-amplitude axial waves. As in the studies by Brownlee and his colleagues, the instability is 'subcritical' in the sense defined in Figure 7.26; to be initiated, a finite disturbance or pulse is required. Thus the motors, for the propellants used, were intrinsically stable for the range of conditions tested.

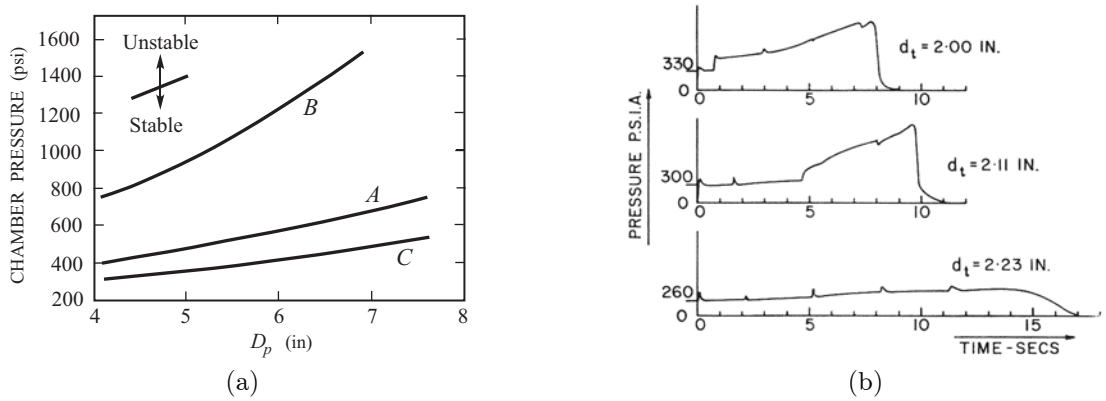

FIGURE 7.47. (a) Stability boundaries for three propellants tested in 80 inch motors and (b) influence of mean pressure (throat diameter) on stability (Dickinson and Jackson 1963).

Although some firings were made with potassium perchlorate, by far most propellants used ammonium perchlorate, the oxidizer used in practice.[13] The binder was PBAN (polybutadiene, acrylic acid, acrilonitrile) which is no longer favored since higher-energy materials are available. Consequently, as often the case with older propellants, the results may be qualitatively suggestive but certainly not valid quantitatively for modern propellants. Figure 7.48 is a compilation of data for a 40 inch series of tests, practically all using AP/PBAN propellants. The similarity with the results obtained by Brownlee, Roberts *et al.* is clear. As in the earlier work, the pressure/burn rate relation was varied by changing the oxidizer particle size, a particularly attractive feature of ammonium perchlorate. The main purpose of the experiments discussed by Capener *et al.* was to obtain results like those shown in Figure 7.48 for a broad range of practical propellant compositions.

Marxman and Wooldridge (1968) apparently were first to attempt to relate the excitation of the finite-amplitude instability to the dynamical properties of the propellant. At that time the subject of the dynamics of propellant burning was a subject of active research; see Section 2.1 and, for example, the extended review by Culick (1968). In particular, Marxman and Wooldridge (1968) had paid special attention to the influence of surface reactions on the response of a burning surface propellant. Using a linearized representation of the propellant response (see Section 2.1) they found that surface reactions can have substantial effect on the amplitude of the propellant response.[14] So far as the present context is concerned, the importance of this work is the use Marxman and Wooldridge made of it in their interpretation of travelling waves in a solid propellant rocket, the axial-mode instability.

The main idea is that the oscillating wave in the chamber is a weak shock wave presenting to the surface an oscillating pressure. That oscillation of pressure causes the burning rate to oscillate. It is the oscillation of burning rate that sustains the shock in the presence of losses, notably attenuation accompanying partial reflection by the exhaust nozzle. Thus the dynamical burning process, travelling with the shock wave, "acts essentially as an annular piston behind the shock wave, ... similar to the role of exothermic chemical reactions in supporting a detonation wave." This idea was developed by requiring that the frequency of the wave should be close to the value at which the propellant response is maximum; and that the response at this frequency should be at least as large as required to support the shock wave.

[13]For unknown reasons, propellants containing potassium perchlorate were also stable to pulsing. There are practical reasons for not using potassium perchlorate in operational propellants.

[14]Marxman and Wooldridge were critical of alternative treatments of surface reactions by Brown *et al.* (1968); Friedly and Peterson (1966)a,b; and Krier *et al.* (1968). The similarities and differences among the analyses lie outside the range of the present discussion.

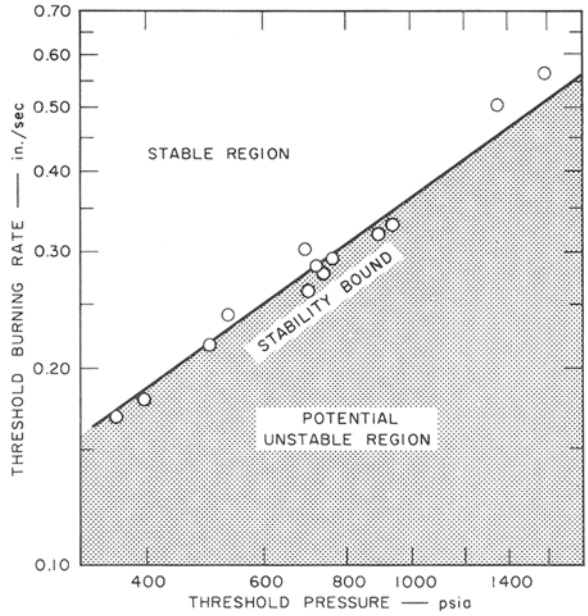

FIGURE 7.48. Stability boundary for 40 inch rockets, 5 inch diameter showing chamber pressure and burning rate below which pulses of pressure are stable (Capener, Dickinson and Kier 1967).

For typical conditions in the experiments examined, the value of the response required was about 1–1.2, ignoring other losses, notably that provided by the nozzle. The response required is reasonable, and overall the model proposed has several appealing features. However, despite the quantitative estimates, the results cannot be used, or extended, for predicting details of the instabilities produced in practice.

With a series of papers[15] in the period 1981–1986, Levine and co-workers have given the most successful and thorough numerical solutions for instabilities with steep-fronted waves in solid-propellant rockets. The success of the work was established by good comparison of the computed results with specially conducted experiments in cold flow as well as motor firings. While the calculations cannot give the fine details of the flow field found with LES simulations, the waveforms produced are remarkably close to those observed, and the consequences of changing physical parameters in the problem are generally explicable and fairly well-understood.[16]

In the early 1970s, numerical methods were first applied to instabilities in solid-propellant rockets, independently in two efforts by Levine and Culick (1972, 1974); and by Kooker (1974), reported also by Kooker and Zinn (1973). Particularly to be noted is that Kooker found a form of triggering in his work. Figure 7.49 reproduces one of his results showing a clear qualitative change of the response with amplitude of a continuously applied pressure oscillation. He reported no results for responses to input pulses.

The requirements of the problems taxed computing capabilities to the extent that only a few (c. 20 at most) cycles of an unstable oscillation could be produced with the numerical methods used. There was therefore strong practical motivation for developing approximate methods (Culick 1973a,b; Powell 1970,

[15]Levine and Baum (1982, 1983); Baum and Levine (1982, 1986, 1987); Baum, Lovine, and Levine (1983); Baum, Levine, and Lovine (1984); Baum, Levine, Chew and Lovine (1984); Lovine, Baum, and Levine (1985); and Baum, Levine and Lovine (1988).

[16]Recall some basic principles governing the behavior of waves in a compressible medium, formulated by Chu and Kovasznay (1957) and summarized briefly in Sections 3.1 and 7.9.

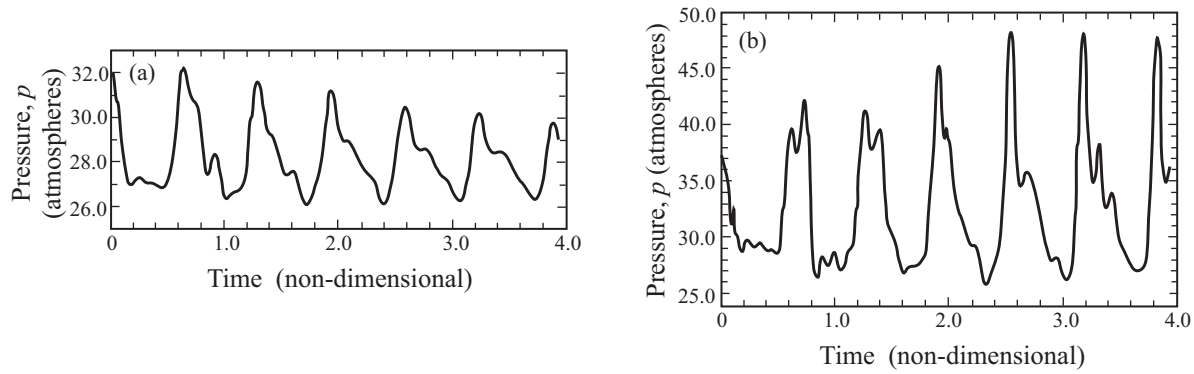

(a) (b)

FIGURE 7.49. Response of the head end of a motor (L = 10 ft.) to a continuously applied input pressure (Kooker and Zinn 1973).

example). Comparison of exact and approximate methods was a central issue (Culick and Levine 1974) in the early work, but in the period covered by the works of immediate concern here, and for the instabilities treated, the principal matter was reconciliation of the results of numerical calculations with observations.

The works in question (see Footnote 15) form a very instructive example of properly applying numerical methods and modeling to internal flows found in solid propellant rockets, accompanied by specially conducted experimental works. It must be recognized, however, that significant limitations are imposed on possible applications because all combustion processes are confined to the lateral surface of a chamber; and the dynamics of combustion are represented by an extension of the model due to Dennison and Baum (1961), as described here in Section 2.1. Most of the cases treated in the references are for uniform chambers.

In the first paper of the series, Baum and Levine (1982) addressed in detail the problem of computing the development of a standing wave or a pulse into traveling waves. They followed the general strategy worked out by Levine and Culick (1972, 1974) but used a combination of three computational methods, the Lax-Wendroff, hybrid, and artificial compression schemes. It was an important achievement that they were able to treat a shock wave as an abrupt discontinuity "without generating artificial pre- or post-shock oscillations" and without introducing artificial viscosity.

With subsequent publications Levine and Baum (1982, 1983) demonstrated that by taking velocity coupling into account, they were able to obtain results for triggering; shifts of the mean pressure when oscillations are present; and some cases when limit cycles were modulated. They also worked with Lovine at Aerojet Tactical Systems to demonstrate the first results comparing numerical computations and oscillations produced by pulsing in cold flow tests (Baum, Levine and Levine 1983). Figure 7.50 shows the three devices used. Figure 7.51 shows the time-evolution of a measured and a predicted pressure perturbation within a chamber containing only the flow from the pulsing unit.

In a paper presented publicly in 1982 but published two years later, Baum, Levine and Lovine (1984) essentially combined the main results presented in their previous works and treated sub-critical instabilities in laboratory motors and full-scale motors. The laboratory motor was 48 in. (1.22 m) long with internal case diameter 2.25 in. (5-7 cm); results were reported for three tests having partial grain either eight or nine inches long, and a fourth test having three short grain elements. In all cases quite good agreement was obtained for the observed and calculated time evolutions of sharp fronted wave following pulses. An example is reproduced as Figure 7.52 showing the results for the first and second pulses of the second test

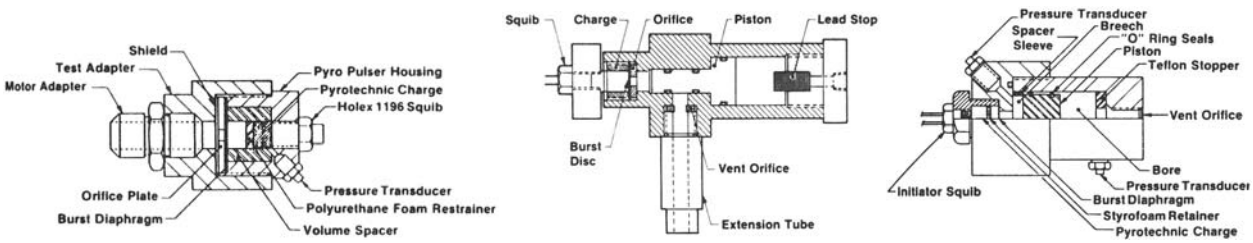

(a) (b) (c)

FIGURE 7.50. Three types of pulsing devices used by Baum, Lovine and Levine (1983). (a) pyro pulser; (b) low-brisance pulser; (c) piston pulser.

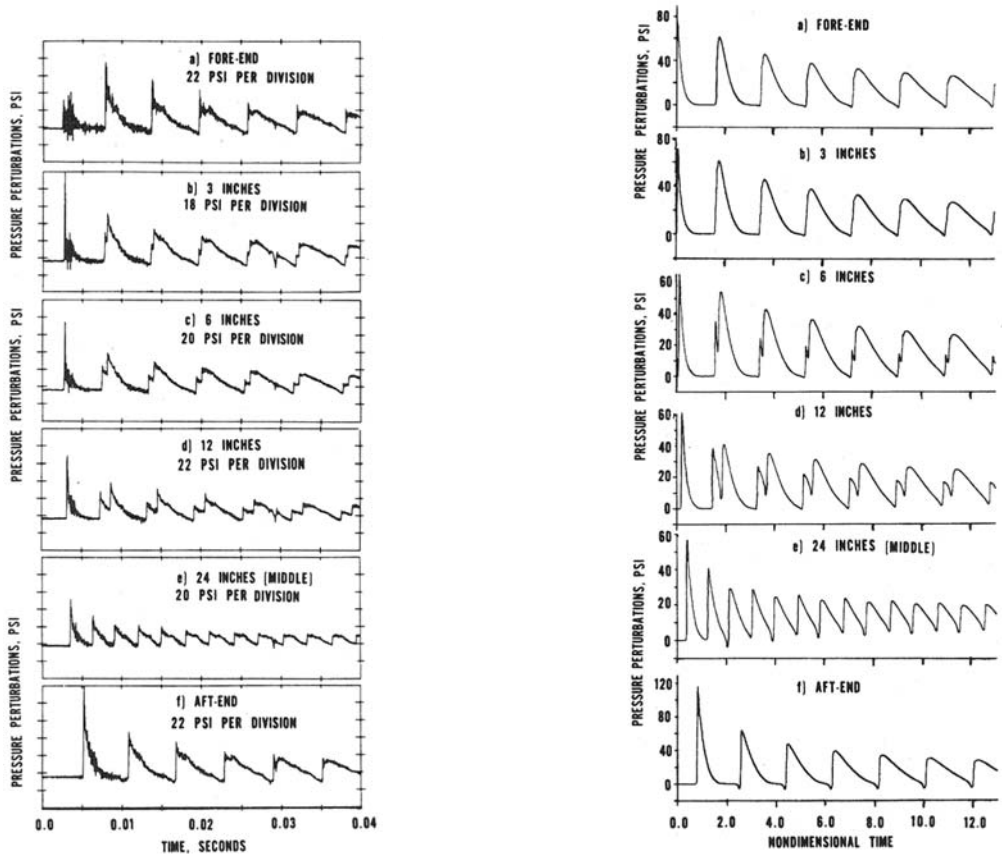

(a) (b)

FIGURE 7.51. Time evolution of pressure perturbations produced by a pyro pulser. (a) measured; (b) calculated (Baum, Lovine and Levine 1983).

called PCC4. The wave following the first pulse was stable and decayed before the second pulse was fired 0.23s after the first.[17]

There is a significant piece of the problem which is certainly not known well, namely representation of the dynamical characteristics of the propellant combustion. Levine *et al.* chose to use the basic result of

[17]Note the horizontal scale in Figure 7.52.

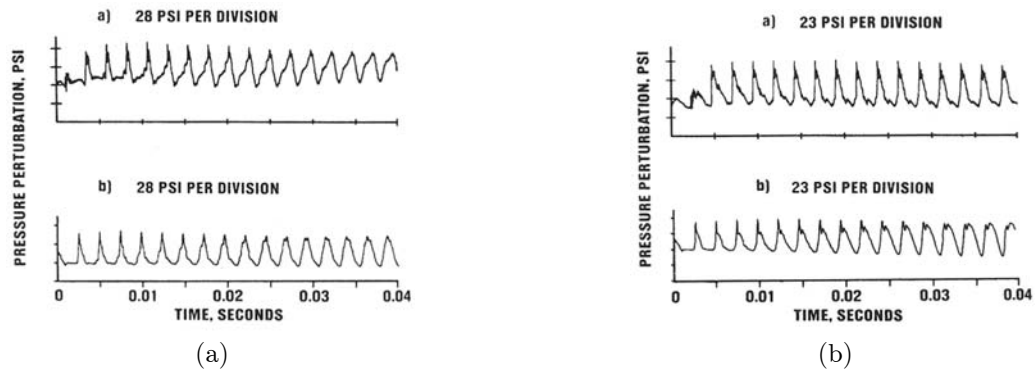

(a) (b)

FIGURE 7.52. Comparison of measured and predicted pressures at the head end, test PCC4 (a) first pulse; (b) second pulse (Baum, Levine and Lovine 1984).

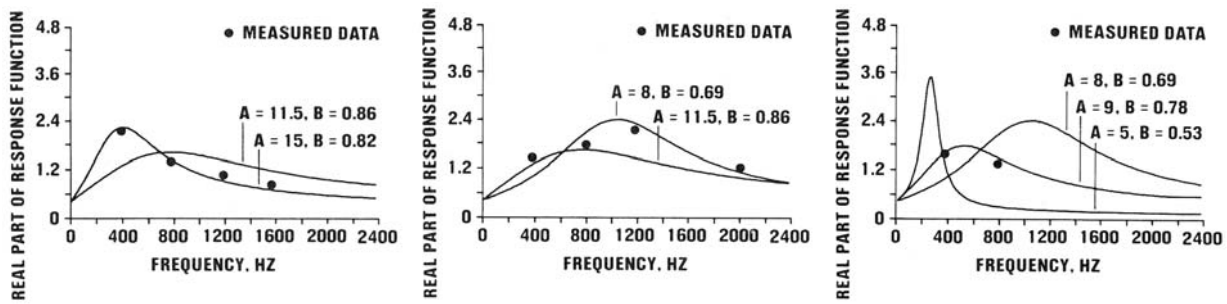

(a) (b) (c)

FIGURE 7.53. Response functions for the three propellants used by Baum, Levine and Lovine (1988).

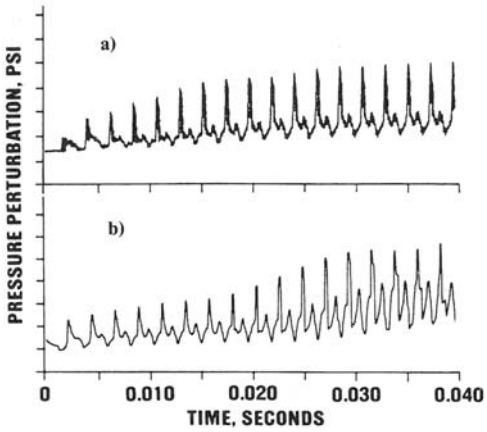

FIGURE 7.54. Comparison of observed and calculated pulsed instabilities in an aft-finocyl motor (a) observed; (b) calculated (Baum, Levine and Lovine 1988).

Dennison and Baum (1961) which forty years later still remains the best starting point. However, to obtain (even qualitatively in some respects) their good results, Levine and Baum found it essential that the surface combustion should be sensitive not only to pressure changes but also to fluctuations of velocity tangential to

the surface, *velocity coupling.* The idea that velocity coupling may be an important aspect of the dynamics of surface combustion is not new, dating back to the late 1950s; see Culick (1970) for a review of early work. In a later paper Baum and Levine (1983) have given a short discussion of their experience with modeling velocity coupling. They eventually chose the form for the fluctuation of mass flux produced by the propellant

$$\dot{m}' = \dot{m}'_{pc}\left[1 + R_{vc}F'(\vec{u})\right] \tag{7.59}$$

where $F(u) = |u'|$ represents the dependence on the magnitude of the velocity and m'_{pc} is related to the response function R_p for pressure coupling by (2.2). Much of the work by Levine *et al.* to obtain good agreement between their predicted results and observations was spent on adjustments to the parameters in (7.59).

The last paper by Baum, Levine and Lovine (1988) not only gives their final results but also summarizes their approach in general. It is probably the best paper of the series, giving an overall view of the work as well as some new findings. Results are present for eighteen pulsed motor tests in motors 8.38 cm (3.3 in) in diameter, having lengths 0.61 m., 0.91 m. and 1.22 m. (24, 36, 48 in). Three reduced-smoke propellants were tested in four different grain designs: cylinder, fore- and aft-finocyls and "dog-bone". In all tests three pulses were planned, a pyrotechnic, an ejected sphere, and a pyrotechnic in that order; ten tests were unstable on the second pulse and nine on the first, leading to amplitudes $\Delta p/\overline{p} = 0.1$ to 0.3. Two of the propellants produced "significantly higher wave amplitudes" in the aft-end finocyl configuration. That configuration also produced consistently greater DC shifts of mean pressure then the fore-end finocyl, a behavior that was found also in numerical predictions.

A limited amount of T-burner data, shown in Figure 7.53, was available for the response functions of the propellants used. These results for the parameters A and B were used to fix the response function according to our form (2.67) of Dennison and Baum's formula. Experience has shown that the values of A and B suggested are quite reasonable; see Section 2.2.3.

The discussion by Baum, Levine and Lovine explains how the values of the various parameters were chosen and fixed for comparison of predicted and observed waveforms. In the paper, six remarkably good comparisons are given. Figure 7.54 shows an example in which a secondary wave grows out of the primary wave. The original reference contains not only further examples but informative discussion and interpretation.

7.12. Dependence of Wall Heat Transfer on the Amplitude of Oscillations

Surface heat transfer is sometimes an important contribution to the loss of acoustic energy for oscillations in chamber. Normally for solid rockets that is not the case, but the T-burner (Figure 2.7) is a special contrary case. The problem of measuring the linear limit of heat transfer under oscillatory conditions has been discussed in Chapter 6 and Annex C. Here we are concerned with the dependence in the amplitude of oscillation, a very significant effect. The most recent work seems to have been reported by Merkli and Thomann (1975) in which oscillations were driven mechanically in a tube containing air. The observed increase of heat transfer rate was shown to be associated with the development of turbulence in part of an oscillatory cycle.

Combustion driven oscillations may reach considerably higher amplitudes than those sustained mechanically. As part of his work with the T-burner, Perry (1970) inferred mean heat transfer rates ($\bar{h}$) over oscillatory amplitudes from 2 to 60 psi, the average pressure being 300 psig. Results are given in Figure 7.55. The notation ($\overline{}$) indicates an average over the length of the T-burner so the dependence shown can be regarded only as approximate. Data taken for five propellants, presented in dimensionless correlations, Nusselt number versus Reynolds number, are plotted in Figure 7.56. The definitions are used

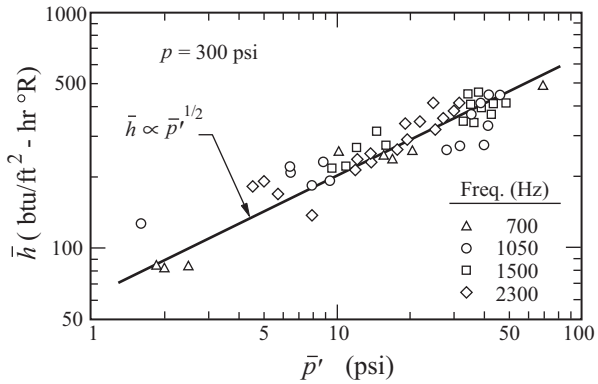

FIGURE 7.55. Mean heat transfer coefficient measured in T-burners showing dependence on amplitude of pressure amplitude (Perry 1970).

$$\overline{Nu} = \frac{\bar{h}\delta}{\bar{k}} \tag{7.60}$$

$$\overline{Re} = \frac{\bar{p}'\delta}{\bar{\mu}\,\bar{a}} \tag{7.61}$$

where $\bar{a}$ is the average speed of sound, and

$$\delta = \sqrt{\frac{\nu}{\pi f}} \tag{7.62}$$

is the 'thickness' of the acoustic boundary layer. The straight line in Figure 7.56 is

$$\overline{Nu} = 0.044\sqrt{\overline{Re}} \tag{7.63}$$

which implies $\bar{h} \propto \sqrt{\bar{p}'}f^{1/4}$. Perry and Culick (1974) note that the data shown in the figures cover a range of maximum velocity fluctuation to mean velocity from near zero to twenty.

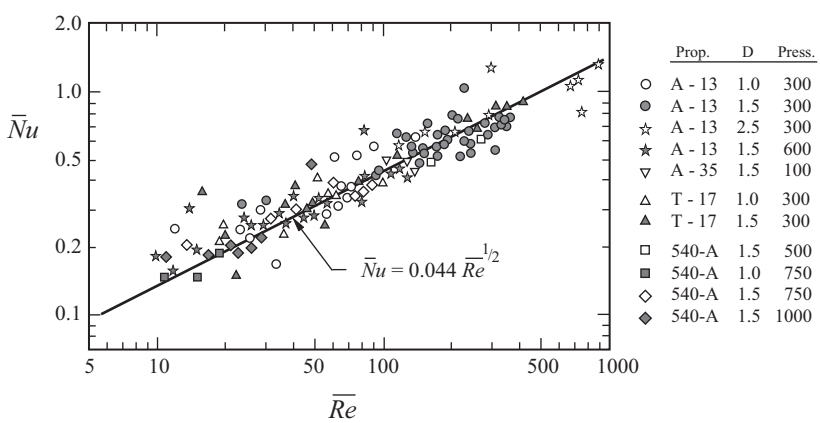

FIGURE 7.56. Mean heat transfer rates correlated as mean Nusselt number versus mean Reynolds number (Perry 1970).

No theory of the behavior shown in Figures 7.55 and 7.56 was given in the original work, or apparently since that time. The quantities defined by (7.60)–(7.62) were chosen as reasonable references and have at best qualitative significance. A brief attempt was made by Perry and Culick (1974) to determine a local

correlation (local heat transfer rate versus local oscillating pressure amplitude) with some reasonable results identical to equation (7.62).

The general problem summarized by the title of this section arises in several practical situations. For example, consequent structural failures in liquid propellant rockets and gas turbine combustors are well-documented. There is a genuine practical need for further clarification of the matter.

7.13. One Way to Analyze the Behavior of Pulses

Levine and Baum achieved remarkably good results using a one-dimensional representation of the wave motions. At least two reasons account for their success in obtaining such close agreement between their computations and observed behavior: careful development and application of the methods to calculate the steep-fronted waves; and close attention to (and modification of) the representation of the unsteady supply of material from the lateral burning surface. The second matter is heavily involved with the problem of velocity-coupling.

It is intrinsic to the works described in the preceding section that the calculations are elaborate and must be entirely done with a computer. In this section we discuss a way of computing the same sorts of problems, which is at best roughly approximate but which offers the possible advantage of investigating some aspects more easily. Although the specific problems discussed in the previous section will not be treated, the possible applications should be clear.

The basis for this calculation has been thoroughly discussed in Chapters 3 and 4. We will use equations (4.64)a,b based on the method of averaging applied to the more general second-order equations (4.36), or (7.5) with $F_n^{NL} = 0$. Since the wave motions that concern us here involve purely longitudinal motions, we assume that they are well-represented by longitudinal modes; the time-averaged equations are therefore (7.28)a,b. A simple example, a square pulse propagating in a quiescent gas contained in a closed tube with no combustion, displays the main idea. As indicated in Figure 7.57, a single pulse within the chamber may be represented as the superposition of two infinitely long trains of pulses, one train moving to the left, and one to the right. At the instant for which the figure is drawn, the pulse A is about to cross the boundary $z = 0$ from left to right, and the pulse B is about to cross from right to left. This represents reflection of a leftward moving pulse at the end, $z = 0$, of the tube. It is easy to deduce from the figure that during reflection the amplitude of the pulse is doubled near the reflecting boundary. Just before reflection, the real pulse within the chamber is represented by pulse B, and after reflection pulse A represents the real pulse. Note that pulses in each of the trains are separated by the distance 2L, twice the length of the chamber. Hence the wave system comprising the two wave trains has period 2L. This represents the pulse within the chamber travelling the distance 2L for a full cycle.

Under the conditions chosen here, the pressure pulse in the chamber must satisfy the homogeneous wave equation subject to the boundary condition for rigid walls at the ends,

$$\frac{\partial^2 p'}{\partial z^2} - \frac{1}{\overline{a}^2}\frac{\partial^2 p'}{\partial t^2} = 0 \tag{7.64}$$

$$\frac{\partial p'}{\partial z} = 0 \quad (z = 0, L) \tag{7.65}$$

The general solution of (7.64) may be written as the sum of rightward and leftward moving waves:

$$\frac{p'}{\overline{p}} = f(z - at) + g(z + at) \tag{7.66}$$

Figure 7.58 shows a special case of this solution. The train of pulses moving to the right is represented by $f(z - at)$ and those moving to the left are contained in $g(z + at)$. It is apparent that in order to satisfy the boundary conditions at the ends of the chamber having length L, the wave trains must have period 2L.

We will be particularly concerned here with the wave motions subsequent to specified initial conditions. Note that the example shown in Figure 7.58 was constructed artificially; it is not immediately obvious what *initial* conditions will produce the wave motion. The simplest initial value problem is that for a pulse initially at rest:

$$(t = 0; \quad 0 \le z \le L) \begin{cases} p'(z, 0) = \overline{p}P(z) \\ \dfrac{\partial p'}{dt}(z, 0) = 0 \end{cases} \tag{7.67}$$

For $t > 0$ such a pulse splits into *two* pulses, one moving to the left and one moving to the right. The solution can be represented as the superposition of two pulse trains as sketched in Figure 7.58. For this case the pulses in each of the trains have half the amplitude of the initial pulse.

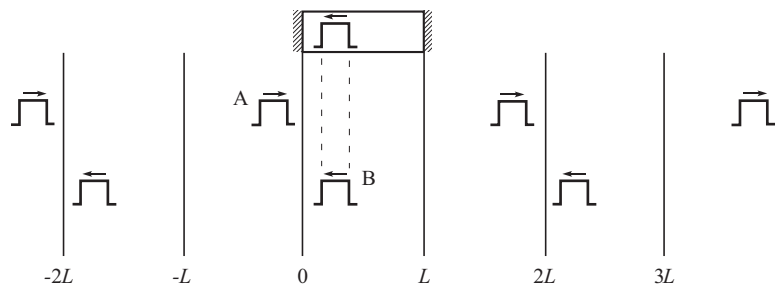

FIGURE 7.57. Superposition of two pulse trains to represent propagation of a single pulse in a closed tube.

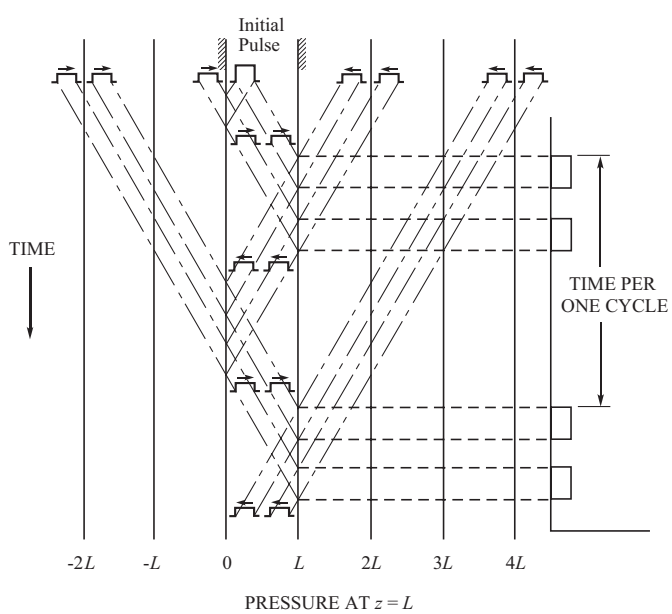

FIGURE 7.58. Propagation of pulses developed from a stationary initial pulse in a closed tube.

Because the initial pulse splits, there are always two pulses in the chamber. Measurement of the pressure at one end produces a signal which is periodic, having period equal to the round trip time for *one* of the pulses. The fundamental frequency of the signal is the fundamental frequency. For example, if a symmetric pulse is introduced at the center of the chamber, then the fundamental frequency of the signal is the frequency of the *second* mode of the chamber.

The case of a single pulse, sketched in Figure 7.57, is the simplest to visualize, and constitutes a special case of the general initial value problem. In order to satisfy the boundary conditions, it is necessary, as Figure 7.57 illustrates, to use wave trains having period twice the length of the chamber. We wish to account for both the initial pulse shape, $P(z)$, and its initial rate of change with time, $Q(z)$; the initial conditions are

$$\frac{p'}{\overline{p}}\,(z,0) = P(z) \tag{7.68}$$

$$\frac{\partial}{\partial t}\frac{p'}{\overline{p}}\,(z,0) = Q(z) \tag{7.69}$$

Define the function $F(z)$ representing leftward and rightward moving pulse trains required to satisfy the initial shape (7.68):

$$F(z) = \begin{cases} P(z) & 0 \le z \le L \\ P(-z) & -L \le z \le 0 \end{cases} \tag{7.70}$$

Outside the region $-2L \le z \le 2L$, $F(z)$ is periodic, having period $2L$:

$$F(z+2nL) = F(z) \qquad -2L \le z \le 2L; \quad n = \pm 1,\ \pm 2,\ \ldots \tag{7.71}$$

Similarly, a function $G(z)$ is defined to represent pulse trains required to satisfy the initial rate of change of the pressure field

$$G(z) = \begin{cases} Q(z) & 0 \le z \le L \\ -Q(-z) & -L \le z \le 0 \end{cases} \tag{7.72}$$

$$G(z+2nL) = G(z) \qquad -2L \le z \le 2L; \quad n = \pm 1,\ \pm 2,\ \ldots \tag{7.73}$$

Note that $F(z)$ is an even function and $G(z)$ is an odd function, with respect to the origin $z = 0$.

The pressure field for any $t \ge 0$ is given by the formula

$$\frac{p'}{\overline{p}} = \frac{1}{2}\left[F(z-at) + F(z+at)\right] + \frac{1}{2a}\int_{z-at}^{z+at} G(\xi)d\xi \tag{7.74}$$

It is easy to confirm that this formula for $p'/\hat{p}$ satisfies the initial conditions (7.68) and (7.69), and because of the definitions of $F(z)$ and $G(z)$ as periodic functions, the boundary conditions at $z = 0, L$ are satisfied.

Now the connection between the solution (7.74) and the normal modes of the chamber is established by expanding $F(z)$ and $G(z)$ in Fourier series:

$$\begin{aligned} F(z) &= \sum_{n=0}^{\infty} B_n \cos k_n z \\ G(z) &= \sum_{n=0}^{\infty} C_n \cos k_n z \end{aligned} \tag{7.75)a,b}$$

The Fourier coefficients are calculated from the formulas

$$
\begin{aligned}
B_0 &= \frac{1}{L}\int_0^L P(z)dz \\
B_n &= \frac{2}{L}\int_0^L \cos(k_n z)P(z)dz \\
C_0 &= \frac{1}{L}\int_0^L Q(z)dz \\
C_n &= \frac{2}{L}\int_0^L \cos(k_n z)Q(z)dz
\end{aligned}
\qquad (7.76)\text{a,b,c,d}
$$

The average values of the pulse and its rate of change are B_0 and C_0. In calculations we will be concerned only with the evolution of departures from the average values. Substitution of (7.75)a,b into (7.49) leads to the Fourier series for $p'(z,t)$:

$$
\begin{aligned}
\frac{p'}{\overline{p}} &= \frac{1}{2}\sum_{n=0}^{\infty} B_n\left[\cos k_n(z-at)+\cos k_n(z+at)\right] \\
&+ \frac{1}{2}\sum_{n=0}^{\infty} C_n\frac{1}{\omega_n}\left[\sin(z-at)+\sin k_n(z+at)\right]
\end{aligned}
\qquad (7.77)
$$

Because C_n has dimensions of frequency, the factor $\omega_n = ak_n$ makes C_n/ω_n dimensionless.

Expansion of the functions in (7.77) leads to the form

$$
\frac{p'}{\overline{p}} = \sum_{n=0}^{\infty}\left[A_n \sin\omega_n t + B_n\cos\omega_n t\right]\cos k_n z \qquad (7.78)
$$

in which A_n has been written from C_n/ω_n. This result is identical with the expansion (4.27), using (4.65) for $\eta_n(t)$. For a pulse which propagates in a passive medium, with unchanging shape, the Fourier coefficients A_n and B_n are constant. For the problems arising in combustion chambers, A_n and B_n vary with time according to equations (4.64)a,b.

Hence we now have a means for analyzing the behavior of an arbitrary pulse in terms of the normal modes of a chamber, and accounting for nonlinear gasdynamics. The procedure may be summarized in the following steps.

1) The initial shape and rate of change of the pressure are specified, giving the functions $P(z)$ and $Q(z)$.
2) The initial values of B_n and $A_n = C_n/\omega_n$ are calculated from the formulas (7.76)a,b.
3) The time evolution is calculated by using the appropriate forms of equations (7.28)a,b.
4) The pressure field can then be calculated at any time by using (7.78).

In principle, any problem of one-dimensional pulse propagation can be handled in this way, accounting for linear and nonlinear processes in the medium. Practical difficulties may arise in the treatment of a steep-fronted pulse requiring a large number of modes for a faithful representation.

7.13.1. Some Results for the Propagation of Pulses. We shall consider here only cases of rectangular pulses with the initial pressure not changing in time. Thus $Q(z) = 0$ in (7.69), and the Fourier

coefficients are given by (7.51)a,b. For a pulse having height Δ, and non-zero in the range $L_1 \leq z \leq L_2$, the coefficients are

$$B_0 = \Delta(L_2 - L_1) \tag{7.79}$$

$$B_n = \frac{2\Delta}{n\pi}\left[\sin\left(n\pi\frac{L_2}{L}\right) - \sin\left(n\pi\frac{L_1}{L}\right)\right] \tag{7.80}$$

Figure 7.59 shows the approximations using 10, 20, 30 and 50 modes for a pulse generated at one end of a chamber in the range $.1L \leq z \leq .4L$.

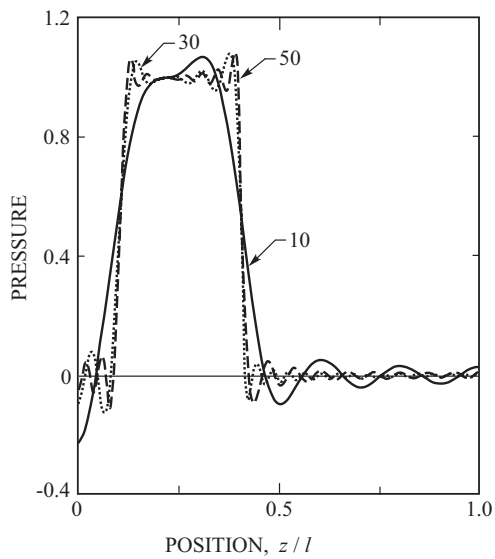

FIGURE 7.59. Approximations to a rectangular initial pulse by 10, 30, 50 modes. Pulse initially in the range $0.1L \leq z \leq 0.4L$.

Equations have been solved here for two cases: $\alpha_n = \theta_n = 0$; and for the values of α_n θ_n chosen to illustrate the propagation of pulses. No results have been obtained for the conditions in a motor. The simplest case is a small amplitude pulse with no losses: $\alpha_n = \theta_n = 0$. Figure 7.60(a) is the pressure at the head end ($z = 0$) for the pulse represented by ten modes, Figure 7.60(b), and $\Delta = 0.006$. Because only ten modes are used, ripples appear in the waveform. The pulse shape in the chamber is shown in Figure 7.60(b) for various times during three cycles. For the small amplitude of this pulse, the second order nonlinearities have no discernible effect on the pulse shape for the short time covered in this figure.

In contrast, the case $\Delta = 0.1$ is a large amplitude pulse, and the influence of nonlinearities appear already in the first cycle. The initial shape is that of Figure 7.60(a). Figure 7.60(a) is the waveform at $z = 0$, and Figure 7.60(b) shows the pulse shape at various times. For comparison, the waveform of a simple cosine, the fundamental mode, is shown in Figure 7.61. Note the steepening into a weak shock after three cycles. The generation of higher harmonics is evident, both in the waveform measured at $= 0$ and in the shape of the pressure distribution, in the chamber. However, an interesting feature is that the smoothness of the spatial distribution is not reflected in the time history, appearing in Figure 7.61(a). The uneven character of the latter is due to the excitation of higher frequencies whose associated spatial waves combine to form the smoothly steeping solitary wave which propagates as shown in Figure 7.61(b).

One of the interesting and potentially useful features exhibited by pulses in motors is the change of shape due to different rates of decay for the modes. In Figure 7.62, the decay of a small amplitude pulse is shown. For this case, $\alpha_n = -40n$, and $\theta_n = 0$ in equations (7.28)a,b; again the initial pulse shape is the

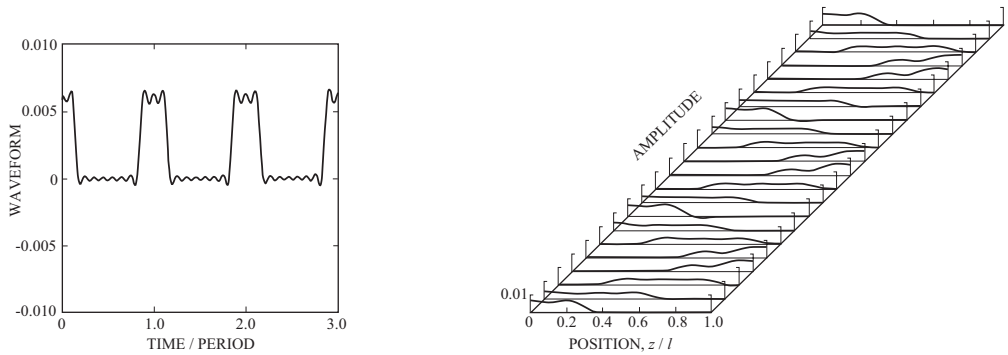

(a) (b)

FIGURE 7.60. Propagation of a rectangular pulse without losses (10 modes): $p'(z,0) = 0.006p_0$; $0 \leq z \leq 0.3L$. (a) Waveform at $z = 0$; (b) pulse shapes for three cycles.

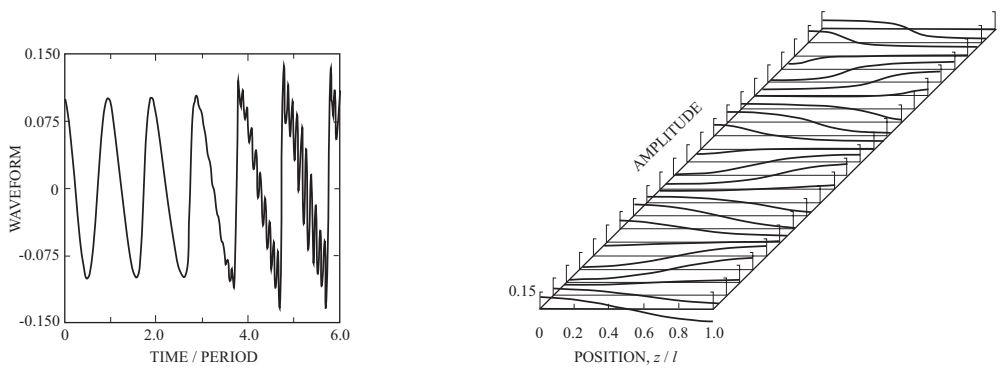

(a) (b)

FIGURE 7.61. Propagation of an evolving cosine wave: $p'(0,0) = 0.01p_o$. (a) Waveform at $z = 0$; (b) pulse shapes for three cycles. Notice the form of the steepened cosine wave shown at the end of the third cycle.

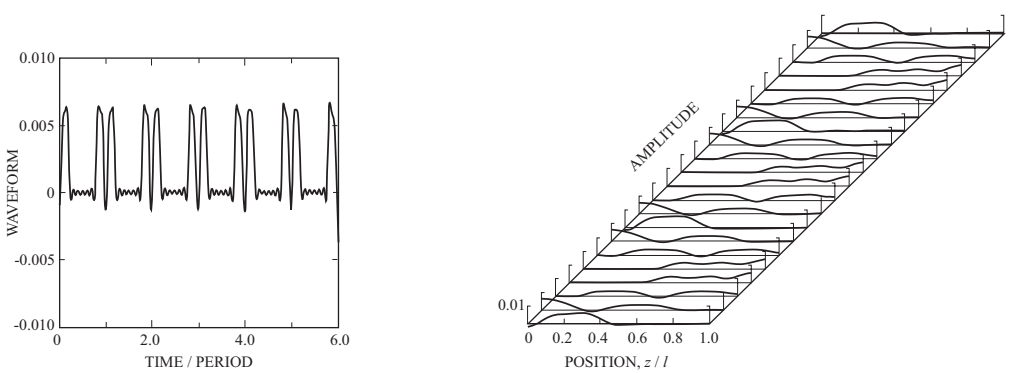

(a) (b)

FIGURE 7.62. Propagation of a rectangular pulse (10 modes): $p'(z,0) = 0.006p_0$; $0.1L \leq z \leq 0.4L$. (a) Waveform at $z = 0$; (b) pulse shapes for three cycles.

approximation for ten modes, Figure 7.62(a). After six cycles there are still substantial amounts of the first five harmonics but the next five are practically absent. The average value of the pulse remains fixed at its initial value, so the pressure fluctuation does not become negative after several cycles.

Finally, in Figure 7.62 the behavior of a rectangular pulse initially displaced from one end is shown. The initial shape is the approximation with ten modes, Figure 7.62(b). This case corresponds to the perfect rectangular pulse sketched in Figure 7.58. The qualitative similarities are obvious.

7.14. Spatial Averaging and Dynamical Systems Theory Applied to Pulsed Instabilities

Attention to the problem of triggering shifted in the 1990s from numerical solutions to use of the method based on spatial averaging as described in Chapters 3 and 4. Although there was no proof, numerous examples had finally led to the conclusion that the equations with linear combustion sources and second order acoustics do not contain triggering. Attempts to find triggering with the equations carried to third order in nonlinear acoustics also failed (Yang, Kim and Culick 1990). The general conclusion was (and is) that the nonlinear acoustics alters the distribution of energy among the modes of oscillation, but since there is no external source of energy, the process cannot support triggering. Therefore, emphasis shifted to the role of the source terms. Due to the conclusion just stated, it is sufficient, at least for the initial work, to consider only second order acoustics. To the present time, third and higher order acoustics have not been considered; there seems to be no need to use an expansion procedure higher than second order.

Earlier work (Yang, Kim and Culick 1990) had shown although the result was not rigorously proven in general, that triggering could occur if either quadratic self-coupling or linear cross-coupling between modes are present. For example, in unpublished work, a model system examined by Awad and Culick (1984) demonstrated the importance of quadratic self-coupling which, however, does not arise in the modal expansion of the purely fluid mechanics contributions ($\rho\vec{u}\cdot\nabla\vec{u}$, etc.). Thus, it appeared again that the resolution of the matter lay with the source terms.

In 1996, Wicker, Green, Kim and Yang (1996) used the time-averaged equations accounting for two modes, to study the conditions under which triggering occurs for five forms of the unsteady burning rate. When $\dot{m}_1'$ is proportional to p'^2, u'^2 or $p'u'$ no triggering. The authors found in that case no linear or quadratic self-coupling so the result is consistent with the conclusion cited above. However for $\dot{m}_b'$ proportional to $|\vec{u}'|$ or $p'|\vec{u}|$. They used the time-averaged equations. An interesting, and probably important, feature of their results was the fact that linear cross-coupling among the acoustic modes and quadratic self-coupling of the fundamental mode were the origin of triggering. A bit unsettling is the conclusion that the "initial phase difference and harmonic content can be just as important as initial composite amplitude in determining the stability of a pulse." This result suggests a certain kind of sensitivity that may be associated with the use of the time-averaged equations. See Jahnke and Culick (1994) for relevant results dealing with the limitations of the time-averaged equations; they did not, however, examine triggering.

Nearly contemporaneous with the work of Wicker *et al.* were results obtained by Jahnke and Culick (1995) using the continuation method described in Section 7.4. They used two models for nonlinear combustion, that of Levine and Baum (1983), and a slightly simpler one by Greene (1990) in which $\dot{m}_b' \sim |\vec{u}'|$. We will discuss only the first here, for which the fluctuation mass flux departing the burning surface is computed with a slightly more complicated form of (7.59). Assume that the *total* mass flux (not just $\dot{m}'$) is given by (7.59) so the fluctuation is now

$$\begin{aligned}\dot{m}' &= \dot{m} - \overline{\dot{m}} \\ &= \left(\dot{m}_{pc}' + \overline{\dot{m}_{pc}'}\right)\left[1 + R_{vc}|\mathbf{U}'|\right] - \overline{\dot{m}_{pc}'}\end{aligned}$$

Some rearrangement and introduction of the response function R_b leads to the relation

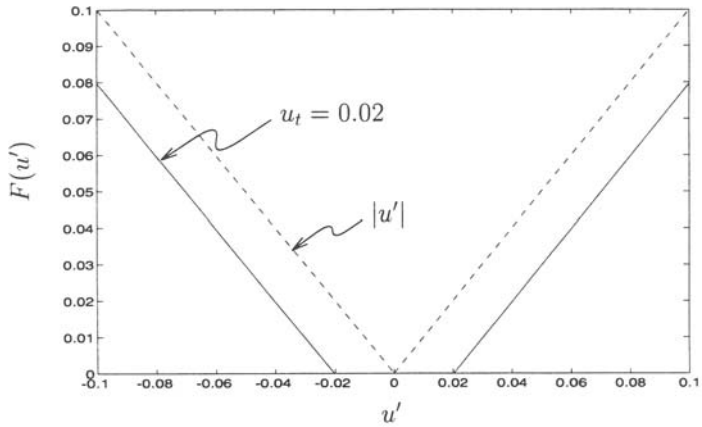

FIGURE 7.63. The function $F(u')$ used in the model having a threshold velocity $u_t > 0$; the value $u_t = 0.02$ is only an example (Burnley 1996).

$$\frac{\dot{m}'}{\overline{m}} = R_b\left(\frac{p'}{\gamma\overline{p}}\right) + R_{vc}R_b\left(\frac{p'}{\gamma\overline{p}}\right)|\mathbf{U}'| + \frac{\dot{m}_{pc}}{\overline{m}}R_{vc}|\mathbf{U}'| \tag{7.81}$$

Substitution into the combustion term of the forcing function ( ) leads to

$$(F_n)_{comb} = \frac{\overline{u}_b}{E_n^2}\left\{C_1\iint\frac{\partial}{\partial t}\left(\frac{p'}{\overline{p}}|u'|\right)\psi_n dS + C_2\iint\frac{\partial|u'|}{\partial t}|u'|\psi_n dS - C_3\iint\frac{p'}{\overline{p}}\frac{\partial}{\partial t}\left(\frac{p'}{\overline{p}}\right)\psi_n dS\right\} \tag{7.82}$$

where

$$C_1 = R_{vc}R_b\ , \quad C_2 = \frac{1}{\gamma}R_{vc}\ , \quad C_3 = \frac{2}{\gamma}(R_b - 1) \tag{7.83}$$

Note that R_{vc} is a constant but R_b is in general a function of frequency, as for example in (2.52). To simplify the calculations in order to understand more easily the qualitative behavior, we set the imaginary part of R_b equal to zero, that is, in (2.40), $R_b = R_b^{(r)}$ given as the real part of (2.52), with $n_s = 0$.

The functions $|u'|$ and $|u' - u_t|$ are shown in Figure 7.63, with $|u' - u_t|$ by definition zero for $u' < u_t$; u_t is called the threshold velocity. Burnley (1996) gave an extended discussion of the consequences of truncation; various simplifications of the combustion model; the threshold velocity; and time-averaging. Results obtained with the second-order equations (7.27) compared with those based on time-averaging have shown that time-averaging must be used with care, for it can lead to misleading results (see Wicker *et al.* 1996, Burnley and Culick 2000 and Wicker and Yang 2000).

A main general conclusion reached by Culick, Burnley and Swenson is that triggering exists only if both nonlinear combustion and nonlinear gasdynamics are included. The point is made most strikingly and clearly with the bifurcation diagram, Figure 7.64.

The role of velocity coupling is clearly important and the results *suggest* that it is important for triggering to occur under practical circumstances, but proof of the point has not been established beyond all doubt. Much remains to be done on this aspect of the problem.

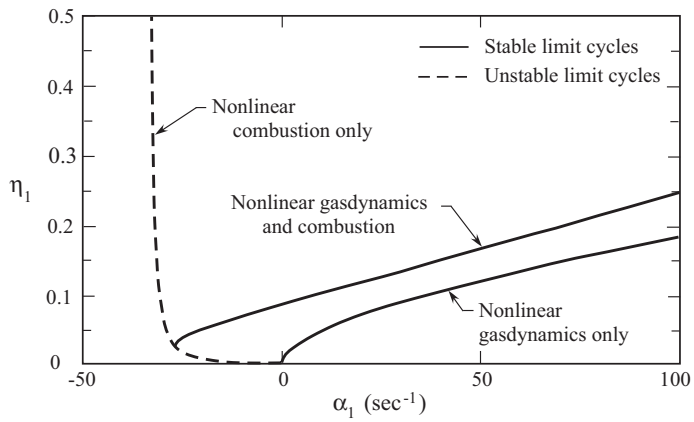

FIGURE 7.64. Maximum amplitude of the first acoustic mode in the limit cycle showing the contribution of nonlinear gasdynamics and combustion (Culick, Burnley and Swenson 1995).

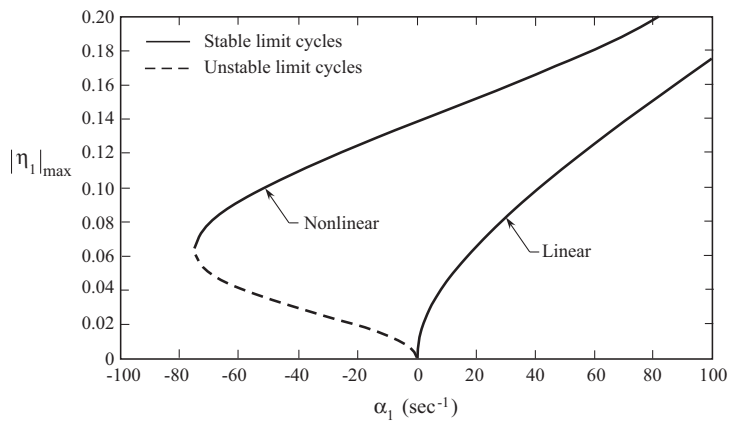

FIGURE 7.65. Maximum amplitude of the first acoustic mode in the limit cycle showing a subcritical bifurcation with a turning point only if both nonlinear gasdynamics and nonlinear combustion dynamics are accounted for (Culick, Burnley and Swenson 1995).